

**SUPRAMOLECULAR STRUCTURAL STUDY ON
MALARIA PIGMENT MODEL SYSTEMS**

Saifon Archanachai Kohnhorst

The image contains a large, faint watermark of the Suranaree University of Technology logo. The logo is circular and features a central figure of a person standing on a pedestal, surrounded by a gear-like border. The Thai text 'มหาวิทยาลัยเทคโนโลยีสุรนารี' (Mahavithayalai Techno Suranaree) is written around the bottom of the circle.

**A Thesis Submitted in Partial Fulfillment of the Requirements for the
Degree of Doctor of Philosophy in Biochemistry
Suranaree University of Technology
Academic Year 2012**

การศึกษาโครงสร้างทางซูปรามอเลคิวลาร์ของระบบแบบจำลองของสารสีมาลาเรีย

นางสายฝน อาชนะชัย คอห์นฮอ์สต์



วิทยานิพนธ์นี้เป็นส่วนหนึ่งของการศึกษาตามหลักสูตรปริญญาวิทยาศาสตรดุษฎีบัณฑิต

สาขาวิชาชีวเคมี

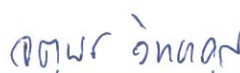
มหาวิทยาลัยเทคโนโลยีสุรนารี

ปีการศึกษา 2555

**SUPRAMOLECULAR STRUCTURAL STUDY ON MALARIA
PIGMENT MODEL SYSTEMS**

Suranaree University of Technology has approved this thesis submitted in partial fulfillment of the requirements for the Degree of Doctor of Philosophy.

Thesis Examining Committee



(Assoc. Prof. Dr. Jatuporn Wittayakun)

Chairperson



(Assoc. Prof. Dr. Kenneth J. Haller)

Member (Thesis Advisor)



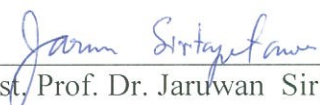
(Dr. Ratchadaporn Puntharod)

Member



(Prof. Dr. James R. Ketudat-Cairns)

Member



(Asst. Prof. Dr. Jaruwat Siritapetawee)

Member



(Prof. Dr. Sukit Limpijumnong)

Vice Rector for Academic Affairs



(Assoc. Prof. Dr. Prapun Manyum)

Dean of Institute of Science

สายฝน อาชนะชัย คอห์นฮอว์สต์ : การศึกษาโครงสร้างทางซูปราโมเลคิวลาร์ในระบบแบบจำลองสารสีมาลาเรีย (SUPRAMOLECULAR STRUCTURAL STUDIES ON MALARIA PIGMENT MODEL SYSTEMS) อาจารย์ที่ปรึกษา : รองศาสตราจารย์ ดร.เค็นเนท เจ. แสเลออร์, 100 หน้า.

มาลาเรียเป็นโรคติดต่อที่เกิดขึ้นโดยมีพาหะนำโรคชนิดโปรโตซัว *Plasmodium falciparum*, ซึ่งเข้าไปอาศัยอยู่ในเม็ดเลือดแดง โปรโตซัวย่อยสลายฮีโมโกลบินของเม็ดเลือดแดงเป็นอาหารและลดการเป็นพิษของฮีโมโกลบินโดยการตกตะกอนเรียกว่าสารสีมาลาเรีย นอกจากนี้ได้มีการศึกษาระบบแบบจำลองของสารสีมาลาเรียใหม่ซึ่งเรียกว่า คลอโรโอรอน(สาม) ออกตะเอทิลพอไพร์ริน Fe(OEP)Cl 5-โคออร์ดิเนต สปินสูง ด้วยเครื่องมือยิงผลึกเดี่ยว โดยผลที่ได้จากศึกษาทางด้านผลึกเดี่ยว ที่อุณหภูมิ 100 องศาเคลวิน ผลึกที่ได้จำแนกอยู่ในกลุ่ม triclinic *P*-1 และประกอบด้วย 2 อะซิมเมตริก ยูนิต ความหนาแน่นเท่ากับ 1.287 กรัมต่อลูกบาศก์เซนติเมตรเมื่อทำการวิเคราะห์โครงสร้างด้วยเครื่องมือยิงผลึกเดี่ยว พบว่า โครงสร้างของ triclinic Fe(OEP)Cl ประกอบด้วย ความยาวพันธะของ Fe—N มีค่า 2.071(2) อังสตรอม และความยาวพันธะของ Fe—Cl มีค่าเป็น 2.220(8) อังสตรอม ในขณะที่อะตอมของเหล็กอยู่เหนือระนาบของวงพอไพร์รินเป็น 0.51(7) อังสตรอม โครงสร้างของวงพอไพร์รินที่ไม่มีหมู่แทนที่มีลักษณะเป็นคลื่นและจากการคำนวณค่าเฉลี่ยของอะตอมที่อยู่ในและนอกระนาบของวงพอไพร์รินทั้ง 24 อะตอมมีค่าเท่ากับ 0 อังสตรอม แสดงให้เห็นว่าวงพอไพร์รินอยู่ในแนวแบนราบ นอกจากนี้ยังได้มีการรายงานภาวะที่มีหลายรูปแบบชนิดใหม่ของ Fe(OEP)Cl พบว่าโครงสร้างในการศึกษาครั้งนี้หมู่เอทิล 4 หมู่ ชี้ขึ้นด้านบน และหมู่เอทิลอีก 4 หมู่ ชี้ลงด้านล่าง ซึ่งการเรียงตัวของหมู่เอทิลเป็นผลมาจากการเกิดสเตอริก และนำไปสู่การเชื่อมต่อกันของโมเลกุลแบบไม่แข็งแรงซึ่งพบในโครงสร้างนี้ นอกจากนี้ยังมีหลายปัจจัยที่ยับยั้งการเชื่อมต่อกันระยะสั้นของผลึก ซึ่งจากการศึกษาโครงสร้างซูปราโมเลคิวลาร์ในระบบแบบจำลองสารสีมาลาเรียนี้ ความยาวพันธะของ C—H...Cl ยับยั้งการเกิดอันตรกิริยาแบบสั้นระหว่างวงพอไพร์รินสองวง ดังนั้นการเกิดโครงสร้างทางซูปราโมเลคิวลาร์ในสารสีมาลาเรียอาจจะเกิดขึ้นโดยอันตรกิริยาของ van der Waals และเนื่องจากความหนาแน่นน้อยจึงมีความเสถียรต่ำ

สาขาวิชาชีวเคมี
ปีการศึกษา 2555

ลายมือชื่อนักศึกษา _____
ลายมือชื่ออาจารย์ที่ปรึกษา _____

SAIFON ARCHANACHAI KOHNHORST : SUPRAMOLECULAR
STRUCTURAL STUDY ON MALARIA PIGMENT MODEL SYSTEMS
THESIS ADVISOR : ASSOC. PROF. KENNETH J. HALLER, Ph.D.
100 PP.

MALARIA PIGMENT/ MODEL SYSTEMS/ HEME/IRON
PORPHYRINS/SUPRAMOLECULAR INTERACTIONS/ PORPHYRINS

Malaria is an infectious disease caused by the parasite, *Plasmodium falciparum*, invading red blood cells. Toxic free heme released by the parasites destruction of hemoglobin is detoxified by conversion to malaria pigment. A new polymorph of malaria pigment model systems is reported in this study, chloroiron(III) octaethylporphyrin, Fe(OEP)Cl five-coordinated high-spin was determined by single-crystal X-ray diffraction at 100 K. The crystallographic structure result demonstrated that the crystal belongs to the triclinic, *P*-1 space group and contains two asymmetric per unit cell. The density of the triclinic, Fe(OEP)Cl is 1.287 Ggm⁻³. The Fe–N bond distance is 2.071(2) Å and Fe–Cl distance is 2.220(8) Å, and the Fe atom is displacement out of the 24-atom mean plane of the porphyrin ring by 0.51(7) Å. The porphyrin core exhibited the wave shape, while the porphyrin core is nearly planar with the average displacement of the 24 atoms of the porphyrin core of nearly 0 Å. A new polymorphism of Fe(OEP)Cl in this study is reported with the four ethyl groups “up”/ “down” which resulted by steric effects of the methyl groups on the periphery, which favors the staggered conformation. The crystal packing is in a slipped parallel arrangement, which indicate that the weak supramolecular interactions are stabilizing

in this structure. Several factors inhibit the close contact in the crystal packing. In this study, the C–H...Cl interaction is preventing the close contact between two porphyrin rings and the supramolecular interactions in malaria pigment model systems may occurred by van der Waals interactions. Thus, these results suggested that malaria pigment may be form by van der Waals interactions.



School of Biochemistry

Academic Year 2012

Student's Signature _____

Advisor's Signature _____

ACKNOWLEDGEMENTS

I dedicate this dissertation to my child, Lynne, who is my source of joy and my inspiration. In loving memory of Dr. Andrew Lloyd Kohnhorst, for his patience and sacrifices, and for his unconditional love. This work would not be possible without the love and support of my family who always believed in me and taught me to persevere.

I acknowledge, first of all, my research advisor Assoc. Prof. Dr. Kenneth J. Haller, for his guidance throughout my Ph.D. research. Thanks also to the dissertation committee members, especially Dr. Ratchadaporn Puntharod and I would also like to thank Dr. Haller's research group members for their guidance and helpful discussions.

I acknowledge the Commission on Higher Education, Thailand for financial support (CHE-PHD-TH-2550) for my Ph.D. program.

Saifon Archanachai Kohnhorst

CONTENTS

	Page
ABSTRACT IN THAI.....	I
ABSTRACT IN ENGLISH	II
ACKNOWLEDGEMENTS.....	IV
CONTENTS.....	V
LIST OF TABLES.....	VII
LIST OF FIGURES	VIII
LIST OF ABBREVIATIONS.....	IX
CHAPTER	
I INTRODUCTION.....	1
1.1 General Structural Features	1
1.2 Porphyrin Core Conformations.....	3
1.3 Iron Porphyrins	8
1.4 Malaria Pigment and Heme Derivatives	13
1.5 Structural Spectroscopy of Malaria Pigment Model Systems	16
1.6 Supramolecular Interactions.....	22
1.7 References	25

CONTENTS (Continued)

	Page
II CONFORMATIONAL STUDY ON μ-OXO- IRON(III) PORPHYRIN MALARIA PIGMENT MODEL COMPOUNDS.....	35
2.1 Introduction.....	35
2.2 Experimental.....	39
2.3 Results and Discussion.....	41
2.4 Conclusion.....	51
2.5 References.....	52
III A NEW POLYMORPH STUDY ON CHLORO (2,3,7,8,12,13,17,18-OCTAETHYLPORPHYRINATO)IRON(III).....	59
3.1 Introduction.....	59
3.2 Experimental.....	61
3.3 Results and Discussion.....	77
3.4 Conclusion.....	93
3.5 References.....	93
IV CONCLUSION.....	98
APPENDICES.....	100
APPENDIX A.....	101
APPENDIX B.....	105
APPENDIX C.....	111
CURRICULUM VITAE.....	137

LIST OF TABLES

Table	Page
1.1 Comparison of Iron(III) Nitrogen Distances, Axial Ligand Distances and Spin State in Six-coordinate $[\text{Fe}(\text{OEP})(3\text{-Clpy})_2]^+$ Perchlorate	12
2.1 Comparison of High Frequency Raman Spectra of μ -oxo iron(III) Porphyrins	37
2.2 Comparison of Structural Parameters of μ -oxo Iron(III) Porphyrins	48
3.1 Crystal Data and Refinement Details for Triclinic $\text{Fe}(\text{OEP})\text{Cl}$	65
3.2 Fractional Triclinic Atomic Coordinates, and Equivalent Isotropic Atomic Displacement Parameters (\AA^2) for the Nonhydrogen Atoms of $\text{Fe}(\text{OEP})\text{Cl}$.	67
3.3 Anisotropic Triclinic Atomic Displacement Parameters for the Nonhydrogen Atoms of $\text{Fe}(\text{OEP})\text{Cl}$	69
3.4 Fractional Triclinic Coordinates and Isotropic Atomic Displacement Parameters (\AA^2) for the Hydrogen Atoms of $\text{Fe}(\text{OEP})\text{Cl}$	71
3.5 Selected Bond Distances and Angles of Triclinic $\text{Fe}(\text{OEP})\text{Cl}$	73
3.6 Summary of Crystal Data, Intensity Data Collection Parameters, and Final Statistics of the Refinement of $\text{Fe}(\text{OEP})\text{Cl}$	81
3.7 Selected Structural Parameters (\AA) of $\text{Fe}(\text{OEP})\text{Cl}$	82
3.8 Selected van der Waals Contact in Triclinic and Monoclinic on $\text{Fe}(\text{OEP})\text{Cl}$	90

LIST OF FIGURES

Figure	Page
1.1 Projection view of porphyrin core..	2
1.2 Porphyrin core diagram with ring substituent positions numbered..	2
1.3 Schematic diagram show normal-coordinate deformations used to describing the planar distortions of the porphyrin cores..	4
1.4 Basic structure of protoporphyrin IX..	10
1.5 Basic structure of octaethylporphyrin..	10
1.6 Basic structure of tetraphenylporphyrin..	11
1.7 Iron(III) protoporphyrin IX..	15
1.8 Diagram of malaria pigment..	17
2.1 IR spectra of [Fe(PPIX*)] ₂ O..	41
2.2 Resonance Raman spectrum in 400-1800 cm ⁻¹ region of [Fe(PPIX*)] ₂ O.....	43
2.3 The simulation PXRD of μ-oxo iron(III) porphyrins.	44
2.4 Formal diagrams of the two crystallographically independent porphinato cores of [Fe(PPIX*)] ₂ O, [Fe(TPP)] ₂ O, and [Fe(OEP)] ₂ O, displaying the perpendicular displacements, in units of 0.01 Å, from the mean plane of the 24-atom core.	41
3.1 <i>ORTEP</i> diagram showing molecular structure of the triclinic form of Fe(OEP)Cl.....	64
3.2 Absorbance spectrum of triclinic Fe(OEP)Cl.....	78

LIST OF FIGURES (Continued)

Figure	Page
3.3 FT-IR spectrum of Fe(OEP)Cl in present work.....	79
3.4 Formal diagram of the single molecule triclinic form of Fe(OEP)Cl showing bond lengths in angstrom and angles in degrees, the values in parentheses are the distances corrected for thermal motion. Also showed the displacement of the 24 atoms displacement out of the mean plane.....	80
3.5 Formal diagrams of the porphyrin core of Fe(OEP)Cl.....	83
3.6 X-Ray Powder Diffraction spectra of Fe(OEP)Cl calculated by Mercury a: monoclinic form. b: triclinic form. c: solvate form.	85
3.7 Different stereochemistry of Fe(OEP)Cl.....	86
3.8 <i>ORTEP</i> drawing shows the hydrogen bonds in the triclinic form of Fe(OEP)Cl.....	86
3.9 Projection view of the packing in the triclinic form of Fe(OEP)Cl showing the C–H...Cl hydrogen bond to form a Fe(OEP)Cl dimer via stacking.....	88
3.10 Nonbonded interaction between two porphyrin rings in the triclinic form showing the C–H... π and C–H...Cl distances.....	88
3.11 Projection view of the packing in the monoclinic form of Fe(OEP)Cl showing the C–H...Cl hydrogen bonds to form Fe(OEP)Cl dimer via stacking.....	89
3.12 Nonbonded interactions between two porphyrin rings in the monoclinic form of Fe(OEP)Cl showing the C–H... π and C–H...Cl distances.....	89

LIST OF ABBREVIATIONS

AERS	Aggregated Enhanced Raman Scattering
CSD	Crystal Structure Database
C _α	α-Carbon
C _β	β-Carbon
C _m	Methine Carbon
C _t	Center of Gravity of the Four Nitrogen Atoms
D	Density
DMF	<i>N,N'</i> Dimethylformamide
CHCl ₂	Dichloromethane
CHCl ₃	Chloroform
EXAFS	Extended X-ray Absorption Fine Structure
Fe(OEP)Cl	Iron(III) Octaethylporphyrin Chloride
Fe(PPIX)Cl	Iron(III) Protoporphyrin IX Chloride
[Fe(OEP)] ₂ O	μ-Oxo-bis(octaethylporphinato) Iron(III)
[Fe(PPIX*)] ₂ O	μ-Oxo-bis(protoporphyrin IX Dimethyl ester) Iron(III)
[Fe(TPP)] ₂ O	μ-Oxo-bis(tetraporphinato) Iron(III)
Fe(EtioP)I	Iodo(2,7,12,17-tetraethyl-3,8,13,18-tetramethylporphyrinato) Iron(III)
Fe(EtioP)Cl	Chloro(2,7,12,17-tetraethyl-3,8,13,18-tetramethylporphyrinato) Iron(III)

LIST OF ABBREVIATIONS (Continued)

Fe(EtioP)F	Fluoro(2,7,12,17-tetraethyl-3,8,13,18-tetramethylporphyrinato) iron(III)
FTIR	Fourier Transforms Infrared Spectroscopy
g	Gram
NiOEP	Nickel(II) Octaethylporphyrin
OEP	2,3,7,8,12,13,17,18-Octaethylporphyrin
<i>ORTEP</i>	Oak Ridge Thermal Ellipsoid Plot Program
PPIX	3,8,13,17-Tetramethyl-7,12-divinylporphyrin-2,18-dipropionic acid
PPIX*	Protoporphyrin IX Dimethyl Ester
PXRD	X-ray Powder Diffraction
Pyr	Pyrrole
Tl(OEP)Cl	Chloro(2,3,7,8,12,13,17,18-Octaethylporphinato)thallium(III)
TPP	5,10,15,20-Tetraphenylporphyrin
RR	Resonance Raman Spectroscopy

CHAPTER I

INTRODUCTION

1.1 General Structural Features

The natural porphyrins are generally formed by adding substituents to beta carbon (C_b) and methine carbon (C_m) positions and are named according to the number and type of substituents (Moss, 1987). The center of gravity of the four nitrogen atoms is denoted C_t as shown in Figure 1.1. The carbon-nitrogen skeleton of the porphyrin is illustrated schematically for an idealized porphyrin core with eleven formal double bonds. The Roman numeral after the name indicates the pattern of substitution and the compounds formed by adding substituents to the nucleus of porphine (Figure 1.2). Ring current of the porphyrin macrocycle is an 18 π -electron porphyrin and can be altered when electrons are removed from or added to the porphyrin π -system by oxidation or reduction of the macrocycle. A porphyrin dianion is a nearly 20 π -electron system which should be anti-aromatic according to the Huckle $4n+2$ aromaticity rule and give paratropic shifts while in a 22 π -electron porphyrin tetraanion aromatic should give diatropic shifts (Medforth, 2000).

The free-base porphyrin possesses idealized D_{2h} symmetry with the two protons occupying the center of the porphyrin core. The removal of the two amine protons to form a dianion raises the symmetry to D_{4h} . Metallation of the dianionic porphyrin

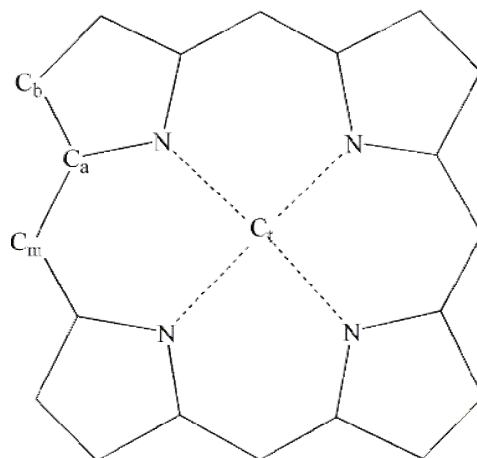


Figure 1.1 Projection view of porphyrin core.

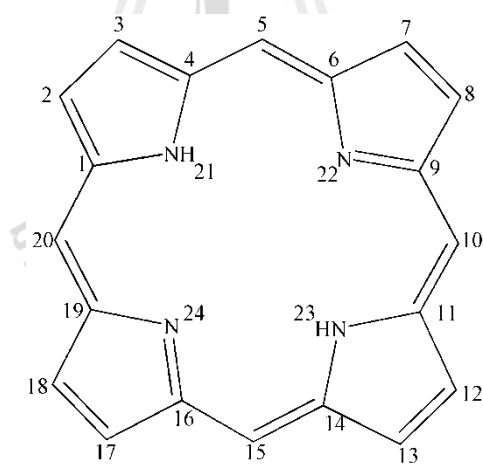


Figure 1.2 Porphyrin core diagram with ring substituent positions numbered.

macromolecule retains the D_{4h} symmetry (Suslick and Watson, 1992; Larsen and Mikšovská, 2007).

Removal of the two nitrogen bound protons of a porphine gives a delocalized planar dianion with four lone pairs directed towards Ct. The metalloporphyrins form a set of compounds in which the metal may be four-coordinate with a square-planar geometry, five-coordinate with square-pyramidal geometry, six-coordinate with distorted octahedral geometry. An eight-coordinate to form a sandwich also known as a square antiprismatic geometry. Coordination of a metal ion thus tends towards a planar metalloporphyrin system with or without axial ligands above and below the plane (Fleischer, 1970).

1.2 Porphyrin Core Conformations

The conformational distortion in nonplanar porphyrin core can be described by five different main distortion modes (Figure 1.3). Two parameters can be used to describe the distortion from the planarity. One is the difference between the displacement of the metal ion from the mean plane (the P_n plane) and the average displacement out of the mean plane of the 24 atom porphyrin core. For the planar macrocycle this difference should be zero or very small for nonplanar macrocycle with approximately D_{2d} , S_4 , or C_{2v} symmetry (Cullen, Meyer, and Smith, 1977).

Ruffled allows the core to contract; the ruffled uses two parameters leading to distinct ruffling modes pyrrole twisting ($C_\alpha N-NC_\alpha$) and pyrrole tilting (N-Ni-N) angles (Shelnutt, Medforth, Berber, Barkigia, and Smith, 1991) and the alternating displacement of the C_m positions above and below the mean plane (Senge, 2000), the

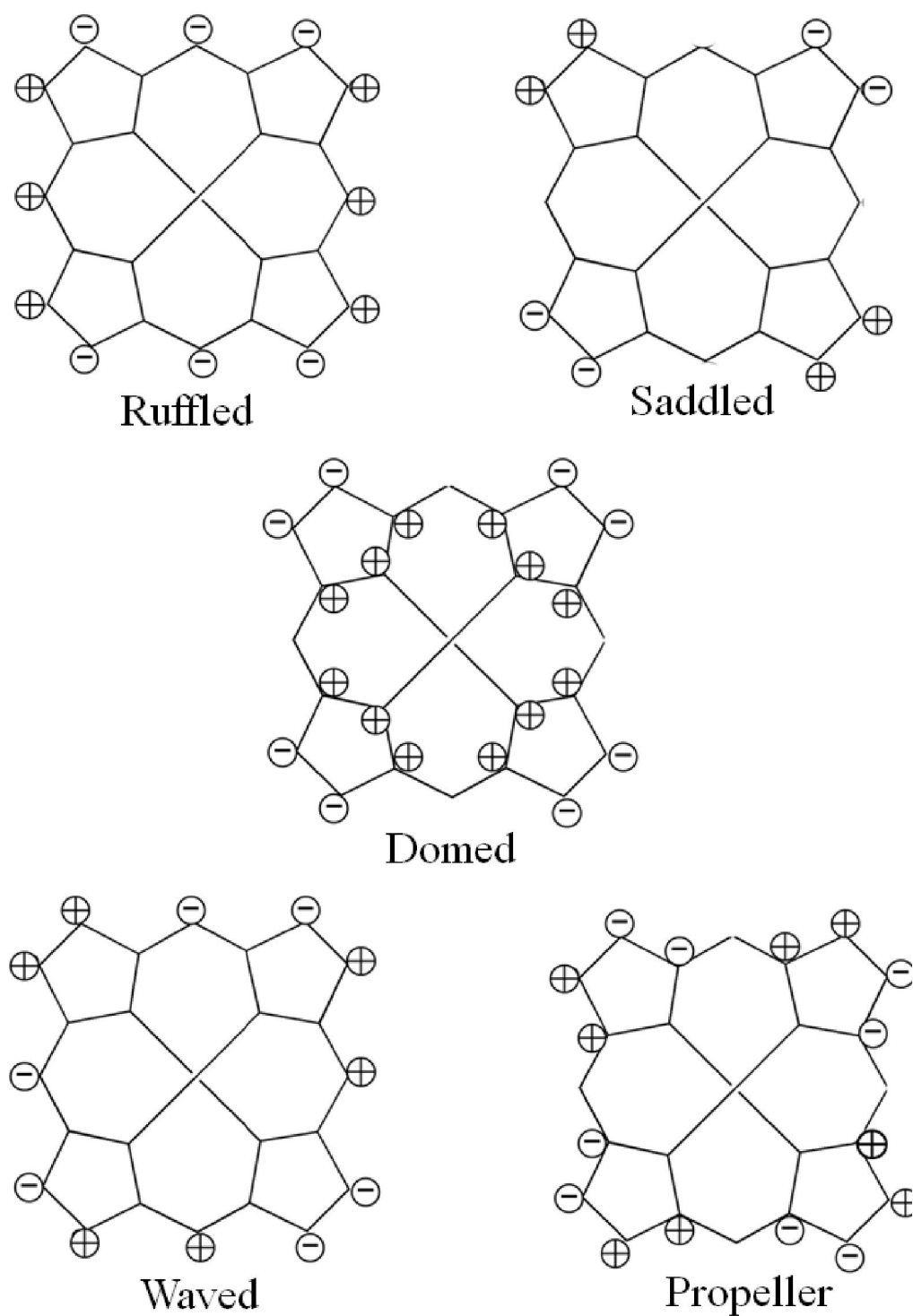


Figure 1.3 Schematic diagram showing normal-coordinate deformations used to describe planar distortions of the porphyrin core.

best example is nickel(II) octaethylporphyrin, NiOEP (Cullen, Meyer, and Smith, 1977). The saddled conformation is involved the two opposite pyrrole rings are above and below the mean plane while the C_m positions remain or less in plane. A good example of the saddled porphyrin cores are the crystal structure of metal octaethyltetraphenylporphyrins (Jentzen, Simpson, Hobbs, Song, Ema, Nelson, Medforth, Smith, Veyrat, Mazzanti, Ramasseul, Marchon, Takeuchi, Goddard, and Shelnut, 1995) and iron(III) chloro(2,3,7,8,12,13,17,18-octaethylporphyrinato)iron(III), Fe(OEP)Cl (Senge, 2005). The domed mode has an axial ligand cause the metal ion displacement out-of-plane which is found in the large central metal ion. The waved conformations are found in molecular mechanics calculations as the lowest energy structures. Two forms wave x and wave y are 90° rotated about the normal to the porphyrin plane (Senge, 2000).

Several factors can influence the porphyrin core conformation including central metal ion (Sparks, Medforth, Park, Chamberlain, Ondrias, Senge, Smith, and Shelnut, 1993), axial ligands (Ohgo, Neya, Ikeue, Takashi, Takeda, Funasaki, and Nakamura, 2002) peripheral substituents (Jentzen, Simpson, Hobbs, Song, Ema, Nelson, Medforth, Smith, Veyrat, Mazzanti, Ramasseul, Marchon, Takeuchi, Goddard, and Shelnut, 1995), or the environment (Anderson, Hobbs, Luo, Stanley, Quirke, and Shelnut, 1993).

Cullen and co-workers (1974) have studied triclinic and tetragonal forms of NiOEP which several differences in the structures. The most differences in the structures were found in Ni–N bond distance in two crystalline forms. The Ni–N bond distances for the triclinic form are 1.959(2) and 1.957(2) Å, and are significantly longer than the Ni–N bond distances in tetragonal form, which a 1.929(3) Å. The angle

between plane of adjacent pyrrole rings in tetragonal is 3.8° while the angle between planes of the adjacent pyrrole rings of the triclinic form is 2.1° which is most planar of the porphyrin cores having the angle between adjacent pyrrole rings in the range of $3-5^\circ$.

Moreover, the tetragonal NiOEP is markedly nonplanar and showed severe S_4 ruffling of the porphyrin core but the triclinic form is approximately planar. The four opposite ethyl groups are pointed up/down relative to the porphyrin ring in the triclinic form while the four ethyl groups on the opposite pyrrole rings are up and down from the porphyrin ring in the tetragonal form. They conclude that the planarity of the porphyrin cores is effectively planar with an angle between the planes of adjacent pyrrole rings of 2.1° which is found in the triclinic form.

In addition, Cullen and co-workers (1977) have been studied the effect of large metal ions like Tl(III) on the geometry of the porphyrin core and on its chemical reactivity. The complex of chloro(2,3,7,8,12,13,17,18-Octaethylporphinato)thallium(III), Tl(OEP)Cl is a five-coordinate square-pyramidal metalloporphyrin with a chlorine atom as an axial ligand. The thallium atom is displaced of the mean plane by 0.44 \AA , the Tl–N bond distance is 2.449 \AA , the thallium atom is significantly out-of-plane with a doming mode, C_{4v} distortion from planarity toward the metal ion. The crystal packing utilities the chlorine atom to form a weak dimers with centrosymmetrically related molecules. The pattern of all eight CH_3 group is pointing down below the porphyrin ring.

Hoard (1970) postulated that the overlong Fe–N bond with high-spin iron(III) ion in a porphyrin constrained it to lie out-of-plane. The observations of large out-of-plane displacement of the high-spin iron(III) in methoxy iron(III) mesoporphyrin IX dimethyl

ester (MeOFeMeso) and chlorohemin result from Ct–N radius of 2.01-2.02 Å is very small relative to the bonds and minimizes skeleton strain. Hoard (1973) suggested that the planar form of the porphyrin cores would be favored in an unconstrained environment.

The central metal ion can be modulated the planarity of the porphyrin cores was investigated by Sparks and co-workers (1993). The effect of the central metal ion such as Ni(II), Cu(II), Zn(II), Co(II), and Fe(III) on the 2,3,7,8,12,13,17,18-octaethyl-5,10,15,20-tetraphenylporphyrin (OETP) was determined by using molecular mechanics force field derived from structural and vibrational data. The results indicated that the large metal central ions were less effect on the porphyrin core planarity as the large metal ion size OEP and OETP can expanded the C_m bridge by increasing C_α – C_m bond distance and C_α – C_m – C_α bond angle. Moreover, the tip over of the coordinating nitrogen away from the metal central ion would increase the M–N bond distance while decrease the C_α –N and C_α –N– C_α bond angle.

Ohgo and coworkers (2002) have studied the molecular structures of five-coordinated halide ligated iron(III) porphyrin, porphyrincene, and corphycene complexes. The structural and spectroscopic results indicated that the spin state of the complex related to the Fe–N bond distance, core geometry, cavity areas, and iron displacement value. The 2,7,12,17-tetraethyl-3,8,13,18-tetramethylporphyrin iron(III) , Fe(EtioP) shows the iron(III) ion displacement out-of-plane decreased when changing axial ligands from F^- to I^- . The porphyrin core of the Fe(EtioP)F, Fe(EtioP)Cl, and Fe(EtioP)Br complex are rather planar with the iron ion displacement out-of-plane are 0.409(1), 0.444(2), and 0.440(3) Å, respectively. These results suggested that the degree of distortion depend on the halide axial ligands.

The influence of the peripheral substituted on the planarity of the porphyrin cores has been extensively studied by molecular mechanics calculation. Jentzen and co-workers (1995) investigated the series of *meso*-tetrasubstituted porphyrins which vary size of substituents; methyl, ethyl, propyl, etc, to increase steric crowding at the periphery. The result indicated that the tetrasubstituted porphyrin at the *meso* carbons generally exhibit the ruffled porphyrin core conformation due to a small movement out-of-plane of the *meso* substituted is sufficient to minimized steric interaction between the substituted atom bonded to the *meso* carbon and the pyrrole ring.

1.3 Iron Porphyrins

Metalloporphyrins perform numerous important functions in living systems. Porphyrin rings tend to be planar (Shelnutt, Song, Ma, Jia, Jentzen, and Medforth, 1998), but flexible, and able to adapt their conformation to different axial ligation and peripheral substitution (Hoard, 1973). They have been described as the pigments of life (Battersby and Macdonald, 1979). Metalloporphyrin complexes have been synthesized to serve as models to understand the functions (Ogoshi, Kuroda, Mizutani, and Hayashi, 1996) and structure (Scheidt, 2000) of the active site for oxygen transport and storage heme proteins (hemoglobin/myoglobin), the incorporation of molecular oxygen into organic substrates (P_{450} model systems) involved in terminal oxidation (copper oxidase and *b*- and *c*-type cytochromes), the metabolism of H_2O_2 (catalase, peroxidase), various electron transfer reactions in cytochromes (Senge, 2006), and vitamin B_{12} (Ogoshi, Kuroda, Mizutani, and Hayashi, 1996). In photosynthesis heme may function as a reaction center pigment (charge transfer) or as an antenna pigment (exciton transfer) in light-harvesting complexes, such as chlorophyll a (Senge, 2006). In many cases, these

hemoproteins function by forming complexes via coordination of various ligands at the metal center followed by oxidation/reduction reactions (Kurtikyan and Ford, 2008). Currently varieties of microbe pigments are used as virulence factors to enhance treatment of certain difficult infectious disease conditions (Liu and Nizet, 2009). The contribution of metalloporphyrins as models are mainly studied on the basis of different synthetic metalloporphyrin model complexes. Iron(III) porphyrins five-coordinate high-spin are used as model systems for study of hemes and byproducts of parasites from various diseases such as malaria pigments from *Plasmodium falciparum* (Egan, 2003) and black pigment a byproduct of *Porphyromonas gingivalis* (Smalley, Silver, Marsh, and Birss, 1998).

Protoporphyrin IX (PPIX) is one of the most abundant naturally occurring porphyrins as shown in Figure 1.4. Historically, octaethylporphyrin (OEP) has been suggested to be a close analog to natural porphyrins because the eight ethyl groups substituted at the β -positions on the porphyrin ring (Figure 1.5) are similar to the natural substituents PPIX while tetraphenylporphyrin (TPP) has been popular due to ease of synthesis and purification, and low cost (Figure 1.6). Iron porphyrin, which is the heme in hemoglobin, generally exhibits d^6 iron(II) ion in high-spin or low-spin states and d^5 iron(III) ion in the high-spin state (Hoard, 1971). The spin state and stereochemistry of the iron ion in hemes is controlled by the number and the nature of the axial ligands (Scheidt, Geiger, and Haller, 1982). Iron(III) ions with five d electrons can exhibit three possible spin states, low-spin $S = 1/2$ spin state, intermediate-spin $S = 3/2$ spin state, and high-spin $S = 5/2$ spin state. Strong field ligands generally favor six-coordinate iron(III) hemes (Hoard, 1973), while weak field ligands favor the five-coordinate high-spin hemes.

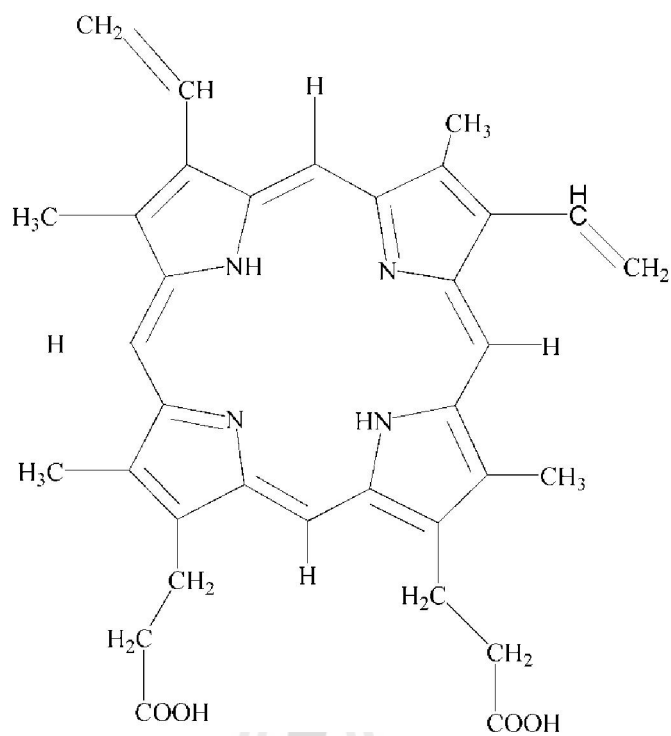


Figure 1.4 Basic structure of protoporphyrin IX.

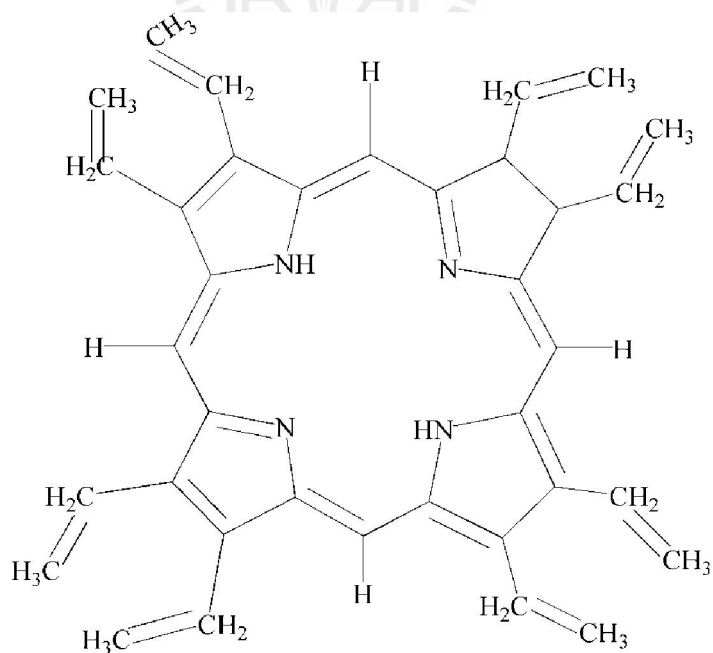


Figure 1.5 Basic structure of octaethylporphyrin.

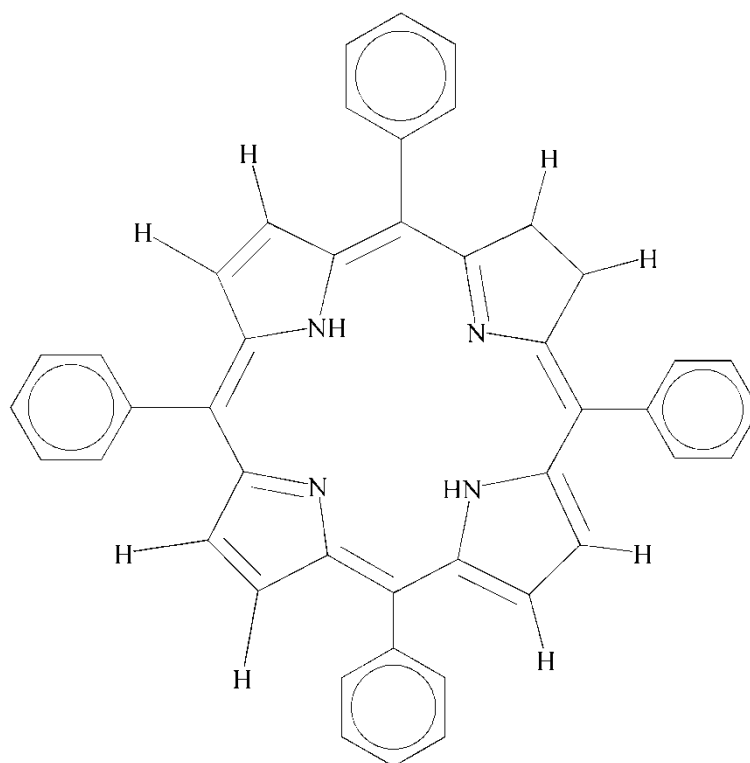


Figure 1.6 Basic structure of tetraphenylporphyrin.

Table 1.1 illustrates the variability of the equatorial and axial Fe-N bond distances as a function of the spin state as seen from the structures determined from three independent polymorphic crystal forms of the six-coordinate iron(III) complex, $[\text{Fe}(\text{OEP})(3\text{-Clpy})_2]\text{ClO}_4$. The complex exhibits an $S = 5/2$, $S = 1/2$ thermal spin equilibrium with 55% high-spin in solution and in the first-studied (triclinic) crystalline phase at room temperature (Scheidt, Geiger, and Haller, 1982). At 98 K the molecule exhibits the low-spin form with an average equatorial Fe-N distance of 1.994(6) Å and an axial ligand Fe-N distance of 2.031(2) Å. At 293 K the thermal spin mixture leads to an average structure with an equatorial Fe-N distance of 2.014 Å and an axial Fe-N distance of 2.194 Å (Scheidt, Geiger, and Haller, 1982). Crystallographic resolution of the low- and high-spin states at 293 K showed axial Fe-N lengths of 2.043 Å and 2.316

Å for the low-spin and high-spin forms, respectively. Determination of a second polymorph (monoclinic) gave an example of a stereochemically controlled spin state. Steric hindrance due to the crystal packing precluded an axial low-spin distance and resulted in a quantum-admixed intermediate-spin state in the monoclinic polymorph of [Fe(OEP)(3-ClPy)₂][ClO₄] (Scheidt, Geiger, Hayes, and Lang, 1983).

Table 1.1 Comparison of Iron(III) Nitrogen Distances, Axial Ligand Distances and Spin State in Six-coordinate [Fe(OEP)(3-Clpy)₂]⁺ Perchlorate.^a

Spin state	Spin	Temp. (K)	d[Fe–N _p] (Å)	d[Fe–N _{ax}] (Å)	Space Group
Low-spin	S = 1/2	98	1.994(6)	2.031(2) ^b	Triclinic
		293	(1.990) ^c	2.043 ^b	Triclinic
Intermediate-spin	S = 3/2 ^e	293	2.005(6)	2.310(17) ^d	Monoclinic
		292	2.006(8)	2.304 ^f	Orthorhombic
High-spin	S = 5/2	293	(2.045) ^c	2.316 ^b	Triclinic
Spin equilibrium	S = 1/2, 5/2	293	2.014(4)	2.194(2) ^b	Triclinic

^a Three crystalline polymorphs of this structure ^d Scheidt, Geiger, Hayes, and Lang, 1983.

have been structurally characterized.

^e Quantum-admixed intermediate-spin state.

^b Scheidt, Geiger, and Haller, 1982.

^f Scheidt, Geiger, Lee, Reed, and Lang, 1987.

^c Average Fe–N_p values from Scheidt and Reed, 1981.

The smaller equatorial size of the intermediate- and low-spin state heme complexes allows the iron(III) atom with relatively short Fe–N bond lengths, 1.990–2.005 Å (Table 1.1). The low-spin complex also has a short, 2.031 Å, axial Fe–N distance. On going from low spin to intermediate spin one electron enters the d_z^2 orbital. Thus, the equatorial distances remain short, but the axial Fe–N bonds lengthen to 2.310 Å. Further, addition of the unpaired electron to the $d_{x^2-y^2}$ orbital in going to high-spin iron induces a concomitant elongation of the equatorial Fe–N bonds (Scheidt, Geiger and Haller, 1982). At the same time, the iron(III) ions in high-spin hemes are substantially displaced out of the plane of the four nitrogen atoms and of the porphyrin plane (about 0.4–0.5 Å) due to the larger ionic radius of high-spin iron(III) (Scheidt and Reed, 1981). These phenomena, along with other effects due to the metal ion environment, aid in understanding how the protein influences the electronic structure of its prosthetic group.

A third polymorph has also been prepared and exhibits a similar intermediate-spin state with similar equatorial and axial Fe–N distances (Scheidt, Geiger, Lee, Reed, and Lang, 1987).

1.4 Malaria Pigment and Heme Derivatives

Hemes can be further subdivided into three different forms as heme *a*, heme *b*, and heme *c* depending on changes in the vinyl groups. Iron protoporphyrin IX Fe^{n+} (PPIX), heme *b* is found in hemoglobin and myoglobin, while heme *a* and heme *c* are found in cytochromes.

Malaria is a tropical disease and a cause of mortality and morbidity in tropical regions. The four principal strains infecting humans are *Plasmodium falciparum*, *Plasmodium vivax*, *Plasmodium malariae*, and *Plasmodium ovale*. The most virulent species is *Plasmodium falciparum*, and its life cycle is complicated with many different forms of offspring (Egan, Mavuso, and Ncokazi, 2001; Egan, 2003). The life cycles of parasites have three major stages, consisting of the mosquito, liver, and blood stages. Following the bite of an infected mosquito, *Plasmodium falciparum* invades human liver cells, emerging into the bloodstream after about one week and invading the red blood cells of the host. Only the blood stage is pathogenic and curative drugs must act at this stage. During the blood stage, the malaria parasites live in red blood cells of humans and use hemoglobin as their primary food source for development and cell division.

The degradation of host hemoglobin occurs inside the parasite's food vacuole under acid conditions with pH 4.5-5.5. Cleavage of hemoglobin by an enzyme releases a high concentration of free heme or ferric iron protoporphyrin IX, Fe^{3+} (PPIX) as a byproduct inside the malaria parasite's food vacuole. The free heme is toxic to the parasite, but is converted into a highly insoluble nontoxic form under physiological conditions (Slater, Swiggard, Orton, Flitter, Golberg, Cerami, and Henderson, 1991; Trivedi, Chand, Maulik, and Bandyopadhyay, 2005) called hemozoin or malaria pigment (Choi, Cerda, Chu, Babcock, and Maretta, 1999; Egan, Mavuso, and Ncokazi, 2001). Malaria pigment is an inert dark microcrystalline material and its black color reveals the chromophoric nature of heme (Bohle, Debrunner, Jordan, Madsen, and Schulze, 1998).

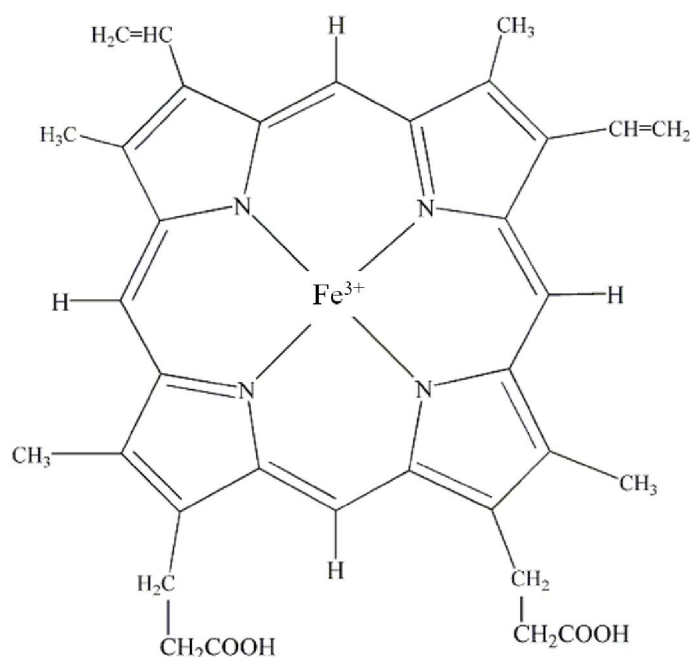
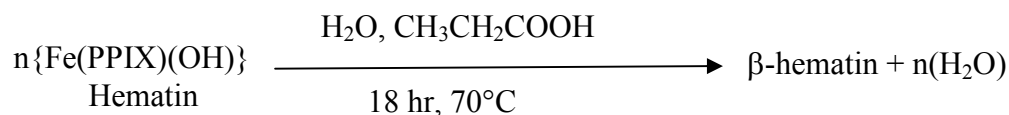


Figure 1.7 Iron(III) protoporphyrin IX.

1.5 Structural Spectroscopy of Malaria Pigment Model Systems

Brown (1911) used spectroscopy to study the chemical nature of malaria pigment and hematin based on the parallelism of their solubility, and reported the first spectroscopic characterization of hemozoin. His examination of malaria pigment showed its spectra to be identical to hematin. The structure of malaria pigment from *Plasmodium falciparum* culture and β -hematin prepared by chemical synthesis under acidic conditions have subsequently been characterized by infrared spectroscopy and X-ray absorption spectroscopy. The infrared and X-ray absorption spectroscopy pattern indicated that a polymeric structure with the molecule linked between the central iron(III) ion of one heme and a carboxylate side-group oxygen of another heme (Slater, Swiggard, Orton, Flitter, Goldberg, Cerami, and Henderson, 1991). Bohle and Helms

(1993) synthesized β -hematin by dehydrohalogenation, with a noncoordinating base solvent in anhydrous conditions as shown below.



The dark black solid is obtained and characterized by FT-IR. The spectroscopic results were identical to β -hematin and supporting hypothesis which the carboxylic acid are involved in an organized regular hydrogen bonded network. The polymerization of hematin to β -hematin in acidic conditions was found to occur spontaneously and showed the carboxylate ligation peaks (Egan, Ross, and Adams, 1994). Synchrotron X-ray powder diffraction patterns of malaria pigment from the malarial *Plasmodium falciparum* and β -hematin prepared from hemin by treating with bases in anhydrous conditions are identical. Several researchers obtained similar results leading to the conclusion that malaria pigment is a coordination polymer of iron(III)(protoporphyrin IX) with hydrogen-bonded propionic dimerization between chains as shown in Figure 1.8 (Bohle, Dinnebier, Madsen, and Stephens 1997).

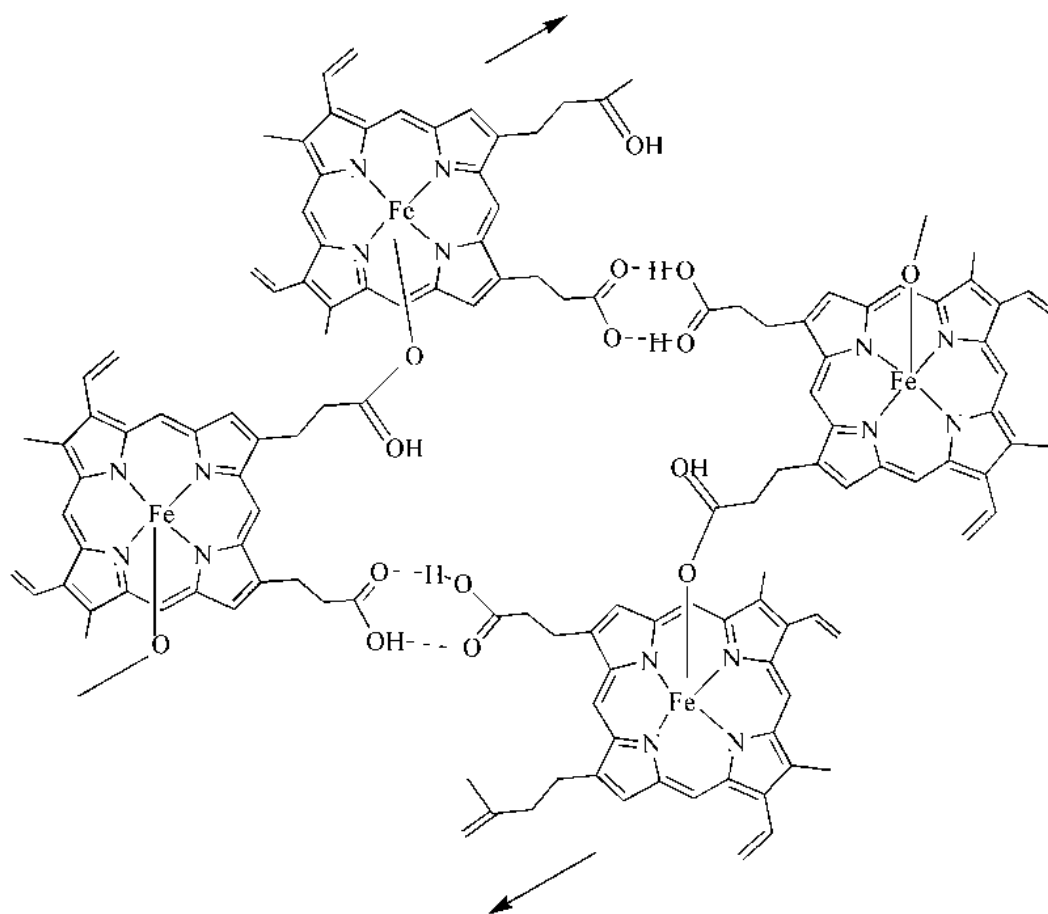


Figure 1.8 A diagram of malaria pigment.

Simulated annealing techniques were used to analyze data of β -hematin obtained from synchrotron powder X-ray diffraction. The Rietveld refinement method shows the molecular structure to be linked through reciprocal iron-carboxylate bonds using one propionate side chain from each porphyrin. The remaining propionic acid side chains from hydrogen bonds link the dimers into a larger supramolecular framework (Pagola, Stephens, Bohle, Kosar, and Madsen, 2000). In 2010, malaria pigment prepared from a culture of *Plasmodium falciparum* was analyzed by the maximum entropy-based pattern

fitting approach (MPF) which combined the Rietveld refinement and maximum entropy method has been reported in 2010 (Klonis, Dilanian, Hanssen, Darmanin, Streltsov, Deed, Quiney, and Tilley, 2010). The structure was solved by the fractional coordinates of iron, using rigid body constrain for all atoms and finally refined using strong nonlinear restraints. The malaria pigment structure was similar β -hematin (Pagola, Stephens, Bohle, Kosar, and Madsen, 2000). The unit cell consisted of two iron(III) porphyrins units stack parallel with the linkage between iron-propionate linkage. The Fe–O is more distorted and leads to greater disordered in the crystal packing of malaria pigment than β -hematin (Klonis, Dilanian, Hanssen, Darmanin, Streltsov, Deed, Quiney, and Tilley, 2010).

The electronic structure of β -hematin can be studied by Raman and resonance Raman (RR) spectroscopy, which have been used to provide structural information corresponding to various electronic properties (excited states, stereochemistry/spin state, oxidation state, structural, bonding arrangements, etc.), and their response to change in the environment of the π -system of the porphyrin skeleton, such as changing of metal center, peripheral substituents, and axial ligands on the metal center, all of which can reduce the symmetry of the porphyrin from ideal D_{4h} of a planar heme group (Gaughan, Shriver, and Boucher, 1975; Shelnutt, 1981; DeVito and Asher, 1989; Unger, Bobinger, Dreybrodt, and Schweitzer-Stenner, 1993; Bhuiyan, Seth, Yoshida, Osuka, and Bocian, 2000; Wood and McNaughton, 2002).

Raman excitation spectra provide the Soret band which is called Type-A and Type-B. The A-term (B band, Soret) is characterized by totally symmetric modes, A_{1g} (A_{1g} modes in the D_{4h} point group but A_1 modes in the C_{4v} point group) which are principally Frank-Condon overlap. The B-term involves transitions of the π system of

the degenerate components of E_u symmetry and the Jahn-Teller active modes (B_{1g} and B_{2g}) giving a rich variety of vibronic mixing of excited states (Spiro, 1974; Spiro and Streckas, 1974). Although, the intensity of the B_{1g} and A_{2g} modes are low but they facilitate intrastate vibronic coupling enhancement (Shelnutt, 1981). The vibration of these symmetries and the coupling of vibrational levels in electronic state provide the enhancement and are considered for interpretations of Raman excitation spectra (Gaughan, Shriver, and Boucher, 1975; Shelnutt, 1981). The enhancement mechanism of vibrational modes can be explained in terms of an increased size effect and near-resonance, polarizability. The excitonic coupling will essentially split the electronic states into a broad band of states with different geometries, energies, and oscillator strengths (Wood, Langford, Cooke, Lim, Glenister, Duriska, Unthank, and McNaughton, 2004).

Spin- and oxidation- states of malaria pigment and β -hematin have been studied by a variety of spectroscopic techniques (Adams, Berman, Egan, Marsh, and Silver, 1996; Adams, Egan, Ross, Silver, and Marsh, 1996) including Raman and RR spectroscopy. The electron paramagnetic resonance (EPR) spectra of malaria pigment and β -hematin both have a distinct rhombic pattern with $g = 5.79$ and 3.80 (Slater, Swiggard, Orton, Flitter, Golberg, Cerami, and Henderson, 1991) showing correspondence to high-spin, monomeric iron(III) protoporphyrin IX acetate (Bohle, Debrunner, Jordan, Madsen, and Schulze, 1998). Mössbauer spectroscopy of malaria pigment and β -hematin was observed at 78°K . The isomer shifts of 0.20 ± 0.03 , 0.24 ± 0.01 , and 0.039 ± 0.01 (Adams, Berman, Egan, Marsh, and Silver, 1996; Adams, Egan, Ross, Silver, and Marsh, 1996) are characteristic of high-spin iron(III). A combination

Mössbauer and EPR study on β -hematin at 4.2 K exhibited the characteristics of a high-spin, $S = 5/2$ environment (Bohle, Debrunner, Jordan, Madsen, and Schulze, 1998).

Raman and RR spectroscopy have been used to characterize the chemical nature and structural properties for malaria pigment and β -hematin (Wood, Langford, Cooke, Lim, Glenister, Duriska, Unthank, and McNaughton, 2004; Webster, McNaughton, and Wood, 2009), and a correlation has been found between RR enhancement of the totally symmetric modes and the number of supramolecular interactions (Puntharod, Webster, Asghari-Khiavi, Bambery, Safinejad, Rivadehi, Langford, Haller, and Wood, 2010). Enhancement of A_{1g} modes (1570, 1371, 795, 677, and 344 cm^{-1}), ring breathing modes (850-650 cm^{-1}), and out-of-plane modes including iron-ligand modes (400-200 cm^{-1}) has been observed in the RR spectra of β -hematin and hemin. Raman excitation was observed in the near-IR region, including 780 and 830 nm. Strong enhancement occurs for β -hematin at 867 nm which can be explained by the aggregation of hemes and allowing charge transfer along the z-axis, z-polarized transition $a_{2u}(\pi) \rightarrow d_z^2$ in C_{4v} symmetry (Wood, Langford, Cooke, Lim, Glenister, Duriska, Unthank, and McNaughton, 2004). Although, the strong enhancement was much greater in β -hematin compared to monomeric hemin, these results suggested that the enhancement is the result of excitonic coupling through the formation of covalent bonds of porphyrins. In addition, the strong enhancement of malaria pigment and heme derivatives may result from the planarity and symmetry of the porphyrin plane when observed by RR spectroscopy.

RR results showed that supramolecular interactions of malaria pigment occur via π - π interactions in dimers but the enhancement of totally symmetric (A_{1g}) modes in the monomer may occur through electron delocalization inside the super-ring (Wood,

Langford, Cooke, Lim, Glenister, Duriska, Unthank, and McNaughton, 2004; Webster, Tilley, Deed, McNaughton, and Wood, 2008; Webster, McNaughton, and Wood, 2009) which is similar to the result for the charge-transfer in the heme derivative (Asher, Vickery, Schuster, and Sauer, 1977).

Unfortunately, both malaria pigment and β -hematin crystals are not suitable for characterization by single crystal X-ray crystallography. The model used to describe malaria pigment is β -hematin prepared in acid and base reaction conditions using hemin as starting material. Both crystalline forms have the same space group and unit cell (Pagola, Bohle, Kosar, and Madsen, 2000) and the structures, determined by X-ray powder diffraction, show the molecules to be heme dimers containing the same iron-carboxylate and propionic acid links as reported before (Bohle, Kosar, and Stephens, 2002). A second model used to explain malaria pigment and β -hematin is Fe(OEP)picrate which, in terms of the RR enhancement of the totally symmetric modes, is the best model to explain β -hematin. These malaria pigment model systems contain a five-coordinate high-spin iron(III) ion coordinated to an oxygen atom from the axial ligand. Intramolecular interactions were found between the oxygen of the NO₂ group of the axial ligand with the porphyrin ring (Puntharod, 2008). A new model for hemozoin and β -hematin is [Fe(OEP)]picrate which showed strong enhancement at 1375 cm⁻¹ which is known as the oxidation state marker band of iron(III) high-spin (Puntharod, 2008).

1.6 Supramolecular Interactions

Supramolecular interactions or noncovalent interactions (ligand-to-metal bonding, hydrogen bonding (H-bond), ionic bonding, van der Waals interactions, and

hydrophobic interactions) play a special role in supramolecular chemistry where supramolecular interactions are known to act at distances of several angstroms (Å) (Muller-Dethlefs and Hobza, 2000). These types of interactions π - π interactions (Hunter and Sanders, 1990), C-H \cdots O (Steiner and Desiraju, 1998), C-H \cdots N (Mascal, 1998; Cotton, Daniels, Jordan, and Murillo, 1997), C-H \cdots Cl, as well as electrostatic interactions, hydrophobic interactions, charge-transfer interactions, and metal coordination bond (Muller-Dethlefs and Hobza, 2000) are found through structural chemistry and biological systems.

Weak hydrogen bonds are believed to play an important role in heme protein function and the intermolecular hydrogen bonding provides additional attractive forces between molecules. Thus, properties and function of heme proteins may be affected by such intramolecular forces and intermolecular interactions (Hu, Noll, Schulz, and Scheidt, 2008). Dimers, oligomers, dendrimers, or polymers due to elaborate dipole-dipole, π -systems, π - π interactions (Hunter and Sanders, 1990), C-H \cdots π interactions (Muller-Dethlefs and Hobza, 2000), hydrogen bonds, and van der Waals interactions (Steiner and Desiraju, 1998) are a normal part of metalloporphyrin chemistry.

The distances and number of hydrogen bonds in monomeric Fe(TPP)Cl and Fe(OEP)Cl, and dimeric [Fe(TPP)]₂O, [Fe(OEP)]₂O, and β -hematin (Puntharod, Webster, Asghari-Khiavi, Bambery, Safinejad, Rivadehi, Langford, Haller, and Wood, 2010). The number of supramolecular interactions was found to correlate with the enhancement of the totally symmetric mode ν_4 of the RR spectra. The enhancement for [Fe(OEP)]₂O was very weak and there are few intermolecular contacts connecting the molecules in the lattice (Puntharod, Webster, Asghari-Khiavi, Bambery, Safinejad,

Rivadehi, Langford, Haller, and Wood, 2010). The extended supramolecular structure study in the malaria pigment model systems was performed with near-IR resonance enhancement at 413 and 514 nm wavelengths in solid and solution phases. The wavelength dependent enhancement of A_{1g} modes increased with increasing concentrations of hemin or hematin in solution, providing insight into the nature of aggregated enhanced Raman scattering (AERS) and suggesting that the excitonic coupling occurs through supramolecular interactions, probably by the formation of π - π interactions of Fe(PPIX) in solution (Webster, Tilley, Deed, McNaughton, and Wood 2008; Webster, McNaughton, and Wood, 2009).

To date, the best model of hemozoin in terms of resonance Raman enhancement is Fe(OEP)picrate, which shows strongest enhancement of the totally symmetry mode than other known model compounds, second only to that of malaria pigment itself (Puntharod, 2008). The frequency and intensity of Raman scattering essentially depends on the nature and conformation heme complexes, properties of solvents, pH, temperature (Stavrov, 1993; Unger, Bobinger, Dreybrodt, and Schweitzer-Stenner, 1993) and excitation wavelength (Webster, McNaughton, and Wood, 2009). However, these depend on the model used to describe hemozoin, β -hematin, and other model for study of the enhancement of the A_{1g} mode (Wood, Langford, Cooke, Lim, Glenister, Duriska, Unthank, and McNaughton, 2004).

The total energy is a result of the increase in Van der Waals interactions of the substituents at the periphery of the porphyrin. The mixture of increase in torsion, angle, and bond strain energies that results from the adjacent of the structure to the mounting Van der Waals repulsion as the size of the C_b substituents increase (Shelnutt, Medforth,

Berber, Barkigia, and Smith, 1991). The majority of the increase in energy among the structures shows up in the Van der Waals energy and the torsional angles. The torsion force constants primarily act to maintain the planarity of the porphyrin core, and, hence are most affected by nonplanar distortions. Distortion from planarity is caused by steric congestion at the periphery of the porphyrin (Shelnutt, Medforth, Berber, Barkigia, and Smith, 1991).

The important factors and interactions for stereochemistry in malaria pigment model system are the spin state, oxidation state and coordination number of iron, intermolecular distances and angles. The nature of the axial ligand ligation through the oxygen with the plane of porphyrin ring leads to changes in the geometry, symmetry and planarity of the porphyrin plane, which may also be important.

In this research syntheses of potential new model compounds of malaria pigment was attempted to investigate the flattening of the porphyrin core and supramolecular structure for comparison with malaria pigment and the existing malaria pigment model systems described above in an effort to understand the malaria pigment structure and what contributes to the enhancement of totally symmetric mode (A_{1g}) in Raman/RR.

Studies of heme model systems shows that many factors, including noncovalent interactions can play an important role in the properties of these metalloporphyrins. The purpose of this work is to observe the effect of supramolecular interactions in malaria pigment model compounds and other heme derivatives to gain more insight into the structure of malaria pigment.

1.7 References

- Adams, P. A., Berman, P. A. M., Egan, T. J., Marsh, P. J., and Silver, J. (1996). The iron environment in heme and heme-antimalarial complexes of pharmacological interest. **Journal of Inorganic Biochemistry**. 63: 69-77.
- Adams, P. A., Egan, T. J., Ross, D. C., Silver, J., and Marsh, P. J. (1996). The chemical mechanism of β -haematin formation studied by Mossbauer spectroscopy. **Biochemistry Journal**. 318: 25-27.
- Anderson, K. K., Hobbs, J. D., Luo, L., Stanley, K. D., Martin, J. M., Quirke, E., and Shelnut. (1991). Planar-nonplanar conformational equilibrium in metal derivatives of octaethylporphyrin and *meso*-nitrooctaethylporphyrin. **Journal of the American Chemical Society**. 115: 12346-12352.
- Asher, S. A., Vickery, L. E., Schuster, T. M., and Sauer, K. (1977). Resonance Raman spectra of methemoglobin derivatives. Selective of enhancement of axial ligand vibrations and lack of effect of inositol hexaphosphate. **Biochemistry**. 16: 5849-5856.
- Battersby, A. R. and McDonald, E. (1979). Origin of the pigments of life: The type-III problem in porphyrin biosynthesis. **Accounts of Chemical Research**. 12: 14-22.
- Bhuiyan, A. A., Seth, J., Yoshida, N., Osuka, A., and Bocian, D. F. (2000). Resonance Raman characterization of excitonically coupled meso, meso-linked porphyrin arrays. **The Journal of Physical Chemistry B**. 104: 10757-10764.
- Bogdanović, G. A., Medaković, V., Milčić, M. K., and Zarić, S. D. (2004). Intramolecular C–H \cdots π interactions in metal-porphyrin complexes. **International Journal of Molecular Science**. 5: 174-185.

- Bohle, D. S., Debrunner, P., Jordan, P. A., Madsen, S. K., and Schulze, C. E. (1998). Aggregated heme detoxification byproducts in malaria trophozoites: β -hematin and malaria pigment have a single $S = 5/2$ iron environment in the bulk phase as determined by EPR and Magnetic Mossbauer spectroscopy. **Journal of the American Chemical Society**. 120: 8255-8256.
- Bohle, D. S., Dinnebier, R. E., Madsen, S. K., and Stephens, P. W. (1997). Characterization of the products of the heme detoxification pathway in malaria late trophozoites by X-ray diffraction. **Journal of Biological Chemistry**. 272: 713-716.
- Bohle, D. S. and Helms, J. B. (1993). Synthesis of β -hematin by dehydrohalogenation of hemin. **Biochemica Biophysica Research Communications**. 193: 504-508.
- Choi, C. Y. H., Cerda, J. F., Chu, H.-A., Babcock, G. T., and Marletta, M. A. (1999). Spectroscopic characterization of the heme-binding sites in *Plasmodium falciparum* histidine-rich protein 2. **Biochemistry**. 38: 16916-16924.
- Choi, S., Spiro, T. P., Langry, K. C., and Smith, K. M. (1982). Vinyl influences on protoheme resonance Raman spectra: Nickel(II) protoporphyrin IX with deuterated vinyl groups. **Journal of the American Chemical Society**. 104: 4337-4344.
- Collins, D. M. and Hoard, J. L. (1970). The crystal structure and molecular stereochemistry of $\alpha,\beta,\gamma,\delta$ -tetra(4-pyridyl)porphinatomonopyridinezinc(II). An appraisal of bond strain in the porphine skeleton. **Journal of the American Chemical Society**. 92: 3761-3770.

- Cotton, F. A., Daniels, L. M., Jordan IV, T. G., and Murillo, C. A. (1997). The crystal packing of bis(2,2'-dipyridylamido)cobalt(II), $\text{Co}(\text{dpa})_2$, is stabilized by C-H \cdots N bonds: Are there any real precedents? **Chemical Communications**. 1673-1674.
- Cullen, D. L. and Meyer, E. F. (1974). Crystal and molecular structure of the triclinic form of 1,2,3,4,5,6,7,8-octaethylporphinatonicel(II). A comparison with tetragonal form. **Journal of the American Chemical Society**. 96: 2095-2102.
- Cullen, D. L., Meyer, E. F., and Smith, K. M. (1977) Porphyrins and large metal ions. Crystal and molecular structure of 2,3,7,8,12,13,17,18-octaethylporphinatochlorothallium(III). **Inorganic Chemistry**. 16: 1179-1186.
- DeVito, V. L. and Asher, S. A. (1989). UV Resonance Raman enhancement of vinyl stretching in ferric protoporphyrin IX: conjugation and preservation of the vinyl π - π^* transition. **Journal of the American Chemical Society**. 111: 9143-9152.
- Egan, T. J. (2003). Haemozoin (malaria pigment): A unique crystalline drug target. **Target**. 2: 115-124.
- Egan, T. J., Mavuso, W. W., and Ncokazi, K. (2001). The mechanism of β -hematin formation in acetate solution. Parallels between hemozoin formation and biomineralization processes. **Biochemistry**. 40: 204-213.
- Egan, T. J., Ross, D. C., and Adams, P. A. (1994). Quinoline anti-malarial drugs inhibit spontaneous formation of β -hematin (malaria pigment). **FEBS Letters**. 352: 54-57.
- Fleischer, E. B. (1970). The structure of porphyrins and metalloporphyrins. **Accounts of Chemical Research**. 3: 105-112.

- Gaughan, R. R., Shriver, D. F., and Boucher, L. J. (1975). Resonance Raman spectra of manganese(III) tetraphenylporphyrin halides. **Proceedings of the National Academy of Sciences of the United State of America**. 72: 433-436.
- Geiger, D. K., Lee, Y. J., and Scheidt, W. R. (1984). Control of spin state in (porphinato)iron(III) complexes. An axial ligand orientation effect on the spin state in bis(2-methylimidazole)(octaethylporphinato)iron(III) perchlorate. **Journal of the American Chemical Society**. 106: 6339-6343.
- Gouterman, M. (1959). Study of the effects of substitution on the absorption spectra of porphin. **Chemical Physics**. 30: 1139-1161.
- Hoard, J. L. (1973). Some aspects of metalloporphyrin stereochemistry. **Annals of the New York Academy of Sciences**. 270: 18-30.
- Hoard, J. L. (1971). Stereochemistry of hemes and other metalloporphyrins. **Science**. 174: 1295-1302.
- Hu, C., Noll, B. C., Schulz, C. E., and Scheidt, W. R. (2008). Hydrogen bonding influence of 1,10-phenanthroline on five-coordinate high-spin imidazole-ligated iron(II) porphyrinate. **Inorganic Chemistry**. 47: 8884-8895.
- Hunter, C. A. and Sanders, J. K. M. (1999). The nature of π - π interactions. **Journal of the American Chemical Society**. 112: 5525-5534.
- Jentzen, W., Simpson, M. C., Hobbs, J. D., Song, X., Ema, T., Nelson, N. Y., Medforth, C. J., Smith, K. M., Veyrat, M., Mazzanti, Ramasseul, R., Marchon, J. C., Takeuchi, T., Goddard, III, W. A., and Shelnut, J. A. (1995). Ruffling in a series of nickel(II) meso-tetrasubstituted porphyrins as a model for the conserved ruffling of the heme of cytochromes *c*. **Journal of the American Chemical Society**. 117: 11085-11097.

- Klonis, N., Dilanin, R., Hanssen, E., Darmanin, C., Streltsov, V., Deed, S., Quiney, H., and Tilley, L. (2010). Hematin-hematin self-association states involved in the formation and reactivity of malaria parasite pigment, hemozoin. **Biochemistry**. 49: 6804-6811.
- Kurtikyan, T. S. and Ford, P. C. (2008). FTIR and optical spectroscopic studies of the reactions of heme models with nitric oxide and other NO_x in porous layered solids. **Coordination Chemistry Reviews**. 252: 1486-1496.
- Larsen, R. W. and Mikšovská, J. (2007). Time resolved thermodynamics of ligand binding to heme proteins. **Coordination Chemistry Reviews**. 251: 1101-1127.
- Liu, G. Y. and Nizet, V. (2009). Color me bad: microbial pigments as virulence factors. **Trends in Microbiology**. 17: 406-413.
- Mascal, M. (1998) Statistical analysis of C–H···N hydrogen bonds in the solid state: There are real precedents. **Chemical Communications**. 303-304.
- Medforth, C. J. (2000). NMR spectroscopy of diamagnetic porphyrins. **The Porphyrin Handbook**. V. 5: 1-80.
- Moss, G. P. (1987). Nomenclature of tetrapyrroles. **Pure & Applied Chemistry**. 59: 779-832.
- Muller-Dethlefs, K. and Hobza, P. (2000). Noncovalent interactions: A challenge for experiment and theory. **Chemical Reviews**. 100: 143-167.
- Ohgo, Y., Neya, S., Ikeue, T., Takashi, M., Takeda, M., Funasaki, N., and Nakamura, M. (2002). Molecular structures of five-coordinated halide ligated iron(III) porphyrin, porphycene, and corphycene complexes. **Inorganic Chemistry**. 41: 4627-4629.

- Ogoshi, H., Kuroda, Y., Mizutani, T., and Hayashi, T. (1996). Synthesis strategies of multifunctional porphyrins as receptors. **Pure & Applied Chemistry**. 68: 1411-1415.
- Pagola, S., Stephens, P. W., Bohle, D. S., Kasar, A. D., and Madsen, S. K. (2000). The structure of malaria pigment β -hematin. **Nature**. 404: 307-310.
- Puntharod, R. (2008). Synthesis and Structural Studies of Malaria Pigment Model systems. **Ph.D. Thesis**, Suranaree University of Technology. p.145-146.
- Puntharod, R., Webster, G. T., Asghari-Khiari, M., Bambery, K. R., Safinejad, F., Rivadehi, S., Langford, S. J., Haller, K. J., and Wood, B. R. (2010). Supramolecular interactions playing an integral role in the near-Infrared Raman "Excitonic" enhancement observed in β -hematin (malaria pigment) and other related heme derivatives. **The Journal of Physical Chemistry B**. 114: 12104-12115.
- Sayer, P. S., Gouterman, M., and Connel, C. R. (1982). Metalloid porphyrins and phthalocyanines. **Accounts of Chemical Research**. 15: 78-79.
- Scheidt, W. R. (2000). Systematics of the stereochemistry of porphyrins and metalloporphyrins. **The Porphyrin Handbook**. V. 3: p.50.
- Scheidt, W. R., Geiger, D. K., and Haller, K. J. (1982). Structural characterization of variable-spin (porphinato)iron(III) complex. Molecular stereochemistry of bis(3-chloropyridine)(octaethylporphinato)iron(III) perchlorate at 98 K ($S = 1/2$) and 293 K ($S = 1/2$, $S = 5/2$). **Journal of the American Chemical Society**. 104: 495-499.
- Scheidt, W. R., Geiger, D. K., Hayes, R. G., and Lang, G. (1983). Control of spin state in (porphinato)iron(III) complexes. An axial ligand orientation effect leading to an

- intermediate-spin complex. Molecular structure and physical characterization of the monoclinic form of bis(3-chloropyridine) (octaethylporphinato)iron(III) perchlorate. **Journal of the American Chemical Society**. 105: 2625-2632.
- Scheidt, W. R., Geiger, D. K. Lee, Y. J. Reed, C. A., and Lang, G. (1987). On the preparation of five-coordinate (3-Chloropyridine) (porphinato)iron(III) complexes. **Journal of the American Chemical Society**. 26, 1039-1045.
- Scheidt, W. R., Kirner, J. F. J., Hoard, L., and Reed, C. A. (1987). Unusual orientation of axial ligands in metalloporphyrins. Molecular structure of low-spin bis(2-methylimidazole)(mesotetraphenylporphinato)iron(III) perchlorate. **Journal of the American Chemical Society**. 109: 1963-1968.
- Scheidt, W. R. and Reed, C. A. (1981). Spin-state/stereochemical relationships in iron porphyrins: Implications for the hemoproteins. **Chemical Reviews**. 81: 543-555.
- Senge, M. O. (2000). Highly substituted porphyrins. **The Porphyrin Handbook**. V. 1: p.6-346.
- Senge, M. O. (2005). Chloro(2,3,7,8,12,13,17,18-octaethylporphyrinato)iron(III). **Acta Crystallographica Section E**, 61: m399-m400.
- Senge, M. O. (2006). Exercises in molecular gymnastics-bending, stretching and twisting porphyrins. **Chemical Communications**. 243-256.
- Shelnutt, J. A. (1981). A simple interpretation of Raman excitation spectra of metalloporphyrins. **Journal of Chemical Physics**. 74: 6644-6656.
- Shelnutt, J. A., Medforth, C. J. Berber, M. D. Barkigia, K. M., and Smith, K. M. (1991). Relationships between structural parameters and Raman frequencies for some planar and nonplanar nickel(II) porphyrins. **Journal of the American Chemical Society**. 113: 4077-4087.

- Shelnutt, J. A., Song, X. -Z. Ma, J. -G. Jia, S. -L., Jentzen, W., and Medforth, C. J. (1998). Nonplanar porphyrins and their significance in proteins. **Chemical Society Reviews**. 27: 31-41.
- Slater, A. F. G., Swiggard, W., Orton, B. R., Flitter, W. D., Golberg, D. E., Cerami, A., and Henderson, G.B. (1991). An iron-carboxylate bond links the heme units of malaria pigment. **Proceedings of the National of Academy of Sciences of the United State of America**. 88: 325-329.
- Smalley, J. W., Silver, J., Birss, A. J., Withnall, R., and Titler, P. J. (2003). The haem pigment of the oral anaerobes *Prevotella nigrescens* and *Prevotella intermedia* is composed of iron(III) protoporphyrin IX in the monomeric form. **Microbiology**. 149: 1711-1718.
- Smalley, J. W., Silver, J., Marsh, P. J., and Birss A. J. (1998) The periodontopathogen *Porphyromonas gingivalis* binds iron protoporphyrin IX in the μ -oxo dimeric form: An oxidative buffer and possible pathogenic mechanism. **Biochemistry Journal**. 331: 681-685.
- Sparks, L. D., Medforth, C. J., Park, M. S., Chamberlin, J. R., Ondiras, M. R., Senge, M. O., Smith, K. M., and Shelnutt, J. A. (1993). Metal dependence of the nonplanar distortion of octaalkyltetraphenylporphyrins. **Journal of the American Chemical Society**. 115: 581-592.
- Spiro, T. G. (1974). Resonance Raman spectroscopy: A new structure probe for biological chromophores. **Accounts of Chemistry Research**. 7: 339-344.
- Spiro, T. G. and Streckas, T. C. (1974). Resonance Raman spectra of heme proteins. Effects of oxidation and spin state. **Journal of the American Chemical Society**. 96: 338-345.

- Stavrov, S. S. (1993). The effect of iron displacement out of the porphyrin plane on the resonance Raman spectra of heme proteins and iron porphyrins. **Biophysics Journal**. 65: 1942-1950.
- Steiner, T. and Desiraju, G. R. (1998). Distinction between the weak hydrogen bond and the van der Waals interaction. **Chemical Communications**. 891-892.
- Suslick, K. S. and Watson, R. A. (1992). The photochemistry of chromium, manganese, and iron porphyrin complexes. **Journal of Chemistry**. 16: 633-642.
- Tang, S. C., Koch, S., Papaefthymiou, G. C., Foner, S., Franke, R., Ibers, J. A., and Holm, R. H. (1976). Axial ligation modes in iron(III) porphyrins. Models for the oxidized reaction states of cytochrome P-450 enzymes and the molecular structure of iron(III) protoporphyrin IX dimethyl ester p-nitrobenzenethiolate. **Journal of the American Chemical Society**. 98: 2414-2434.
- Trivedi, V., Chand, P., Maulik, P. R., and Bandyopadhyay, U. (2005). Mechanism of horseradish peroxidase-catalyzed heme oxidation and polymerization (β -hematin formation). **Biochimica Biophysica Acta**. 1723: 221-228.
- Unger, E., Bobinger, U., Dreybrodt, W., and Schweitzer-Stenner, R. (1993). Vibronic coupling in Ni(II) porphine derived from resonant Raman excitation profiles. **The Journal of Physical Chemistry**. 97: 9956-9968.
- Webster, G. T, McNaughton, D., and Wood, B. R. (2009). Aggregated enhanced Raman scattering in Fe(III)PPIX solutions: The effects of concentration and chloroquine on excitonic interactions. **The Journal of Physical Chemistry B**. 113: 6910-6916.
- Webster, G. T, Tilley, L., Deed, S., McNaughton, D., and Wood, B. R. (2008). Resonance Raman spectroscopy can detect structural changes in haemozoin

(malaria pigment) following incubation with chloroquine in infected erythrocytes.

FEBS Letters. 582: 1087-1092.

Wood, B. R., Langford, S. J., Cooke, B. M., Lim, J., Glenister, F. K., Duriska, M., Unthank, J. K., and McNaughton, D. (2004). Resonance Raman spectroscopy reveals new insight into the electronic structure of β -hematin and malaria pigment.

Journal of the American Chemical Society. 126: 9233-9239.

Wood, B. R., Langford, S. J., Cooke, B. M., Glenister, F. K., Lim, J., Unthank, J. K., and McNaughton, D. (2003). Raman imaging of hemozoin within the food vacuole of *Plasmodium falciparum* trophozoites. **FEBS Letters**. 554: 247-252.

Wood, B. R and McNaughton, D. (2002). Micro-Raman characterization of high- and Low-spin heme moieties within single living erythrocytes. **Biopolymers, (Biospectroscopy)**. 67: 259-262.

Zimmermann, J., Siggel, U., Fuhrhop J.-H., and Roder, B. (2003). Excitonic coupling between B and Q transitions in a porphyrin aggregate. **The Journal of Physical Chemistry B**. 107: 6019-6021.

CHAPTER II

PORPHYRIN CORE CONFORMATION STUDY ON μ - OXO- IRON(III) PORPHYRIN MALARIA PIGMENT MODEL COMPOUNDS

2.1 Introduction

Iron porphyrins perform numerous important functions in living systems. Porphyrin rings tend to be planar (Shelnutt, Song, Ma, Jia, Jentzen, and Medforth, 1998), but flexible, and able to adapt their conformation to different axial ligation and peripheral substitution (Hoard, 1973). They have been described as the pigments of life (Battersby and McDonald, 1979). Heme complexes including μ -oxo TPP (Swepston and Ibers, 1985) and OEP (Cheng, Hobbs, Debrunner, Erlebacher, Shelnutt, and Scheidt, 1995) complexes have been studied as a supramolecular interaction on malaria pigment model systems for (Puntharod, Webster, Asghari-Khiavi, Bambery, Safinejad, Rivadehi, Langford, Haller, and Wood, 2010).

Iron(III) ion five-coordinate high-spin is square-pyramidal with long bonds to porphinato nitrogen atoms, but a short bond to the axial ligand (Scheidt and Reed, 1981). The origin of the frequency shift would be due to a stretching of the Fe–O bond due to nonbonding interactions with van der Waals radii of the pyrrole nitrogen; the Fe–O linkage cannot rigidly follow the iron movement to the proximal side of the

heme plane. The resulting elongation of the bond results in the decreased bond order and force constant (Asher and Schuster, 1979).

Resonance Raman spectroscopy of iron porphyrins are shown in Table 2.1. It is well known that the highest frequency ring modes, between 1350 and 1650 cm^{-1} are sensitive to spin state of the iron atom. The frequencies respond to ligation changes because these changes alter the spin state, the size of Fe, and therefore its displacement out-of-plane. These factors influence the size of the porphyrin central cavity and, therefore, the force constants and vibrational frequencies associated with the ring bond stretches. Thus, the “core size” frequencies can establish the spin state and coordination number for heme proteins in both iron(II) and iron(III) oxidation states (Spiro, 1985). The correlation of ν_4 to the movement of the core size marker is observed and has a possible explanation in terms of the metal's interaction with the porphyrin π system. The position of ν_4 has been observed to shift with core size for the iron porphyrins. However, iron interacts with the porphyrin π system in number of ways, including π back-bonding. These complications are largely absent in nickel porphyrins. The behavior observed in ν_4 of nickel porphyrins may reflect, in part, the sensitivity to changes in core size in manner similar to ν_3 (Findsen, Shelnut, and Ondrias, 1988).

Table 2.1 Comparison of high wave number Raman spectra of μ -oxo iron(III) porphyrins.

Complex	Displacement out of plane (Å)	Excitation wavelength (nm)	ν_4 (cm^{-1})	Degree of enhancement	References
[Fe(TPP)] ₂ O	0.54 ^a	530.8	1357	s	Adar and Srivastava, 1975
		568.2	1358	m	
[Fe(TPP)] ₂ O		413	1361	s	Puntharod et al., 2010
[Fe(TPP)] ₂ O		457.9	1359	s	Burke et al., 1978
		571.6	1359	w	
[Fe(TPP)] ₂ O		457.9	1364	s	Kowalewski et al., 1988
[Fe(TPP)] ₂ N	0.41 ^b	413.1	1362	s	Schick and Bocian 1980
[Fe(TPP)] ₂ N		530.9	1367	m	Schick et al., 1983
[Fe(TPP)] ₂ C	0.36 ^c	406.7	1365	m	Crisanti et al., 1984
[Fe(OEP)] ₂ O		406.7	1377	s	Hofmann and Bocian, 1984
		568.2	1377	m	
[Fe(OEP)] ₂ N		406.7	1378	s	Hofmann and Bocian, 1984
		514.5	1378	s	
[Fe(OEP)] ₂ O	0.54 ^d	413	1376	w	Puntharod et al., 2010
[Fe(DPDE)] ₂ O		457.9	1371	s	Kowalewski et al., 1988
[Fe(PDPE)] ₂ O		413	1372	s	Brémard et al., 1992
		530.9	1372	m	
[Fe(PPDE)] ₂ O		413	1375	s	
		530.9	1375	s	
[Fe(PPIX*)] ₂ O	0.33, 0.40	530	1365	s	This work

^a Swepston and Ibers, 1985

^d Cheng et al., 1995

^b Scheidt et al., 1976

s=strong, m=medium, w=weak

^c Goedken et al., 1982

In particular, a good correlation between the splitting of the α -band and the Soret band for a series of copper porphyrins and the Hammett constants for the substituents is explained by a relationship between the electron-withdrawing ability of substituents and strength of configuration interaction that mixes one-electron excited states of porphyrin. Variations among the porphyrins in the configuration interaction energy result from delocalization of ring charge caused by increased mixing of p-orbitals of the substituent α -carbons with ring orbitals as the “electronegativity” of the substituents increase. Delocalization of ring charge onto substituent carbons lowers the electron-electron repulsion, and therefore the configuration interaction (Shelnutt and Ortiz, 1985).

The distortion of the porphyrin via tilting or twisting of the pyrrole rings can influence the frequencies found in heme model compounds (Czernuszewicz, Li, and Spiro, 1989; Shelnutt, Medforth, Berber, Barkigia, and Smith, 1991; Sparks, Medforth, Park, Chamberlin, Ondrias, Seng, Smith, and Shelnutt, 1993) and in cytochrome *c* which occurs via protein linkage and contacts (Hu, Morris, Singh, Smith, and Spiro, 1993). The binding of π acid ligands such as CO, NO, and O₂ to Fe(II) hemes increasing the frequencies of the ring due to the Fe-porphyrin back-bonding (Spiro, 1995).

Studies of heme model systems shows that many factors, including noncovalent interactions can play an important role in the properties of these metalloproteins. The current study focuses on structure of μ -oxo TPP and OEP complexes and [Fe(PPIX*)]₂O (Cheng, Lee, Powell, and Richter-Addo, 2004) in an effort to better understand the spectra of malaria pigment and the μ -oxo heme complexes. The

purpose of this work is to observe polymorphism, porphyrin core conformation, planarity of the porphyrin core, and supramolecular interactions in malaria pigment model compounds and other heme derivatives to gain more insight into the structure of malaria pigment.

2.2 Experimental

2.2.1 μ -oxo-Iron(III) Protoporphyrin IX Dimethyl Ester, $[\text{Fe}(\text{PPIX}^*)]_2\text{O}$

μ -oxo-Iron(III) protoporphyrin IX dimethyl ester, $[\text{Fe}(\text{PPIX}^*)]_2\text{O}$ was prepared by modified literature method (O'Keeffe, Barlow, Smythe, Fuchsman, Moss, Lilienthal, and Caughey, 1975). Hemin chloride, $\text{Fe}(\text{PPIX})\text{Cl}$ (0.5 g) was added to a mixture of anhydrous methanol (MeOH) and sulfuric acid (36 N, 25 ml) and allowed to stir overnight at room temperature. Chloroform (CHCl_3) extract were washed with water, with saturated sodium bicarbonate solution, and again with water, and then dried over anhydrous sodium sulfate. Evaporation to dryness gave a product that was dissolved in CHCl_3 and chromatographed in CHCl_3 on alumina (deactivated with 10% water). The major band was eluted from the column with $\text{CHCl}_3:\text{MeOH}$ (3:1) and evaporated to dryness. Crystallization from $\text{CHCl}_3:\text{MeOH}$ yields 0.4 g.

2.2.2 Infrared Spectroscopy

Infrared spectra were recorded on a Perkin-Elmer Model Spectrum GX spectrometer as KBr pellets. Both $\text{Fe}(\text{PPIX})\text{Cl}$ and $[\text{Fe}(\text{PPIX}^*)]_2\text{O}$ crystalline powder were measured with these parameters: resolution 4 cm^{-1} , interval 1 with 250 scans.

2.2.3 Raman Spectroscopy

Raman spectra were recorded on HORIBA Jobin Yvon power 0.5 mW, 2 min, 3 accumulations.

2.2.4 Crystallography Geometry Calculations

The crystallographic data of [Fe(OEP)]₂O (CSD reference codes YIKJOR and YIKJOR01) and [Fe(TPP)]₂O (CSD refcode PPORFE10) were retrieved from the Cambridge Structural Database, and of [Fe(PPIX*)]₂O from the Acta Crystallographica website (Cheng, Lee, Powell, and Richter-Addo, 2004). The coordinates were utilized for structure parameter calculations. Least squares planes were calculated by the SHELXL program (Sheldrick, 2008). The computational analysis of geometrical supramolecular features, including hydrogen bonds, intra- and inter-atomic distances, angles, torsional angles, and graphical analysis reported herein were computed by the ORTEP-III program (Burnett and Johnson, 1997).

2.3 Results and Discussion

Infrared Spectroscopy. The ligand-exchange and dimerization reactions of iron(III) derivatives including Fe(III) porphyrins have been characterized by FTIR spectroscopy of microcrystalline samples. The IR absorption band in the region 800-900 cm⁻¹ has been used as evidence of the μ-oxo-bridged for several transition metal complexes (Sadasivan, Elberspacher, Fuchsman, and Cauhey, 1969; O'Keeffe, Barlow, Smythe, Fuchsman, Moss, Lilienthal, and Caughey, 1975). The FTIR spectra of [Fe(PPIX*)]₂O is shown in Figure 2.1. Figure 2.1a exhibits the band near 831 cm⁻¹, assign as asymmetric stretching vibration of Fe–O–Fe in Fe(PPIX)Cl, while this band

shifted to lower frequency as observed at 824 cm^{-1} (7 cm^{-1}) in $[\text{Fe}(\text{PPIX}^*)]_2\text{O}$ as shown in Figure 2.5b (Fleisher and Srivastava, 1969), this result can be interpreted as indicating an oxo-bridged linkage.

The spectrum of $[\text{Fe}(\text{PPIX}^*)]_2\text{O}$ clearly shows the most intense bands at 1731 and 1255 cm^{-1} assigned to the carbonyl stretching mode and the C–O stretching vibration of the propionate linkage. These can be compared with 1731 cm^{-1} in $\text{Fe}(\text{PPIX})\text{Cl}$ and the hydrogen bonded value of 1721 cm^{-1} . The 10 and 6 cm^{-1} shift of C–O stretching in $[\text{Fe}(\text{PPIX}^*)]_2\text{O}$ to the lower wave number compared with $\text{Fe}(\text{PPIX})\text{Cl}$ (1261 cm^{-1}), this suggested the hydrogen bond formation reduces the frequency of the adjoining C–O link due through the dimethyl ester bond.

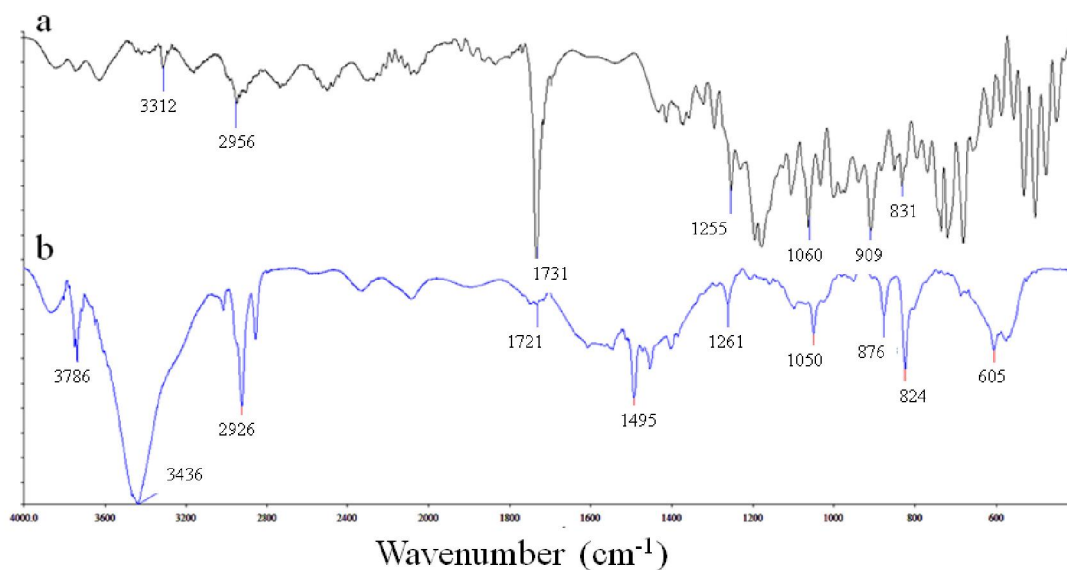


Figure 2.1 IR spectra of $[\text{Fe}(\text{PPIX}^*)]_2\text{O}$; a: $[\text{Fe}(\text{PPIX}^*)]_2\text{O}$. b: $\text{Fe}(\text{OEP})\text{Cl}$.

Solid-state resonance Raman Spectroscopy. Figure 2.2 shows a RR spectrum of $[\text{Fe}(\text{PPIX}^*)]_2\text{O}$ obtained by excitation near the Soret bands. Bands in the core size (or spin state marker) band region $1650\text{-}1500\text{ cm}^{-1}$ and relative intensity of Soret band/or 514 nm excitation wavelengths for $[\text{Fe}(\text{PPIX}^*)]_2\text{O}$ is shown in Figure 2.2.

The most intense band region is comprised of three principal bands, totally symmetric modes appearing at 1613 , 1562 , and 1361 cm^{-1} assigned to ν_{10} , ν_2 , and ν_4 , respectively. The ν_{10} is involved in $\nu(\text{C}_b\text{C}_b)$, ν_2 assigned as $\nu_{\text{sym}}(\text{C}_a\text{C}_m)$, and ν_4 band is related to $\text{C}\alpha\text{N}$ or pyrrole breathing mode. These frequency region are similar with the 514 nm excitation wavelength in $[\text{Fe}(\text{OEP})]_2\text{O}$ (Puntharod, Webster, Asghari-Khiavi, Bamberg, Safinejad, Rivadehi, Langford, Haller, and Wood, 2010). The band near lower frequency region is unclear to assign since this band is mixed with background. The Raman spectra are dominated by the porphyrin vibrational modes which are enhanced by resonance with allowed electronic transitions in the visible and near-ultraviolet region (Spiro, 1974). These $\pi\text{-}\pi^*$ transitions, polarized frequencies shifts in the porphyrin plane, and the strong Raman bands are at frequency shifts ($1000\text{-}1700\text{ cm}^{-1}$) appropriate for in-plane stretching vibrations of the ring and the different bands are enhanced depending on the excitation wavelength (Spiro, 1974).

Figure 2.4 represent the simulation of powder X-ray diffraction pattern to compare the polymorphism of $[\text{Fe}(\text{PPIX}^*)]_2\text{O}$, triclinic $[\text{Fe}(\text{OEP})]_2\text{O}$, monoclinic $[\text{Fe}(\text{OEP})]_2\text{O}$, and $[\text{Fe}(\text{TPP})]_2\text{O}$, respectively.

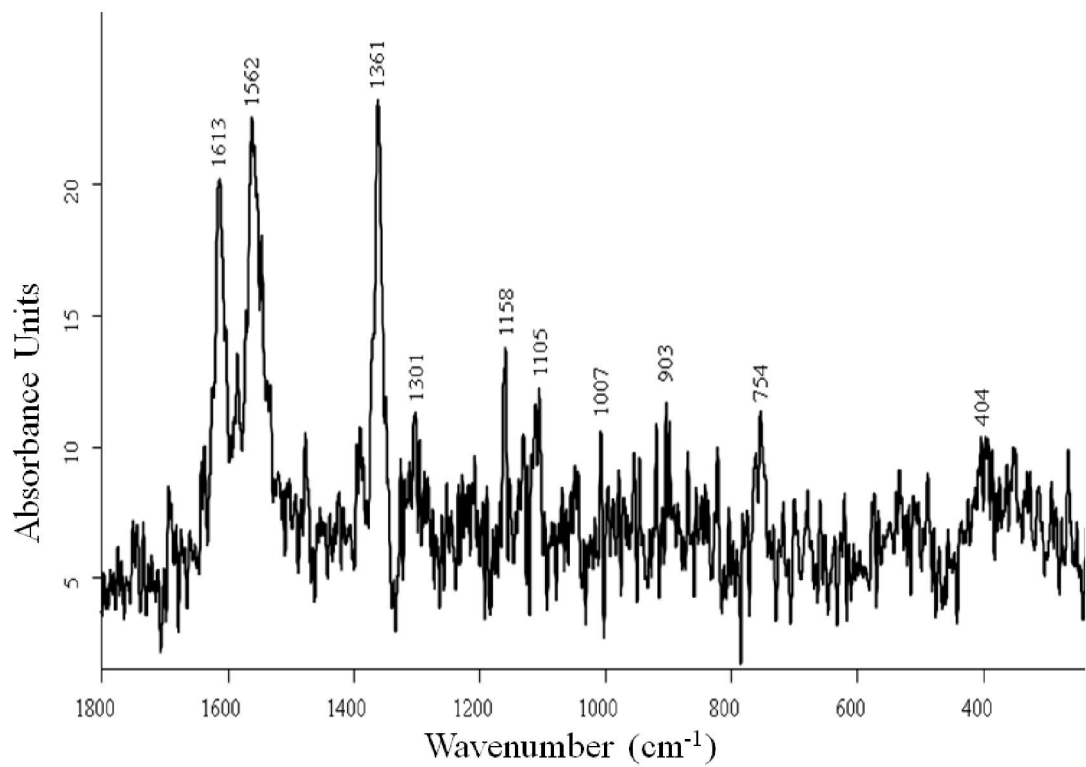


Figure 2.2 Resonance Raman spectrum in 400-1800 cm⁻¹ region of [Fe(PPIX*)]₂O.



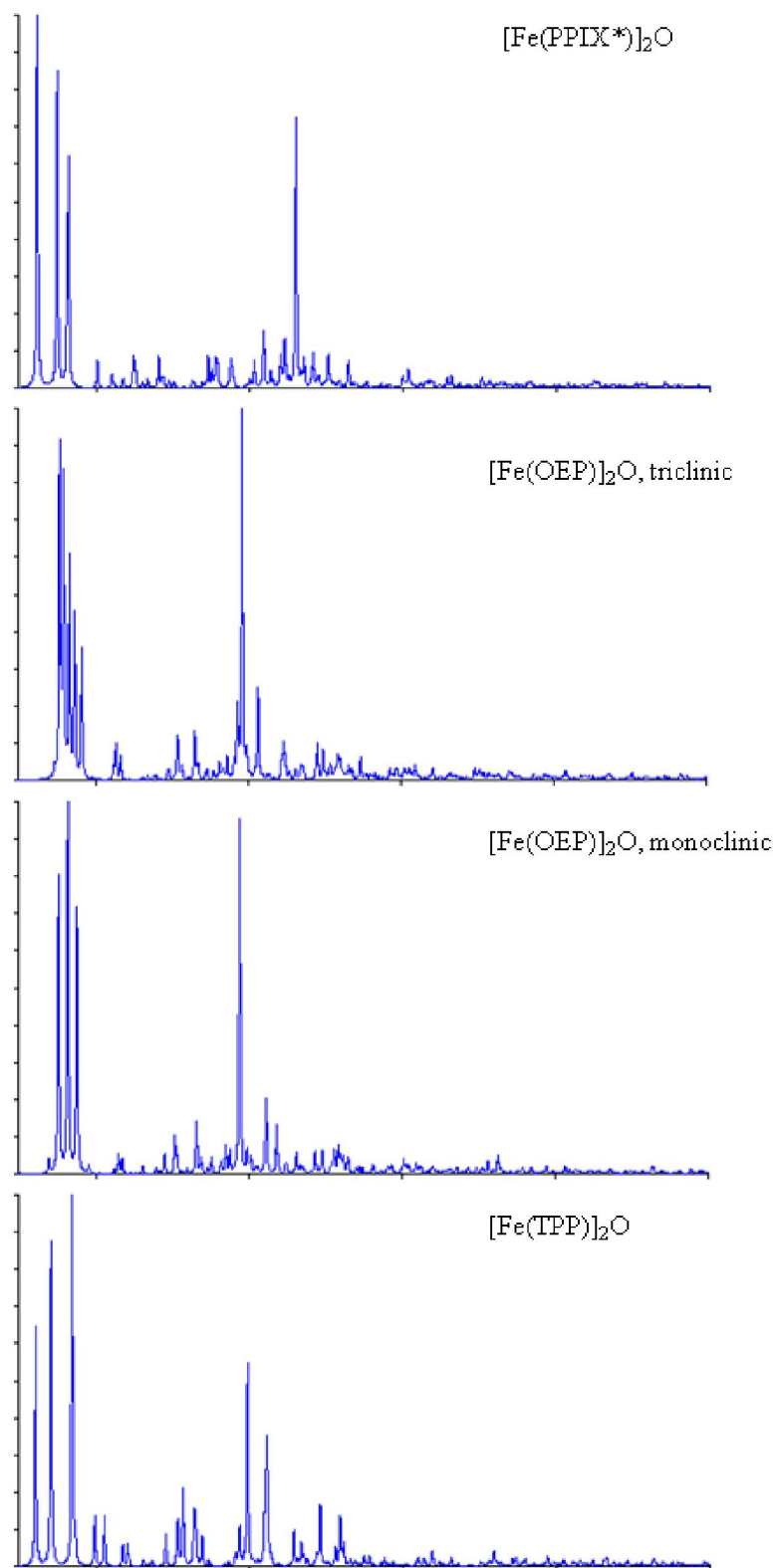
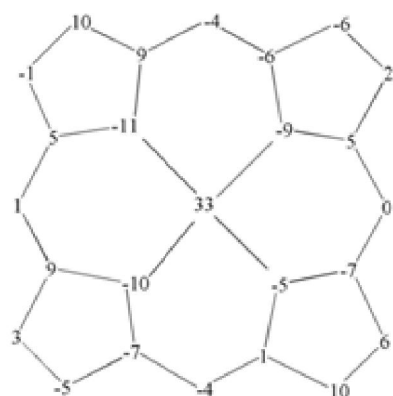


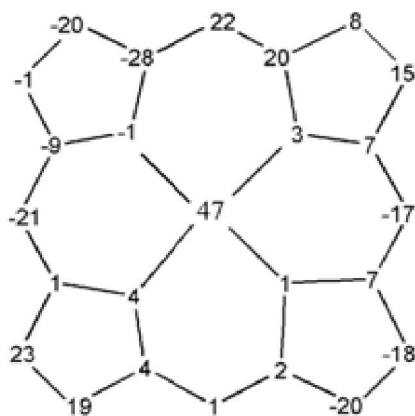
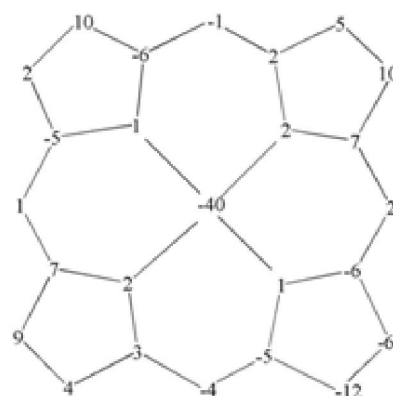
Figure 2.4 Simulated PXRD of μ -oxo iron(III) porphyrins.

Crystallographic Calculations. Formal diagrams of the porphinato cores for the two crystallographically independent porphyrin moieties with perpendicular displacements of the individual atoms from the least squares planes through the 24-atom cores of $[\text{Fe}(\text{PPIX}^*)]_2\text{O}$ are shown in Figure 2.3. The relative planarity of the cores is easily seen. The average displacement of the 24 atoms core in $[\text{Fe}(\text{PPIX}^*)]_2\text{O}$ are -10 and 28 \AA for two rings and the porphyrin core showed a wave conformation for both two rings. In contrast, the average displacement of the 24 atoms core in β -hematin, triclinic $[\text{Fe}(\text{OEP})]_2\text{O}$, and $[\text{Fe}(\text{TPP})]_2\text{O}$ are -11 , -10 , and 1 \AA , respectively. The porphyrin core conformation of β -hematin, triclinic $[\text{Fe}(\text{OEP})]_2\text{O}$, and $[\text{Fe}(\text{TPP})]_2\text{O}$ are showed saddled mode. While the average displacement of the 24 atoms core in monoclinic $[\text{Fe}(\text{OEP})]_2\text{O}$ is -1 \AA and the porphyrin core conformation is exhibited domed mode. These results indicated that the planarity of the porphyrin core in $[\text{Fe}(\text{PPIX}^*)]_2\text{O}$ is not related to β -hematin and triclinic $[\text{Fe}(\text{OEP})]_2\text{O}$, while the porphyrin core conformation may be resulting in the arrangement of peripheral substituted on C_β of pyrrole ring.

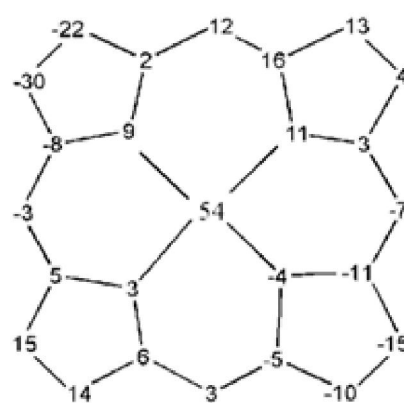
The Fe displacement out of the mean plane is 0.37 and 0.40 \AA for $[\text{Fe}(\text{PPIX}^*)]_2$ which is smaller than the 0.47 in β -hematin, 0.50 and 0.54 \AA displacement in the triclinic and monoclinic forms of $[\text{Fe}(\text{OEP})]_2\text{O}$ (Cheng, Hobbs, Debrunner, Erlebacher, Shelnut, and Scheidt, 1995), and 0.54 \AA in $[\text{Fe}(\text{TPP})]_2\text{O}$ (Swepston and Ibers, 1985), respectively. The iron(III) in $[\text{Fe}(\text{PPIX}^*)]_2\text{O}$ is more in plane and lies closer to the four pyrrole nitrogen plane.



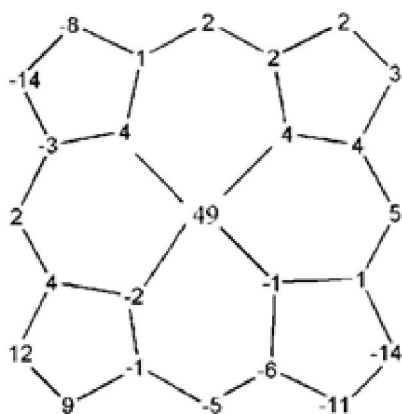
[Fe(PPIX*)]₂O



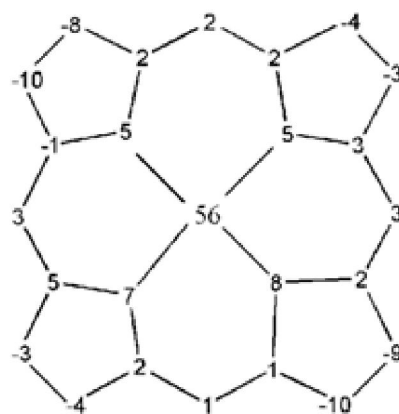
β -hematin



[Fe(TPP)]₂O



[Fe(OEP)]₂O triclinic



[Fe(OEP)]₂O monoclinic

Figure 2.4 Formal diagrams of the two crystallographically independent porphyrato cores of [Fe(PPIX*)]₂O, [Fe(TPP)]₂O, and [Fe(OEP)]₂O, displaying the perpendicular displacements, in units of 0.01 Å, from the mean planes of the 24-atom core.

The molecular structural parameters of the three μ -oxo heme compounds are given in Table 2.2. The average Fe–N bond distances in the three complexes are the same within one standard deviation. The $[\text{Fe}(\text{PPIX}^*)]_2\text{O}$ molecule follows the typical pattern for high-spin iron(III) ion porphyrins (Scheidt and Reed, 1981). The average Fe–N_p bond distance of $[\text{Fe}(\text{PPIX}^*)]_2\text{O}$, 2.077(4) Å, is similar to those in $[\text{Fe}(\text{TPP})]_2\text{O}$ and both the triclinic and monoclinic forms of $[\text{Fe}(\text{OEP})]_2\text{O}$. The average values of C_t–N in the three μ -oxo iron porphyrins are 2.036, 2.022, and 2.024 Å for $[\text{Fe}(\text{PPIX}^*)]_2\text{O}$, $[\text{Fe}(\text{OEP})]_2\text{O}$, and $[\text{Fe}(\text{TPP})]_2\text{O}$, respectively. The core size of $[\text{Fe}(\text{PPIX}^*)]_2\text{O}$ is significantly larger than those of $[\text{Fe}(\text{OEP})]_2\text{O}$ and $[\text{Fe}(\text{TPP})]_2\text{O}$ leading to a lower average iron atom displacement of 0.37 and 0.40 Å from the 24 atom porphyrin core in $[\text{Fe}(\text{PPIX}^*)]_2\text{O}$ compared to the displacements in $[\text{Fe}(\text{OEP})]_2\text{O}$ and $[\text{Fe}(\text{TPP})]_2\text{O}$. The equatorial Fe–N_p bond length of 2.077 Å is within one standard deviation of those in the OEP and TPP complexes, and is consistent with the $d_{x^2-y^2}$ orbital being occupied. The C_t···N radius, 2.036 Å, in the $[\text{Fe}(\text{PPIX}^*)]_2\text{O}$ corresponds to trivial strain in the porphyrinato core and the concomitant 0.37 Å out-of-plane displacement of the Fe³⁺.

It is evident that the $[\text{Fe}(\text{PPIX}^*)]_2\text{O}$, $[\text{Fe}(\text{OEP})]_2\text{O}$, and $[\text{Fe}(\text{TPP})]_2\text{O}$ molecules in which the square-pyramidal coordination group (Scheidt and Reed, 1981; Hoard, Hamor, Hamor, and Caughey, 1965) has an axial ligand Fe–O distance of 1.748 Å, four Fe–N bonds length of 2.077 Å, and out-of-plane displacement of the iron atom of ~0.33-0.5 Å.

Table 2.2 Comparison of Structural Parameters of μ -oxo Iron(III) Porphyrins.

Types	Complexes				
	[Fe(PPIX*)] ₂ O		[Fe(OEP)] ₂ O	[Fe(OEP)] ₂ O	[Fe(TPP)] ₂ O
	Ring a	Ring b	(triclinic)	(monoclinic)	
Fe-N _p	2.077(4)	2.076(3)	2.077(3)	2.080(3)	2.081(3)
Fe-O	1.748(3)	1.748(3)	1.758(3)	1.755(4)	1.759(1)
Fe-Fe	3.496		3.516	3.510	3.526
Δ_{av}	0.33, 0.40		0.50	0.54	0.54
N-C _t	2.036			2.022	2.024
Torsion	27.2		17.0	16.8	35.4
Fe-O-Fe	170.5(2)		172.2(2)	176.2(2)	174.5(1)

Projection views of the three systems (Figure 2.4), the N–Fe–Fe'–N' torsional angles are 35°, 27°, and 17° for [Fe(TPP)]₂O, [Fe(PPIX*)]₂O, and [Fe(OEP)]₂O, respectively. As noted above, the key stereochemically active orbitals for monomeric heme complexes are d_z^2 , directed toward the axial ligand(s), and $d_{x^2-y^2}$ which interact directly with the macrocyclic N atoms. When two hemes are joined by a linear μ -oxo bridge, the d_{xz} and d_{yz} orbitals on the iron centers and the p_x and p_y orbitals on the bridging oxygen atom are also stereochemically active.

The plus and minus combination of the d_z^2 orbitals interact with the 2s and 2p_z (two sp) μ -oxo orbitals to form σ bonds, while the iron d_{xz} and d_{yz} orbitals engage in π bonding with the μ -oxo p_x and p_y orbitals which are of similar energy. The two $d_{x^2-y^2}$ orbitals remain high-lying and do not interact with the μ -oxo orbitals, and the two d_{xy}

orbitals become lowest energy. The interaction of the in- and out-of-phase combinations of d_{xz} and d_{yz} with the μ -oxo p_x and p_y orbitals is enhanced.

The relative orientations of the two rings within the molecules (Figure 2.4), one group of propionate side chains in ring *a* pointing downward directly to the another one vinyl chain in ring *b*, while the vinyl groups in ring *a* pointing upward but one propionate side chain in ring *b* is pointing opposite direction. The vinyl group tends to stay in the middle between two propionate side chains and pointing directed to the O atom in propionate since the O atom is more electronegative. The orientation of peripheral substituents in $[\text{Fe}(\text{PPIX}^*)]_2\text{O}$ are differ from $[\text{Fe}(\text{OEP})]_2\text{O}$ which is those all the ethyl groups in $[\text{Fe}(\text{OEP})]_2\text{O}$ pointing outward/inward to minimization increased the $\text{N}-\text{Fe}-\text{Fe}'-\text{N}'$ to 31.6° (Cheng, Hobbs, Debrunner, Erlebacher, Shelnut, and Scheidt, 1995). The interactions between the porphinato core in $[\text{Fe}(\text{PPIX}^*)]_2\text{O}$ molecule are less constrained and the role may be play by the vinyl groups. These can be conclude that the relaxation of the steric bulky groups are found in phenyl < vinyl < ethyl group and lead to limitation of the rotation angle of the two interacting porphyrin rings and $[\text{Fe}(\text{PPIX}^*)]_2\text{O}$ is more closely related to $[\text{Fe}(\text{TPP})]_2\text{O}$ than $[\text{Fe}(\text{OEP})]_2\text{O}$. Thus, $[\text{Fe}(\text{PPIX}^*)]_2\text{O}$ may favor staggered conformation to minimized steric hindrance, while $[\text{Fe}(\text{OEP})]_2\text{O}$ favors eclipsed conformation.

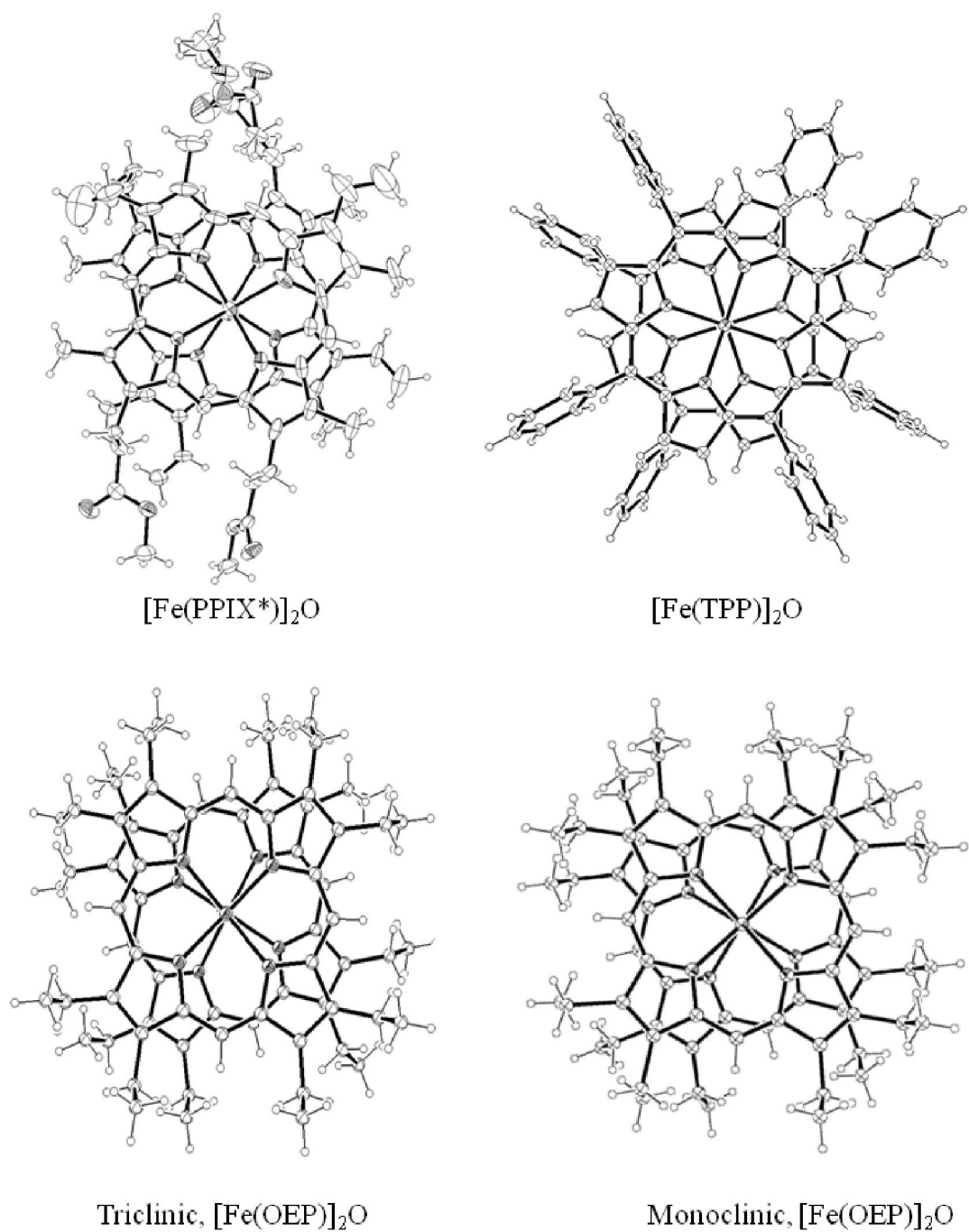


Figure 2.4 Projection diagrams of the μ -oxo dimers showing the relative arrangement of peripheral substituted of the porphyrin cores.

2.5 Conclusion

The FT-IR and RR spectra results were good evidence for study the electronic structure, μ -oxo-bridge linkage and the interaction of the C–O stretching vibration of the propionate linkage between two $[\text{Fe}(\text{PPIX}^*)]_2\text{O}$ molecules. Raman spectroscopy is especially dominated by the porphyrin vibrational modes which are enhanced by resonance with the allowed electronic transitions in the visible and near-ultraviolet. These π – π^* transitions give the enhancement of the porphyrin plane and the strong enhancement Raman bands are at 1000-1700 cm^{-1} , which is appropriate for the in-plane stretching modes of the ring. In this study, the resonance Raman spectra of $[\text{Fe}(\text{PPIX}^*)]_2\text{O}$ is incomplete, since the Raman bands depend on the excitation wavelength and excited one wavelength.

The crystal structural parameters in the three μ -oxo iron(III) porphyrin malaria pigment model compounds considered herein are good evidence for five-coordinate high-spin heme complexes with square-pyramidal geometry about the iron atoms. The crystallographic data showed that the iron(III) ion displacement out-of-plane are 0.33 and 0.40 Å which is more in plane than those found in $[\text{Fe}(\text{TPP})]_2\text{O}$ and $[\text{Fe}(\text{OEP})]_2\text{O}$. The N–Fe–Fe'–N' torsional angles are 35°, 27°, and 17° for $[\text{Fe}(\text{TPP})]_2\text{O}$, $[\text{Fe}(\text{PPIX}^*)]_2\text{O}$, and $[\text{Fe}(\text{OEP})]_2\text{O}$, respectively. Firstly, the bending of the rotational angle in $[\text{Fe}(\text{PPIX}^*)]_2\text{O}$ may promote the overlap of iron d orbitals and oxygen 2p orbitals and thus decrease the energy of μ -oxo \rightarrow Fe(III) charge transfer transition. Secondly, the interactions between the porphyrato core in $[\text{Fe}(\text{PPIX}^*)]_2\text{O}$ molecule are sterically less constrained and may be played by the vinyl groups. These can be conclude that the relaxation of the steric bulky groups are found in phenyl < vinyl < ethyl group and lead to limitation of the rotation angle of the two interacting

porphyrin rings and $[\text{Fe}(\text{PPIX}^*)]_2\text{O}$. Thirdly, the conformation of $[\text{Fe}(\text{PPIX}^*)]_2\text{O}$ appears to be controlled by the steric factors and favors the staggered conformation.

2.6 References

- Adar, F. and Srivastava, T. S. (1975). Resonance Raman effect in μ -oxo-bis[iron(III) tetraphenylporphyrin]. **Proceedings of the National Academy of Sciences of the United States of America**. 72: 4419-4424.
- Asher, S. A. and Schuster, T. M. (1979). Resonance Raman examination of axial ligand bonding and spin-state equilibria in metmyoglobin hydroxide and other heme derivatives. **Journal of the American Chemical Society**. 18: 5377-5386.
- Battersby, A. and McDonald, E. (1979). Origin of the pigments of life: the Type-III problem in porphyrin biosynthesis. **Accounts of Chemical Research**. 12: 14-22.
- Brémad, C., Kowalewski, P., and Merlin, J. C. (1992). Resonance Raman enhancement of the oxo-bridged dinuclear iron center: Vibrational modes in iron(III) physiological-type porphyrin complexes. **Journal of Raman Spectroscopy**. 23: 325-333.
- Brown, W. H. (1911). Malaria pigment (so-called melanin): Its nature and mode of production. **Journal of Experimental Medicine**. 13: 290-99.
- Burke, J. M., Kincaid, J. R., and Spiro, T. G. (1978). Resonance Raman spectra and vibrational modes of iron(III) tetraphenylporphine μ -xo dimer. Evidence for phenyl interaction and lack of dimer splitting. **Journal of the American Chemical Society**. 100: 6077-6083.

- Burnett, M. N. and Johnson, C. K. (1996). *ORTEP-III: Oak Ridge Thermal Ellipsoid Plot Program for Crystal Structure Illustration*, Report ORNL-6895, **Oak Ridge National Laboratory**, Tennessee, USA.
- Cheng, B., Hobbs, J. D., Debrunner, P. G., Erlebacher, J., Shelnut, J. A., and Scheidt, W. R. (1995). An unusual near-eclipsed porphyrin ring orientation in two crystalline forms of $(\mu\text{-oxo})\text{bis}[(\text{octaethylporphinato})\text{iron(III)}]$. Structural and molecular mechanics studies. **Inorganic Chemistry**. 34: 102-110.
- Cheng, L., Lee, J., Powell, D. R., and Richter-Addo, G. B. (2004). $\mu\text{-oxo-bis}[(\text{protoporphyrin IX dimethyl ester})\text{-iron(III)}]$. **Acta Crystallographica E**. 60: m1340-m1342.
- Crisanti, M. A., Spiro, T. G., English D. R., Hendrickson, D. N., and Suslick, K. S. (1984). Resonance Raman spectra of high oxidation state iron porphyrin dimers. **Inorganic Chemistry**. 23: 3897-3901.
- Czernuszewicz, R. S., Li, X.-Y., and Spiro, T. G. (1989). Nickel, octaethylporphyrin ruffling dynamics from resonance Raman spectroscopy. **Journal of the American Chemical Society**. 111: 7024-7031.
- Findsen, E. W., Shelnut, J. A., and Ondrias, M. R. (1988). Photodynamics of nickel porphyrins in noncoordinating solvents: Characterization of d-d excited states using transient Raman spectroscopy. **The Journal of Physical Chemistry**. 92: 307-413.
- Fleischer, E. B. and Srivastava, T. S. (1969). The structure and properties of $\mu\text{-oxo-bis}(\text{tetraphenylporphyrine})\text{iron(III)}$. **Journal of the American Chemical Society**. 91: 2403-2405.

- Geiger, D. K., Lee, J. Y., and Scheidt, W. R. (1984). Control of spin state in (porphinato)iron(III) complexes. An axial ligand orientation effect on the spin State in bis(2-methylimidazole)(octaethylporphinato)iron(III) Perchlorate. **Journal of the American Chemical Society**. 106: 6339-6343.
- Hoard, J. L., Hamor, M. J., Hamor, T. A., and Caughey, W. S. (1965). The crystal structure and molecular stereochemistry of methoxyiron (III) mesoporphyrin IX dimethyl ester. **Journal of the American Chemical Society**. 87: 2312-2319.
- Hoard, J. L. (1971). Stereochemistry of hemes and other metalloporphyrins. **Science**. 174: 1295-305.
- Hoard, J. L. (1973). Some aspects of metalloporphyrin stereochemistry. **Annals of the New York Academy Science**. 18-30.
- Hoffman, A. B., Collins, D. M., Day, V. W., Fleischer, E. B., Srivastava, T. S., and Hoard, J. L. (1972). The crystal structure and molecular stereochemistry of μ -oxo-bis [$\alpha,\beta,\gamma,\delta$ -tetraphenylporphinatoiron(III)]. **Journal of the American Chemical Society**. 94: 3620- 3626.
- Ivanca, M. A., Lappin, A. G., and Scheidt, W. R. (1991). Water-soluble ferric porphyrinates: Solution and solid-state species. **Inorganic Chemistry**. 30: 711-718.
- Kohnhorst, S. A. and Haller, K. J. (2011). **ANSCSE15 Proceeding**, Bangkok University, Thailand. 104-110.
- Kowalewski, P., Merlin, J. C. Bremard, C., and Moreau, S. (1988). Resonance Raman evidence for μ -oxo linkage in ferriporphyrins. **Journal of Molecular Structure**. 175: 55-60.

- Little, R. G., Dymock, K. R., and Ibers, J. A. (1975). The crystal and molecular structure of the ferrihemochrome bis(1-methylimidazole)(protoporphyrin IX)iron-methanol water. **Journal of the American Chemical Society**. 97: 4532-4539.
- Landrum, J. T., Grimmett, D., Haller, K. J., Scheidt, W. R., and Reed, C. A. (1981). Imidazolate- and oxo-bridged metalloporphyrins. **Journal of the American Chemical Society**. 103: 2640-1650.
- Lay, K. L., Buchler, W. J., Kenny, J. E., and Scheidt, W. R. (1986). **Inorganica Chimica Acta**. 123: 91.
- Moss, G. P. (1987). Nomenclature of tetrapyrroles. **Pure & Applied Chemistry**. 59: 779-832.
- O’Keeffe, D. H., Barlow, C. H., Smythe, G. A., Fuchsman, W., Moss, T. H., Lilienthal, H., and Caughey, W. (1975). Magnetic and spectroscopic probes for Fe–Fe linkages in hemin systems. **Bioinorganic Chemistry**. 5: 125-147.
- Puntharod, R. (2008). Synthesis and Structural Studies of Malaria Pigment Model systems. **Ph.D. Thesis**, Suranaree University of Technology. p.145-146.
- Puntharod, R., Webster, G. T., Asghari-Khiavi, M., Bambery, K. R., Safinejad, F., Rivadehi, S., Langford, S. J., Haller, K. J., and Wood, B. R. (2010). Supramolecular interactions playing an integral role in the near-infrared Raman “excitonic” enhancement observed in β -hematin (malaria pigment) and other related heme derivatives. **The Journal of Physical Chemistry B**. 114: 12104-12115.

- Sadasivan, N., Eberspacecher, H. I., Fuchsman, W. H., and Caughey, W. S. (1969). Substituted deuteroporphyrins. VI. Ligand-exchange and dimerization reactions of deuterohemins. **Biochemistry**. 8: 534-541.
- Scheidt, W. R. and Reed, C. A. (1981). Spin-State/Stereochemical relationships in iron porphyrins: Implications for the hemoproteins. **Chemistry Reviews**. 81: 543-553.
- Scheidt, W. R., Geiger, D. K., and Haller, K. J. (1982). Structural characterization of a variable-spin (porphinato)iron(III) complex. Molecular stereochemistry of bis(3-chloropyridine)(octaethylporphinato)iron(III) perchlorate at 98K ($S = 1/2$) and 293 K ($S = 1/2$, $S = 5/2$). **Journal of the American Chemical Society**. 104: 495-499.
- Scheidt, W. R., Geiger, D. K., Hayes, R. G., and Lang, G. (1983). Control of spin state in (porphinato)iron(III) complexes. Axial ligand orientation effect leading to an intermediate-spin complex. Molecular structure and physical characterization of the monoclinic form of bis(3-chloropyridine)-(octaethylporphinato)iron(III) perchlorate. **Journal of the American Chemical Society**. 105: 2625-2632.
- Scheidt, W. R., Geiger, D. K., Lee, Y. J., Reed, C. A., and Lang, G. (1987). On the preparation of five-coordinate (3-chloropyridine)(porphinato)iron(III) complexes. **Journal of the American Chemical Society**. 26: 1039-1045.
- Schick, G. A. and Bocian, D. (1980). Further characterization of the oxidation and spin states of iron in the nitrogen-bridged metalloporphyrin μ -nitrido-bis[(5,10,15,20-tetraphenylporphinato)iron]. **Journal of the American Chemical Society**. 102: 7982-7984.

- Schick, G. A. and Bocian, D. F. (1983). Resonance Raman spectra of the nitrogen-bridged iron porphyrin dimer, (μ -nitrido)bis[5,10,15,20-tetraphinato]iron]. **Journal of the American Chemical Society**. 105: 1830-1838.
- Sheldrick, G. M. (2008). A short history of SHELX. **Acta Crystallographica A**. 64: 112-122.
- Shelnutt, J. A., Song, X.-Z, Ma, J.-G., Jia, S.-L., Jentzen, W., and Medforth, C. (1998). Nonplanar porphyrins and their significance in proteins. **Chemical Society Reviews**. 27: 31-41.
- Shelnutt, J. A., Medforth, C. J., Berber, M. D., Barkigia, K. M., and Smith, K. M. (1991). Relationship between structural parameters and Raman frequencies for some planar and nonplanar nickel(II) porphyrins. **Journal of the American Chemical Society**. 113: 4077-4087.
- Shelnutt, J. A. and Ortiz, V. (1985). Substituent effects on the electronic structure of metalloporphyrins: A quantitative analysis in terms of four-orbital-model parameters. **Journal of Physical Chemistry**. 89: 4733-4739.
- Sparks, L. D., Medforth, C. J., Park, M.-S., Chamberlin, J. R., Ondrias, M. R., Seng, M. O., Smith, K. M., and Shelnutt, J. A. (1993). Metal dependence of the nonplanar distortion of octaalkyltetraphenylporphyrins. **Journal of the American Chemical Society**. 115: 581-592.
- Spiro, T. G. (1974). Resonance Raman spectroscopy: A new structure probe for biological chromophores. **Accounts of Chemical Research**. 7: 339-344.
- Spiro, T. G. (1985). Resonance Raman spectroscopy as a probe of heme protein structure and dynamics. **Advanced Protein Chemistry**. 37: 110-159.

- Spiro, T. G. (1990). Metalloporphyrin structure and dynamics from resonance Raman spectroscopy. **Coordination Chemistry Reviews**. 100: 541-571.
- Spiro, T. G and Czernuszewicz, R. S. (1995). Resonance Raman spectroscopy of metalloproteins, in **Methods in Enzymology**. 246: 417-461.
- Spiro, T. G. and Streckas, T. C. (1974). Resonance Raman spectra of heme proteins. Effects of oxidation and spin state. **Journal of the American Chemical Society**. 96: 338-345.
- Strááso, T., Kappishnikov, S., Kato, K., Takata, M., Als-Nielsen, J., and Leiserowitz, L. (2011). The role of the four stereoisomers of the heme Fe-O cyclic dimer in the crystalline phase behavior of synthetic hemozoin: Relevance to native hemozoin crystallization. **Crystal Growth and Design**. 11: 3342-3350.
- Sweptson, P. N. and Ibers, J. A. (1985). Redetermination of the structure of μ -oxo-bis[5,10,15,20-tetraphenylporphyrinato]iron(III) at 122K, $[\text{Fe}_2\text{O}(\text{C}_{44}\text{H}_{28}\text{N}_4)_2]$. **Acta Crystallographica C**. 41: 671-673.
- Wood, B. R., Langford, S. J., Cooke, B. M., Lim, J., Glenister, F. K., Duriska, M., Unthank, J. K., and McNaughton, D. (2004). Resonance Raman spectroscopy reveals new insight into the electronic structure of β -hematin and malaria pigment. **Journal of the American Chemical Society**. 126: 9233-9239.

CHAPTER III

A NEW POLYMORPH OF CHLORO(2,3,7,8,12,13,17,18-OCTAETHYLPORPHYRINATO)IRON(III)

3.1 Introduction

Complexes of metalloporphyrins have been intensively investigated as model systems for heme proteins (Scheidt, 2000) c-type cytochromes (Teraoka and Kitagawa, 1980), and malaria pigment (Puntharod, Webster, Asghari-Khiavi, Bambery, Safinejad, Rivadehi, Langford, Haller, and Wood, 2010). The electronic structure of metalloporphyrins is dominated by the tetrapyrrole ring because of the extended aromatic π - π^* system, involvement with the central iron atom, axial ligation, and metal atom, spin state (Spiro, 1985). Octaethylporphyrin (OEP) have hydrogen atoms bound to methine carbon (C_m) and various substituents at the outer pyrrole carbon atoms (C_b). Iron octaethylporphyrin has eight ethyl substituents at the C_b atoms, are extensively used for studying heme model systems (Scheidt, 2000) including malaria pigment (Puntharod, Webster, Asghari-Khiavi, Bambery, Safinejad, Rivadehi, Langford, Haller, and Wood, 2010).

As is generally know, the planarity of the porphyrin core is defined by the displacements of the atoms of the 24-atom cores in a directions of perpendicular to the mean plane. The pyrrole rings are always planar, the displacement of the 24-atom core of pyrrole ring above or below the mean plane of the core. The meso carbon

atoms are found to be in, or nearly in 24-atom core (Scheidt and Lee, 1987). The planarity of the porphyrin plane can be characterized by the average of 24 atom mean plane is zero and the displacements of the opposite meso carbons above (+) and below (-) the porphyrin mean plane (Scheidt and Lee, 1987). The two distortion modes found most often are the saddle-shaped and ruffled conformations (Medforth, Haddad, Muzzi, Dooley, Jaquinod, Shyr, Nurco, Olmsteadt, Smith, Ma, and Shelnut, 2003) pointed out that the different porphyrin core conformations are responsible for the substantial difference in the M–N bond lengths. The result is clearly seen in ruffled NiOEP tetragonal form (Meyer, 1972) and the planar NiOEP triclinic form (Cullen and Meyer, 1974). In the triclinic form the porphyrin moiety is essentially planar and the Ni–N distance is the same as found for other nickel(II) metalloporphyrins while the tetragonal form has a severe ruffling of macrocycle (Cullen and Meyer, 1974).

Porphyrin core distortion has attracted attention because of the recent observation that a class of hemoprotein derivatives contains similarly conformationally distorted macrocycles (Shelnutt, Song, Ma, Jia, Jentzen, and Medforth, 1998). The porphyrin macrocycle conformation is rather flexible with respect to nonplanar distortions and can adopt a wide range of nonplanar conformations that have been described as ruffled, saddled, domed and waved which showed in Figure 1.3 (Scheidt and Lee, 1987).

Several porphyrin type cofactors are known to adopt nonplanar conformations in their protein environments, and it has been suggested that nonplanarity may be an important factor (Shelnutt, Song, Ma, Jia, Jentzen, and Medforth, 1998; Jentzen, Ma, and Shelnutt, 1998). Factors that are known to induce nonplanar distortion are the size of the central metal ion, sterically clashing peripheral substituents, and the nature of

the axial ligands (Senge, 2000; Scheidt and Lee, 1987) and packing forces may be another determining factor as to which form is obtained in the crystalline state (Cullen and Meyer, 1974).

Fe(OEP)Cl is crystalline with a number of five-coordinated, including octaethylporphyrinato iron(III) derivative having a picrate as an axial ligand (Uno, Hatano, Nishimura and Arata, 1990; Puntharod, 2008), methoxide (Hatano and Uno, 1990), trichloroacetate (Neal, Cheng, Ma, Shelnut, Schulz, and Scheidt, 1999

Three different crystalline species containing Fe(OEP)Cl have been reported, a monoclinic form (Senge, 2005), a solvated form (Safo, Buentello, Oliver, and Scheidt, 2010), and a two species crystal with a fullerene in the lattice (Olmstead, Costa, Maitra, Noll, Phillips, Van Calcar, and Balch, 1999). The π -cation-radical derivatives of octaethylporphyrinato iron(III), $[\text{Fe}(\text{OEP}^{\bullet})(\text{Cl})]^+$ which is all eight ethyl groups are up (Scheidt, Song, Haller, Safo, Orosz, Reed, Debrunner, and Schulz, 1992). In this study, a new crystalline triclinic form of five-coordinate Fe(OEP)Cl is synthesis and the structural, and physical characterization. It is interesting to compare the triclinic and monoclinic forms of Fe(OEP)Cl, which have different arrangements of the peripheral ethyl groups. The structure determination showed that, although OEP derivatives are not sterically crowded, they are capable of adopting various core conformations and arrangements of the peripheral groups.

3.2 Experimental

Fe(OEP)Cl (15 mg) was recrystallized in 100 mL of 1:10 *N,N*-dimethylformamide: chloroform. The brown-red solution was refluxed to the its boiling point (120°C) and stirred for 6 h, then the solution was filtered and

crystallized by vapor diffusion with methanol, the crystals were harvested after a month at room temperature.

3.2.1 UV-Vis Spectroscopy

Fe(OEP)Cl was dissolved in CH₂Cl₂ and its electronic spectrum recorded on an Agilent model 8453 UV-Vis/NIR spectrophotometer. The spectrum was scanned from 200 to 900 nm.

3.2.2 FT-IR Spectroscopy

Infrared spectra were recorded on sample mixed in KBr disks on a Perkin-Elmer Model Spectrum GX spectrometer. Fe(OEP)Cl crystalline powders was measured with these parameters: resolution 4 cm⁻¹ with 50 scans.

3.2.4 Solution and Refinement of Structure

A suitable single crystal of the triclinic form of Fe(OEP)Cl was obtained by slow diffusion at room temperature of MeOH into CHCl₃ solutions of the complex. An ORTEP perspective diagram showing the numbering scheme and atomic displacement ellipsoids drawn at the 50% probability level is given in Figure 4.5. Programs used to solve structure: SHELXS97 and structure refinement with SHELXL97 (Sheldrick, 1997) to obtain $R_1 = 0.0653$ for 7545 $F_o > 4\text{sig}(F_o)$ and 0.0829 for all 9534 data, $wR_2 = 0.2236$, GooF = S = 1.629, Restrained GooF = 1.629 for all data. Refinement of data obtained at 100 K. Molecular graphics: ORTEP (Burnett and Johnson, 1996) and Mercury (<http://www.ccdc.cam.ac.uk.com>). Software used to prepare material for publication: SHELXL97.

The final cycles included all hydrogen atoms which refined anisotropic atomic displacement parameters, and included the 44 hydrogen atoms as riding model contributions in idealized positions ($d[\text{C}-\text{H}_{\text{methine}}] = 0.95 \text{ \AA}$, $d[\text{C}-\text{H}_{\text{methylene}}] = 0.99 \text{ \AA}$, $d[\text{C}-\text{H}_{\text{methyl}}] = 0.98 \text{ \AA}$).

Refinement converged with $R_1 = \Sigma||F_o|-|F_c|| / \Sigma|F_o| = 0.065$, $R_2 = \Sigma w(|F_o|-|F_c|)^2 / \Sigma w(|F_o|)^2)^{1/2} = 0.2236$, and the standard deviation of an observation of unit weight = 1.1037. For the final cycle refinement the number of observations 7545 reflections with $I > 2\sigma(I)$. The largest peak in the final difference density map was 1.69 e \AA^{-3} and the deepest hole was -0.80 e \AA^{-3} . Crystal structure data and details of the data collection and structural refinement are summarized in Table 3.1. Fractional triclinic atomic coordinates, and equivalent isotropic atomic displacement parameters (\AA^2) for the nonhydrogen atoms and hydrogen are given in Table 3.2 and Table 3.3. An *ORTEP* diagram of Fe(OEP)Cl in the triclinic form of Fe(OEP)Cl including the atom numbering is shown in Figure 3.1.

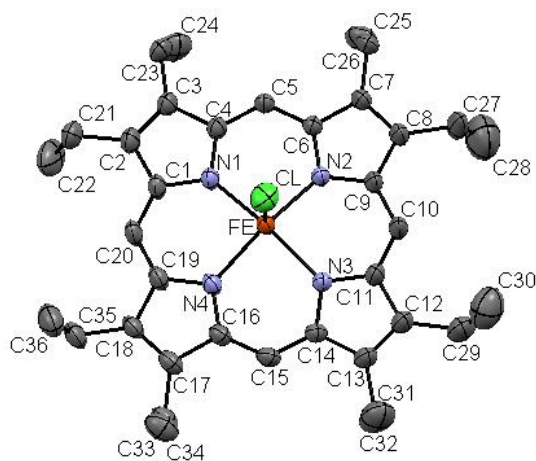


Figure 3.1 A *ORTEP* diagram showing molecular structure of the triclinic form of Fe(OEP)Cl. Hydrogen atoms omitted for clarity.

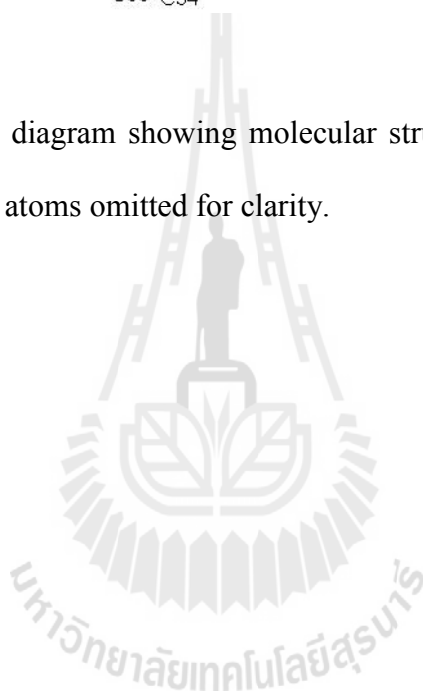


Table 3.1 Crystal Data and Refinement Details for Triclinic Fe(OEP)Cl.

Parameters	Triclinic Fe(OEP)Cl
Empirical formula	Fe(C ₃₆ H ₄₄ N ₄)Cl
M_r	624.05
Temperatur	100 °K
Crystal system	Triclinic
Space group	P-1
a	10.4495(3) Å
b	10.7805(4) Å
c	15.7360(5) Å
α ,	71.949(1) °
β	73.034(1) °
γ	82.440(1) °
V , Å ³	1610.42(9)
Z	2
$F(000)$	662
D_x	1.287 M gm ⁻³
Radiation type/wavelength	Mo K α / λ =0.71073 Å
Crystal dimens, mm	0.22x0.35x0.47

Table 3.1 (Continued).

Data collection	
Radiation source: fine-focus sealed tube	$R_{\text{int}} = 0.021$
Graphite	$\Theta_{\text{max}} = 30.6^\circ$, $\Theta_{\text{min}} = 2.0^\circ$
34934 measured reflections	$h = 14 \rightarrow 14$
9534 independent reflections	$k = -15 \rightarrow 15$
7545 reflections with $I > 2\sigma(I)$	$l = -22 \rightarrow 22$
Refinement	
Refinement on F^2	Primary atom site location: structure-invariant direct method
Least-squares matrix: full	Secondary atom site location: difference Fourier map
$R[F^2 > 2\sigma(F^2)] = 0.065$	Hydrogen site location: inferred from neighboring sites
$wR(F^2) = 0.2236$	H atoms treated by a mixture of independent and constrained refinement
Weighting scheme	calculated $w = 1/[\sigma^2(F_o^2) + (0.1P)^2]$
$S = 1.63$	where $P = (F_o^2 + 2F_c^2)/3$
9534 reflections	$(\Delta/\sigma)_{\text{max}} = 0.023$
387 parameters	$\Delta\rho_{\text{max}} = 1.69 \text{ e } \text{\AA}^{-3}$,
0 restraints	$\Delta\rho_{\text{min}} = -0.80 \text{ e } \text{\AA}^{-3}$

Table 3.2 Fractional Triclinic Atomic Coordinate, and Equivalent Isotropic Atomic Displacement Parameters (\AA^2) for the Nonhydrogen Atoms of $\text{Fe}(\text{OEP})\text{Cl}^a$.

Atom	x	y	z	U_{eq}
Fe	0.058525(3)	0.99220(3)	0.73407(2)	0.0568(2)
Cl	0.72671(7)	1.11839(8)	0.61346(5)	0.0568(2)
N1	0.40162(18)	1.05209(19)	0.70692(14)	0.0339(4)
N2	0.57984(19)	0.83383(18)	0.68811(14)	0.0326(4)
N3	0.70887(19)	0.87677(19)	0.81224(14)	0.0335(4)
N4	0.53030(19)	1.09556(19)	0.83095(14)	0.0352(4)
C1	0.3224(2)	1.1592(2)	0.72517(19)	0.0398(5)
C2	0.2195(2)	1.1888(3)	0.6762(2)	0.0438(6)
C3	0.2354(2)	1.0994(3)	0.62844(19)	0.0405(5)
C4	0.3504(2)	1.0156(2)	0.64712(17)	0.0350(5)
C5	0.4026(2)	0.9137(2)	0.60926(17)	0.0346(5)
C6	0.5078(2)	0.8282(2)	0.62903(16)	0.0321(4)
C7	0.5565(3)	0.7208(2)	0.59096(19)	0.0406(5)
C8	0.6601(3)	0.6612(3)	0.6269(2)	0.0533(8)
C9	0.6733(3)	0.7313(3)	0.6874(2)	0.0431(6)
C10	0.7656(3)	0.7000(3)	0.7395(2)	0.0547(8)
C11	0.7185(3)	0.7649(3)	0.7985(2)	0.0441(6)
C12	0.8760(3)	0.7274(3)	0.8540(2)	0.0533(7)
C13	0.8624(3)	0.8202(3)	0.8982(2)	0.0475(6)
C14	0.7580(2)	0.9107(2)	0.87390(17)	0.0365(5)
C15	0.7071(3)	1.0138(2)	0.91010(17)	0.0398(5)

Table 3.2 (Continued).

Atom	<i>x</i>	<i>y</i>	<i>z</i>	<i>U</i> _{eq}
C16	0.6007(2)	1.0987(2)	0.89150(16)	0.0356(5)
C17	0.5463(3)	1.2032(3)	0.93418(18)	0.0425(6)
C18	0.4445(3)	1.2644(3)	0.89687(18)	0.0409(5)
C19	0.4338(2)	1.1969(2)	0.83281(18)	0.0399(5)
C20	0.3394(3)	1.2258(3)	0.7828(2)	0.0455(6)
C21	0.1153(3)	1.3015(3)	0.6791(2)	0.0586(8)
C22	-0.0006(4)	1.2683(5)	0.7637(3)	0.0924(15)
C23	0.1511(3)	1.0824(3)	0.5705(2)	0.0476(6)
C24	0.0595(3)	0.9675(4)	0.6209(3)	0.0696(10)
C25	0.4978(3)	0.6824(3)	0.5258(2)	0.0474(6)
C26	0.3725(4)	0.6094(3)	0.5743(2)	0.0612(8)
C27	0.7506(5)	0.5459(4)	0.6051(4)	0.0936(17)
C28	0.7085(7)	0.4272(6)	0.6642(5)	0.1360(2)
C29	0.9663(4)	0.6027(4)	0.861(3)	0.0747(11)
C30	1.0829(5)	0.6197(5)	0.7828(4)	0.1039(15)
C31	0.9459(4)	0.8267(3)	0.9604(3)	0.0642(9)
C32	1.0660(5)	0.9087(4)	0.9111(4)	0.906(14)
C33	0.5961(3)	1.2348(3)	1.0046(2)	0.0517(7)
C34	0.7083(4)	1.3269(4)	0.9619(2)	0.0653(9)
C35	0.3599(3)	1.3819(3)	0.9146(2)	0.0543(7)
C36	0.4129(4)	1.5101(3)	0.8447(3)	0.0717(10)

^a The numbers given in parentheses are the estimated standard deviations in the least significant digits.

Table 3.3 Anisotropic Atomic Displacement Parameters for the Nonhydrogen Atoms of Fe(OEP)Cl^a.

Atom	U^{11}	U^{22}	U^{33}	U^{23}	U^{13}	U^{23}
Fe	0.02914(19)	0.0305(2)	0.0375(2)	0.00476(12)	-0.0139(14)	-0.01705(14)
Cl	0.0484(4)	0.0618(5)	0.0546(4)	-0.0049(3)	-0.0120(3)	-0.0094(3)
N1	0.0275(9)	0.0362(10)	0.0460(11)	0.0079(7)	-0.0142(8)	-0.0288(9)
N2	0.0334(9)	0.0317(9)	0.0430(10)	0.0077(7)	-0.0205(8)	-0.0191(8)
N3	0.0365(9)	0.0326(10)	0.0399(10)	0.0062(7)	-0.0199(8)	-0.0166(8)
N4	0.0346(9)	0.0353(10)	0.0433(11)	0.0043(8)	-0.0132(8)	-0.0212(8)
C1	0.0319(11)	0.0392(12)	0.0559(14)	0.0112(9)	-0.0152(10)	-0.0260(11)
C2	0.0343(12)	0.0467(14)	0.0562(15)	0.0118(10)	-0.0169(11)	-0.0237(12)
C3	0.0320(11)	0.0447(13)	0.0527(14)	0.0094(10)	-0.0187(10)	-0.0226(12)
C4	0.0289(10)	0.0359(12)	0.0458(13)	0.0045(8)	-0.0151(9)	-0.0172(10)
C5	0.0350(11)	0.0363(12)	0.0430(12)	0.0038(9)	-0.0193(10)	-0.0200(10)
C6	0.0347(10)	0.0305(11)	0.0389(11)	0.0033(8)	-0.0173(9)	-0.0158(9)
C7	0.0484(13)	0.0364(12)	0.0514(14)	0.0102(10)	-0.0267(12)	-0.0251(11)
C8	0.0635(17)	0.0488(16)	0.0740(2)	0.0268(13)	-0.0440(16)	-0.0427(15)
C9	0.0503(14)	0.0362(12)	0.0608(16)	0.0174(10)	-0.0336(13)	-0.0294(12)
C10	0.0608(17)	0.0503(16)	0.0810(2)	0.0283(13)	-0.0484(16)	-0.0437(15)
C11	0.0456(13)	0.0408(13)	0.0607(16)	0.0159(11)	-0.0324(13)	-0.0257(12)
C12	0.0606(17)	0.0491(16)	0.0708(19)	0.0196(13)	-0.0450(15)	-0.0296(14)
C13	0.0536(15)	0.0469(15)	0.0581(16)	0.0109(12)	-0.0364(13)	-0.0229(13)
C14	0.0400(12)	0.0385(12)	0.0391(12)	0.0017(9)	-0.0197(10)	-0.0154(10)
C15	0.0486(13)	0.0433(13)	0.0381(12)	-0.0029(11)	-0.01977(11)	-0.0182(10)

Table 3.3 (Continued).

Atom	U^{11}	U^{22}	U^{33}	U^{23}	U^{13}	U^{23}
C16	0.0398(12)	0.0371(12)	0.0360(11)	-0.0030(9)	-0.0106(10)	-0.0181(10)
C17	0.0461(13)	0.0417(13)	0.0342(13)	-0.0045(11)	-0.0077(11)	-0.0264(11)
C18	0.0448(13)	0.0392(13)	0.0441(13)	0.0026(10)	-0.0101(11)	-0.0267(11)
C19	0.0384(12)	0.0392(13)	0.0490(14)	0.0047(14)	-0.0102(10)	-0.0265(11)
C20	0.0385(12)	0.0467(14)	0.0643(17)	0.0158(11)	-0.0190(12)	-0.0364(11)
C21	0.0493(16)	0.0653(19)	0.0700(2)	0.0253(14)	-0.0288(15)	-0.0316(16)
C22	0.0610(2)	0.1200(4)	0.0840(3)	0.0400(2)	-0.0110(2)	-0.0380(3)
C23	0.0408(13)	0.0529(16)	0.0604(17)	0.0122(11)	-0.0286(13)	-0.0239(13)
C24	0.0490(17)	0.0900(3)	0.0830(2)	-0.0075(16)	-0.0339(17)	-0.0260(2)
C25	0.0591(16)	0.0470(15)	0.0549(16)	0.0132(12)	-0.0322(14)	-0.0313(13)
C26	0.0760(2)	0.0577(18)	0.0700(2)	-0.0119(15)	-0.0339(17)	-0.0287(16)
C27	0.1270(4)	0.0700(2)	0.1470(4)	0.0570(2)	-0.1070(3)	-0.0790(3)
C28	0.1570(6)	0.1000(4)	0.1720(6)	0.0260(4)	-0.0660(5)	-0.0600(4)
C29	0.0780(2)	0.0830(3)	0.0910(3)	0.0270(2)	-0.0580(2)	-0.0420(2)
C30	0.0780(3)	0.0950(3)	0.1370(4)	0.0040(2)	-0.0370(3)	-0.0270(3)
C31	0.0800(2)	0.0611(19)	0.0820(2)	0.0210(16)	-0.0620(2)	-0.0352(17)
C32	0.0940(3)	0.0860(3)	0.1260(4)	0.0000(2)	-0.0750(3)	-0.0380(3)
C33	0.0548(16)	0.0606(17)	0.0516(15)	-0.0018(13)	-0.0123(13)	-0.0348(14)
C34	0.0680(2)	0.0720(2)	0.0680(2)	-0.0185(17)	-0.0155(17)	-0.0339(17)
C35	0.0552(16)	0.0575(17)	0.0640(18)	0.0119(13)	-0.0160(14)	-0.0424(15)
C36	0.0850(3)	0.0560(2)	0.0750(2)	0.0119(18)	-0.0160(2)	-0.0317(18)

^a The numbers given in parentheses are the estimated standard deviations in the least significant digits.

Table 3.4 Fractional Triclinic Coordinates and Isotropic Atomic Displacement Parameters (\AA^2) for the Hydrogen Atoms of Fe(OEP)Cl.

Atom	x	y	z	U_{iso}
H5	0.3625	0.9014	0.5657	0.042
H10	0.8242	0.6260	0.7340	0.066
H15	0.7493	1.0280	0.9520	0.048
H20	0.2801	1.2993	0.7887	0.055
H21A	0.1580	1.3788	0.6781	0.070
H21B	0.0820	1.3244	0.6231	0.070
H22A	-0.0524	1.2020	0.7596	0.139
H22B	-0.0580	1.3470	0.7678	0.139
H22C	0.0392	1.2344	0.8190	0.139
H23A	0.2104	1.0680	0.5123	0.057
H23B	0.0957	1.1634	0.5540	0.057
H24A	0.1140	0.8857	0.6303	0.104
H24B	-0.0003	0.9658	0.5835	0.104
H24C	0.0060	0.9775	0.6811	0.104
H25A	0.4783	0.7623	0.4787	0.057
H25B	0.5652	0.6275	0.4930	0.057
H26A	0.3931	0.5255	0.6162	0.092
H26B	0.3349	0.5941	0.5284	0.092
H26B	0.3073	0.6608	0.6102	0.092
H27A	0.7562	0.5466	0.5411	0.112

Table 3.4 (Continued).

Atom	x	y	z	U_{iso}
H27B	0.8419	0.5572	0.6075	0.112
H28A	0.7050	0.4245	0.7277	0.204
H28B	0.7711	0.3580	0.6461	0.204
H28C	0.6190	0.4140	0.6612	0.204
H29A	0.9949	0.5800	0.9191	0.090
H29B	0.9153	0.5297	0.8641	0.090
H30A	1.0548	0.6538	0.7253	0.156
H30B	1.1318	0.5354	0.7839	0.156
H30C	1.1412	0.6814	0.7859	0.156
H31A	0.9763	0.7370	0.9900	0.077
H31B	0.8883	0.8629	1.0102	0.077
H32A	1.1269	0.8699	0.8647	0.136
H32B	1.1142	0.9123	0.9561	0.136
H33A	1.0371	0.9972	0.8803	0.136
H34A	0.6273	1.1529	1.0445	0.062
H34B	0.5211	1.2742	1.0446	0.062
H34C	0.6757	1.4113	0.9272	0.098
H35A	0.3553	1.3849	0.9777	0.065
H35B	0.2678	1.3730	0.9127	0.065
H36A	0.5054	1.5180	0.8443	0.108
H36B	0.3571	1.5834	0.8621	0.108
H36C	0.4103	1.5111	0.7827	0.108

Table 3.5 Selected Bond Distances and Angles of Triclinic Fe(OEP)Cl.

Atoms	Distance (Å)	Atoms	Angle (°)
Fe–Cl	2.2202(8)	N1–Fe–N3	153.44
Fe–N1	2.0649 (18)	N2–Fe–N4	153.42
Fe–N2	2.0628 (18)	N1–Fe–Cl	103.20
Fe–N3	2.0702 (18)	N2–Fe–Cl	102.07
Fe–N4	2.0662 (19)	N3–Fe–Cl	103.07
N1–C1	1.3841 (27)	N4–Fe–Cl	104.51
N1–C4	1.3807 (29)	C1–N1–C4	105.47
N2–C6	1.3749 (28)	N1–C1–C2	110.10
N2–C9	1.3759 (28)	C2–C3–C4	106.24
N3–C11	1.3794 (29)	C3–C4–N1	110.75
N3–C14	1.3781 (29)	Fe–N1–C4	126.26
N4–C16	1.3735 (30)	N1–C4–C5	124.62
N4–C19	1.3874 (29)	C4–C5–C6	126.05
C1–C2	1.4471 (36)	C5–C6–N2	124.79
C1–C20	1.3785 (36)	C6–N2–C9	105.27
C2–C3	1.3620 (37)	N2–C6–C7	110.59
C2–C21	1.5232 (35)	C6–C7–C8	106.61
C3–C4	1.4500 (30)	C7–C8–C9	106.94
C3–C24	1.5013 (35)	C8–C9–N2	110.57

Table 3.5 (Continued).

Atoms	Distance (Å)	Atoms	Angle (°)
C4–C5	1.3845 (31)	C9–C10–C11	127.05
C4–N1	1.3807 (29)	C11–N3–C14	105.06
C5–C6	1.3816 (31)	N3–C11–C12	110.08
C5–H5	0.95	C11–C12–C13	106.87
C6–C7	1.4343 (32)	C12–C13–C14	106.90
C7–C8	1.3609 (37)	C13–C14–N3	110.46
C7–C25	1.5144 (34)	N3–C14–C15	124.23
C8–C9	1.4297 (35)	C14–C15–C16	126.59
C8–C27	1.5245 (41)	C16–N4–C19	106.07
C9–C10	1.3869 (36)	N4–C16–C17	110.24
C9–C10	1.3869 (36)	N4–C16–C17	110.24
C10–C11	1.3788 (37)	C16–C17–C18	106.65
C10–H11	0.95	C17–C18–C19	107.20
C11–C12	1.4426 (36)	C18–C19–N4	109.82
C12–C13	1.3589 (39)	N4–C19–C20	124.59
C12–C29	1.5316 (43)	C19–C20–C1	126.82
C13–C14	1.4358 (34)	C20–C1–N1	124.25
C13–C31	1.4961 (37)	C2–C21–C22	112.22
C14–C15	1.3794 (34)	C3–C23–C24	112.25

Table 3.5 (Continued).

Atoms	Distance (Å)	Atoms	Angle (°)
C15–C16	1.3835 (35)	C7–C25–C26	113.13
C15–H16	0.95	C8–C27–C28	114.63
C17–C18	1.3604 (39)	C13–C31–C32	113.84
C17–C33	1.4947 (37)	C17–C33–C34	112.87
C18–C19	1.4493 (34)	C18–C35–C36	113.21
C18–C35	1.4985 (35)	C4–C5–H5	117.00
C19–C20	1.3816 (36)	C9–C10–H10	116.51
C20–H20	0.9500	C14–C15–H15	116.72
C21–C22	1.4985 (50)	C1–C20–H20	116.61
C21–H21A	0.99	C2–C21–H21A	109.19
C21–H21B	0.99	C2–C21–H21B	109.18
C22–H22A	0.98	C3–C23–H23A	109.15
C22–H22B	0.98	C3–C23–H23B	109.15
C22–H22C	0.98	C7–C25–H25A	108.97
C23–C24	1.5292 (46)	C7–C25–H25B	108.97
C23–H23A	0.99	C8–C27–H27A	108.76
C23–H23B	0.99	C8–C27–H27B	108.74
C24–H24A	0.98	C12–C29–H29A	109.45
C24–H24B	0.98	C12–C29–H29B	109.44
C24–H24C	0.98	C13–C31–H31A	108.83

Table 3.5 (Continued).

Atoms	Distance (Å)	Atoms	Angle (°)
C25–C26	1.4953 (45)	C13–C31–H31B	108.84
C25–H25A	0.99	C17–C33–H33A	109.02
C25–H25B	0.99	C17–C33–H33B	109.01
C26–H26A	0.98	C18–C35–H35A	108.94
C26–H26B	0.98	C18–C35–H35B	108.94
C26–H26C	0.98	C21–C22–H22A	109.47
C27–C28	1.3665 (71)	C21–C22–H22B	109.47
C28–H28A	0.98	C21–C22–H22C	109.46
C28–H28B	0.98	C23–C24–H24A	109.47
C28–H28C	0.98	C23–C24–H24B	109.48
C29–C30	1.4440 (68)	C23–C24–H24C	109.47
C31–C32	1.5018 (59)	C25–C26–H26A	109.47
C31–H31A	0.99	C25–C26–H26B	109.49
C31–H31B	0.99	C25–C26–H26C	109.46
C32–H32A	0.98	C27–C28–H28A	109.47
C32–H32B	0.98	C27–C28–H28B	109.47
C32–H32C	0.98	C27–C28–H28C	109.48
C33–C34	1.4988 (45)	C29–C30–H30A	109.46
C33–H33A	0.99	C29–C30–H30B	109.48
C33–H33B	0.99	C29–C30–H30C	109.47
C34–H34A	0.98	C31–C32–H32A	109.48

Table 3.5 (Continued).

Atoms	Distance (Å)	Atoms	Angle (°)
C34–H34B	0.98	C31–C32–H32B	109.46
C34–H34C	0.98	C31–C32–H32C	109.48
C35–C36	1.5266 (48)	C33–C34–H34A	109.46
C35–H35A	0.99	C33–C34–H34B	109.47
C35–H35B	0.99	C33–C34–H34C	109.48
C36–H36A	0.98	C35–C36–H36A	109.48
C36–H36B	0.98	C35–C36–H36B	109.46
C36–H36C	0.98	C35–C36–H36C	109.48

^aThe numbers given in parentheses are the estimated standard deviations in the least significant digits.

3.3 Results and Discussion

3.3.1 Electronic absorption spectra.

The UV-vis spectra of Fe(OEP)Cl (Figure 4.3) in CH₂Cl₂ solution showed the Soret band in the range of 381nm and Q band at 522 and 636 nm, this Soret band is in agreement with the visible absorption spectra of porphyrins and metalloporphyrins (Scheidt, 2000; Senge, 2000; Shelnutt, 2000). The red shift of the Soret band of the visible spectrum for the triclinic form Fe(OEP)Cl suggested that porphyrin ring in the present complex also adopts conformation, which are mostly based on studies of porphyrin complexes with metals other than iron (Weiss, Fischer, Bulach, Schünemann, Gerdan, Trautwein, Shelnutt, Gros, Tabard, and Guillard, 2002).

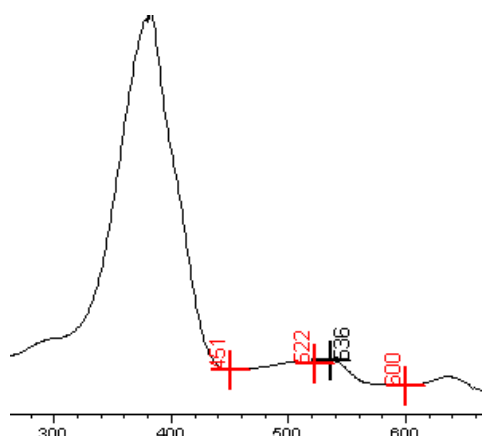


Figure 3.2 Absorbance spectrum of triclinic, Fe(OEP)Cl.

3.3.2 Infrared spectra

The infrared spectrum of Fe(OEP)Cl can be seen in Figure 3.3 and this spectrum is in agreement with that of Fe(OEP)Cl (Puntharod, Webster, Asghari-Khiavi, Bamberg, Safinejad, Rivadehi, Langford, Haller, and Wood, 2010; Ogoshi, Watanabe, Yoshida, Kincaid and Nakamoto, 1973).

The triplet bands near 3000 cm^{-1} were assigned to =C–H stretching in aromatic ring, the band near 1465 cm^{-1} was assigned as antisymmetric CH_3 deformation, which normally is in the $1470\text{--}1440\text{ cm}^{-1}$, and 1268 cm^{-1} region was assigned as in-plane CH deformation. Another band was observed in the $800\text{--}900\text{ cm}^{-1}$ regions which suggested the Fe(OEP)Cl is contaminated with $[\text{Fe}(\text{OEP})]_2\text{O}$ in starting material as reported by Puntharod (2010).

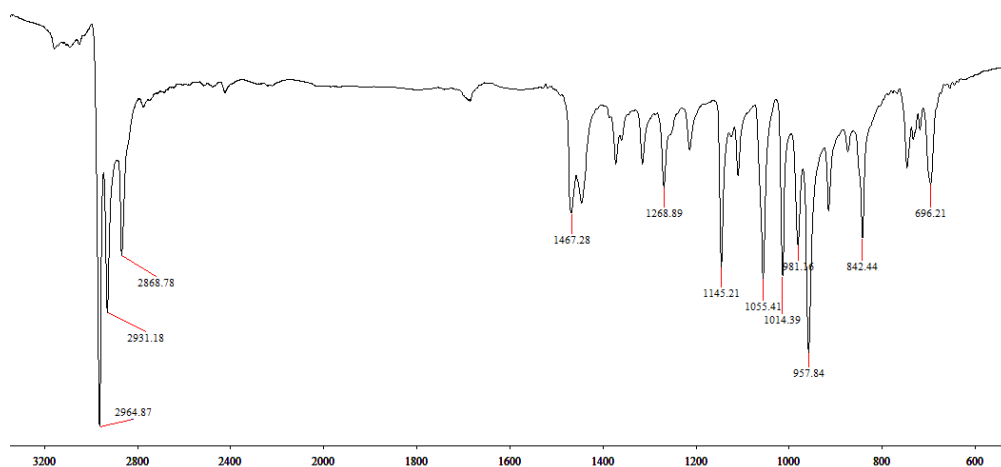


Figure 3.3 FT-IR spectrum of Fe(OEP)Cl in present work.

3.3.4 Crystal Structure of the Triclinic Polymorph of Chloro(2,3,7,8,12,13,17,18-octaethylporphyrinato) Iron(III).

The core diagram of the Fe(OEP)Cl triclinic form is exhibited in Figure 3.4, which shows Fe–N bond distances, the average C_a – C_m bond distance, C_a – C_b , the average C_m angle, and the average C_a angle. Table 3.4 provides a summary of crystal data intensity data collection parameters, and final refinement statistics for the Fe(OEP)Cl triclinic, monoclinic and solvated forms (\AA^2). The crystal of Fe(OEP)Cl in triclinic form belongs to the space group P-1. The Fe(OEP)Cl triclinic form contains two asymmetric units per unit cell, density and volume of Fe(OEP)Cl triclinic form slightly greater than those of Fe(OEP)Cl monoclinic form, but less than the solvate form. From this observation, the Fe(OEP)Cl triclinic form may be less stable than monoclinic form and solvate form.

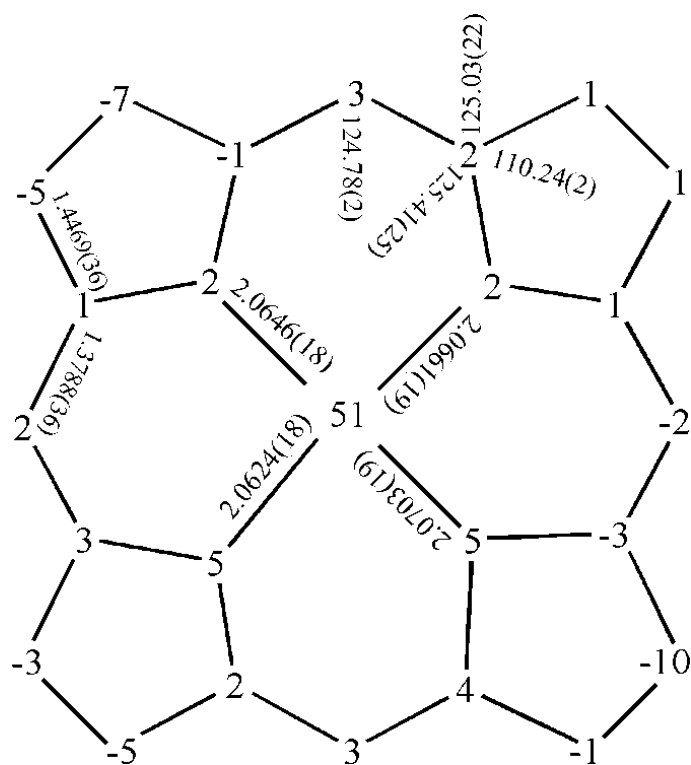


Figure 3.4 Formal diagram of a single molecule of the triclinic form of Fe(OEP)Cl showing bond lengths in Ångstroms, angles in degree, and showed the displacements of the 24 atoms out of the mean plane.

Table 3.6 Summary of Crystal Data, Intensity Data Collection Parameters, and Final Statistics of the Refinement of Fe(OEP)Cl.

Molecule	Monoclinic	Triclinic	Solvate
	Fe(OEP)Cl ^a	Fe(OEP)Cl ^b	Fe(OEP)Cl ^c
Empirical formula	[Fe(C ₃₆ H ₄₄ N ₄)Cl]	[Fe(C ₃₆ H ₄₄ N ₄)Cl]	[Fe(C ₃₆ H ₄₄ N ₄)Cl] · 1.5 CH ₂ Cl ₂
<i>M_r</i>	624.05	624.05	751.44
Temperature, °K	126	100	293
Crystal system	Monoclinic	Triclinic	Triclinic
Space group	P21/c	P-1	P-1
<i>a, b, c, Å</i>	15.045(9)	10.449(3)	10.062(6)
	22.154(12)	15.736(5)	13.767(5)
	9.972(5)	10.780(4)	14.754(5)
<i>α, β, γ, degree</i>	90	71.95(1)	66.46(2)
	106.05(4)	73.03(1)	80.55(2)
	90	82.44(1)	76.10(2)
<i>V, Å³</i>	3194(3)	1610.42	1813.5(14)
<i>Z</i>	4	2	2
<i>d_{calc}</i> , mg/m ³	1.298	1.287	1.376
Crystal dimensions, mm ³	0.53x0.30x0.25	0.22x0.35x0.47	0.02x0.11x0.08
<i>R_I</i>	0.048	0.065	0.059

^a Senge et al. 2005

^bthis work.

^c Safo et al., 2010.

The Fe–Cl distance, 2.2201(8) Å, which is similar with the two crystalline forms of triclinic and monoclinic of Fe(OEP)Cl and the solvate form, while the monoclinic form, 2.231(1) Å (Senge, 2005) and solvate form, 2.243(13) Å (Safo, Buentello, Oliver, and Scheidt, 2010) have a slightly longer Fe–Cl distances as shown in Table 3.6. Also the Fe–Cl distance in the triclinic form is not significantly different with the Fe–Cl distance 2.211(1) Å of Fe(TPP)Cl (Scheidt and Finnegan, 1989). The Fe–Np bond distance on the triclinic form is similar with the monoclinic form and solvated form. The Fe displacement out of the 24-atom mean plane of the triclinic form is 0.51(7) Å which is greater than the monoclinic but similar with the solvated forms.

Table 3.6 Selected structural parameters (Å) of Fe(OEP)Cl.

Heme models	Fe–Np (Å)	Fe–Cl (Å)	displacement of Fe from mean plane (Å)	Form
Fe(C ₃₆ H ₄₄ N ₄)Cl ^a	2.071(2)	2.231(1)	0.50(1)	Monoclinic
Fe(C ₃₆ H ₄₄ N ₄)Cl ^b	2.066(19)	2.220(8)	0.51(7)	Triclinic
Fe(C ₃₆ H ₄₄ N ₄)Cl·1.5CH ₂ Cl ₂ ^c	2.065(3)	2.243(13)	0.51(1)	Solvate

^a Senge, 2005. ^b This work. ^c Safo et al., 2010

Figure 3.5 shows a formal diagram of the porphyrin core with the displacements of the 24 atom porphyrin core. Three pyrrole rings were below and one pyrrole ring was above the mean plane of porphyrin core in the triclinic form. The triclinic form is exhibited the wave core conformation while in the monoclinic, solvate, and $[\text{Fe}(\text{OEP}^\bullet)\text{Cl}]^+$ are exhibited in the saddled core conformation.

However, the average displacement of 24 atoms of the porphyrin mean plane for the monoclinic, triclinic, solvate forms, and $[\text{Fe}(\text{OEP}^\bullet)\text{Cl}]^+$ are 0.08333, 0, 0.04167, and 0.66667 Å, respectively (Figure 3.5). The results indicated that the conformation of the porphyrin core in the triclinic form is nearly planar which is the average of the porphyrin planes is nearly zero Å.

The displacement of the Fe atom in the triclinic form out of the mean plane of the porphyrin core 0.51(7) Å is slightly greater than that in the monoclinic form, 0.50(1) Å while similar to that in the solvate form, 0.51(1) Å, but greater than those $[\text{Fe}(\text{OEP}^\bullet)\text{Cl}]^+$, 0.43 Å. These Fe displacement out-of-plane are consistent with literature values reported in the $\text{Fe}(\text{OEP})\text{Cl}$ monoclinic form (Senge, 2005) and a solvate form of $[\text{Fe}(\text{C}_{36}\text{H}_{44}\text{N}_4)\text{Cl}]\cdot 1.5\text{CH}_2\text{Cl}_2$ (Safo, Buentello, Oliver, and Scheidt, 2010).

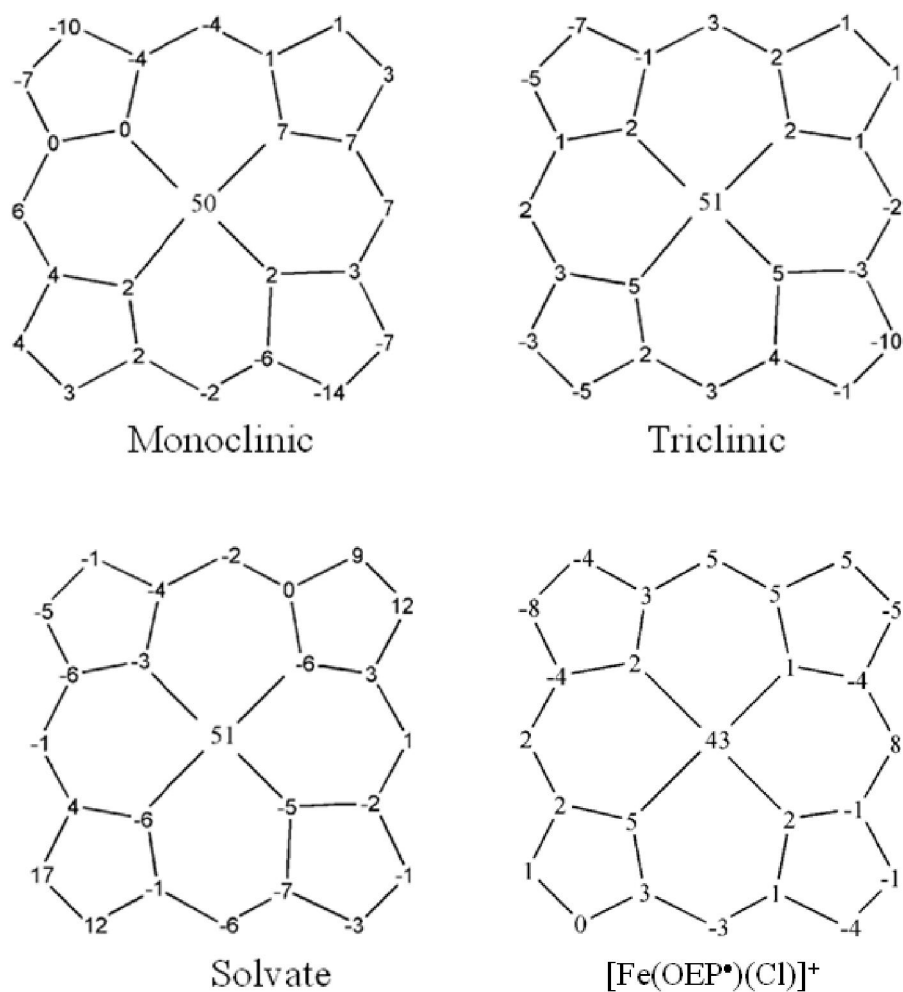


Figure 3.5 Formal diagrams of the porphyrin core of Fe(OEP)Cl: monoclinic form (Senge, 2005). triclinic form (this work); solvate form (Safo et al., 2010). Deviation from the mean plane of 24-atom porphyrin core of the perpendicular displacement of each atom, in units 0.01 Å.

Figure 3.6 shows the calculated X-ray powder diffraction (XRD) patterns of the three forms of Fe(OEP)Cl, the monoclinic, triclinic, and solvate forms, respectively. The relative arrangement of the peripheral methyl groups in the three forms of Fe(OEP)Cl are shown in Figure 3.7. The four peripheral ethyl groups of the two half rings are all up or all down, while the eight ethyl groups of the monoclinic form are disposed five ethyl groups down and three ethyl groups up and all eight ethyl groups in solvate form and a two species with crystal with a fullerene in the lattice are down, called octopus shape (Olmstead, Costa, Maitra, Noll, Phillips, Van Calcar, and Balch, 1999). The four “up”/four “down” orientation of the ethyl groups is commonly seen for OEP derivatives with the degree of interring overlap. The dimeric units are extended by the formation of hydrogen bonding network (Cheng, Safo, Orosz, Reed, Debrunner, and Scheidt, 1994).

The intermolecular interactions between the porphyrin π systems and C–H of the methylene and methyl group, and numerous of C–H \cdots Cl in triclinic form are shown in Figure 3.7 which form dimer via slipped parallel. The C–H \cdots Cl distance is 2.877 Å while the C–H $\cdots\pi$ interactions distance is 3.467 Å. Analysis of the non-hydrogen atoms bonding from the plane defined by the center of the two pyrrole rings showed the interactions between two porphyrin rings indicated that a very weak interaction is formed.

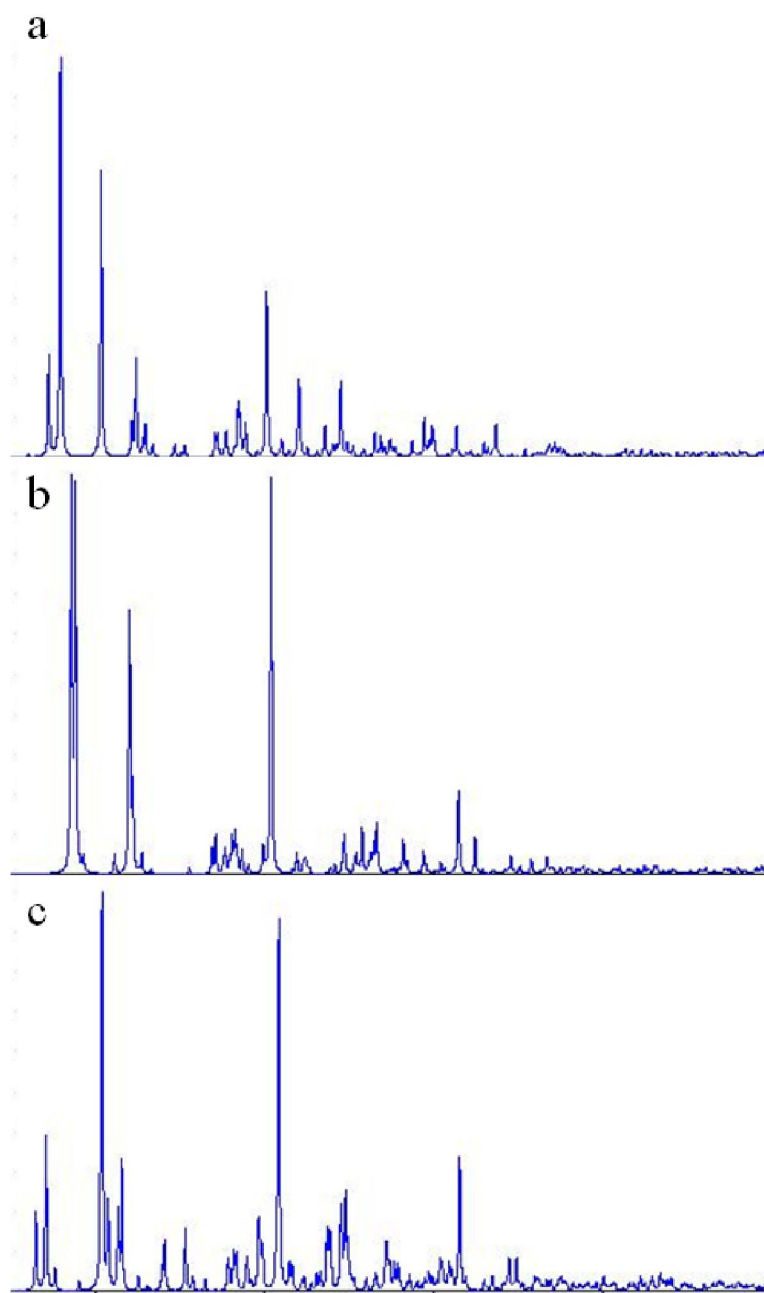


Figure 3.6 X-Ray Powder Diffraction spectra of Fe(OEP)Cl calculated by Mercury a: monoclinic form. b: triclinic form. c: solvate form.

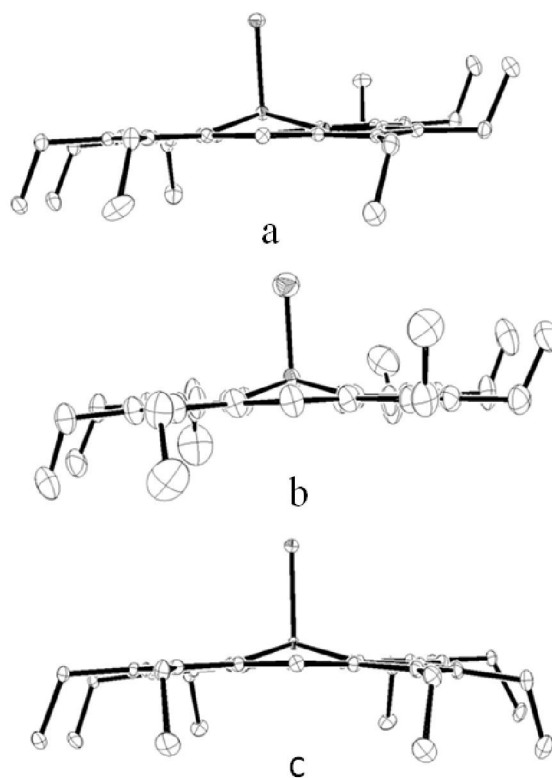


Figure 3.7 Different stereochemistry of Fe(OEP)Cl a: monoclinic form. b: triclinic form; c: solvate form.

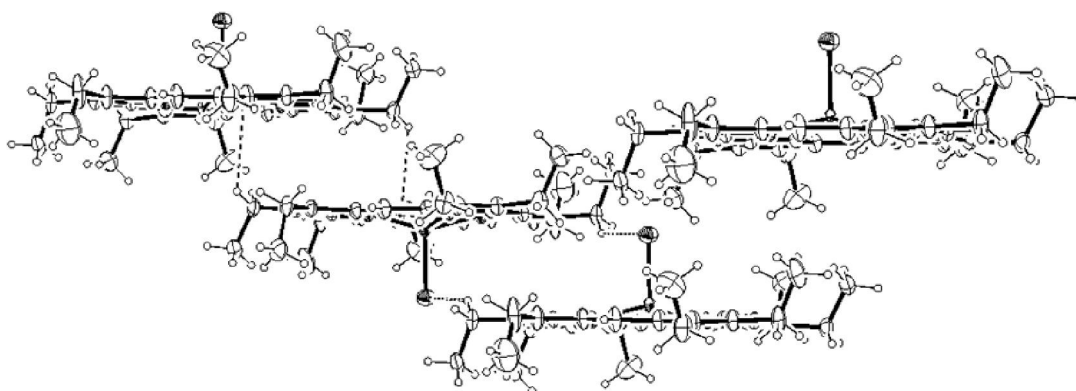


Figure 3.8 ORTEP drawing shows the hydrogen bonds in the triclinic form of Fe(OEP)Cl.

For monoclinic form the distance of C–H···Cl is 2.864 Å while the interactions between two porphyrin rings distance of 3.408 Å indicated that a very weak interaction is formed which is similar with the triclinic form. The molecular packing of monoclinic form is formed dimer by layer stacking. The slipped parallel interaction in triclinic form may be weaker with less density and the stacking distance increase compared to those observed in monoclinic and solvated form.

This study considers the conformation of the two crystal forms, monoclinic and triclinic given the difference in the arrangement of the ethyl groups between them. The conformations seen for the four ethyl groups in the triclinic form (C12, C13, C17 and C18) are quite interesting; these groups are displaced away from the mean plane of the macrocycle. The packing arrangement in the triclinic form is shows the ethyl groups are in a staggered configuration, overlapping in between the pyrrole ring and C_m these generated π cloud along this region (Figure 3.9). The monoclinic form exhibited an eclipsed conformation in between two pyrrole ring (Figure 3.10) via the stacked manner of the pyrrole rings. The van der Waals contacts for triclinic and monoclinic form are shown in Table 3.7. The result suggested that the triclinic dimer and monoclinic dimer are held together within Van der Waals interactions. The orientation of the ethyl groups also facilitates the adjoining porphyrin-porphyrin interactions. However, in Fe(OEP)Cl the position of the C–H···Cl bond prohibits such close contact and leads to weak interaction in face-to-face pattern (Olmstead, Costa, Maitra, Noll, Phillips, Van Calcar, and Balch, 1999) which is methyl groups are within the Van der Waals radius of 2.0 Å (Bürgi, Restori, Schwarzenbach, Balch, Lee, Noll, and Olmstead, 1994).

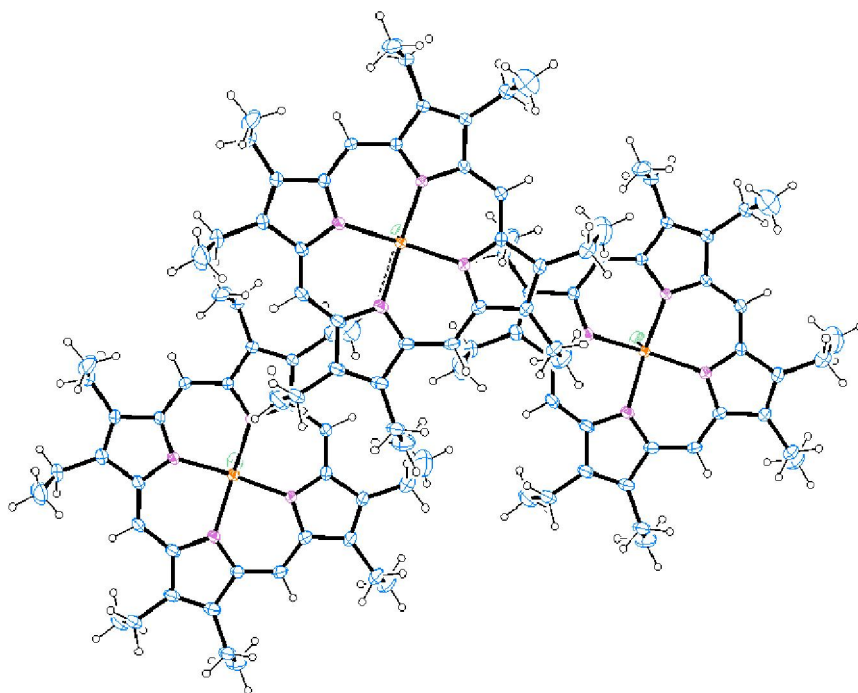


Figure 3.9 Projection view of the packing in the triclinic form of Fe(OEP)Cl showing the C–H...Cl hydrogen bond to form a Fe(OEP)Cl dimer via stacking.

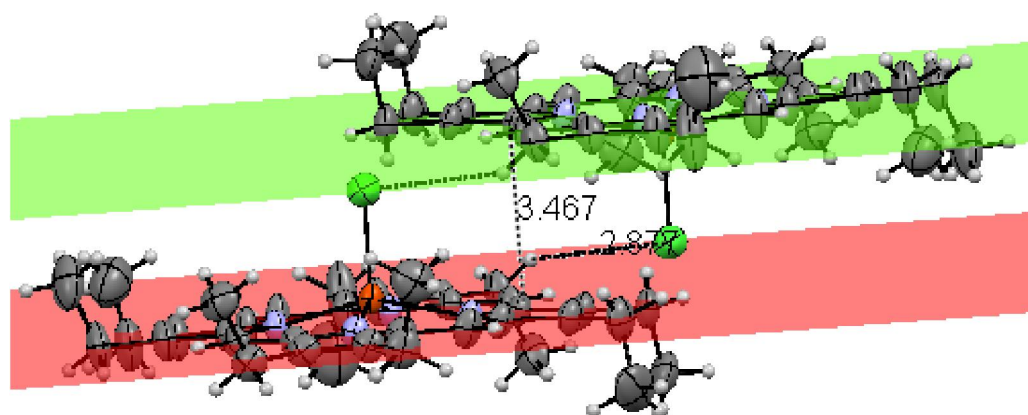


Figure 3.10 Nonbonded interaction between two porphyrin rings in the triclinic form showing the C–H... π and C–H...Cl distances.

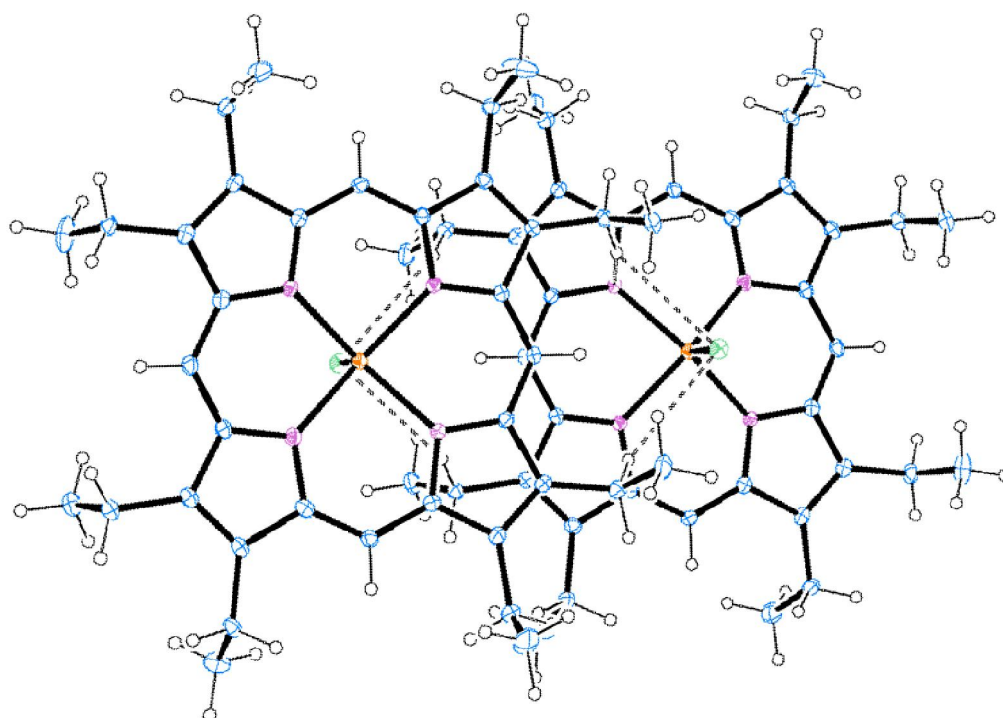


Figure 3.11 Projection view of the packing in the monoclinic form of Fe(OEP)Cl showing the C–H...Cl hydrogen bonds to form Fe(OEP)Cl dimer via stacking.

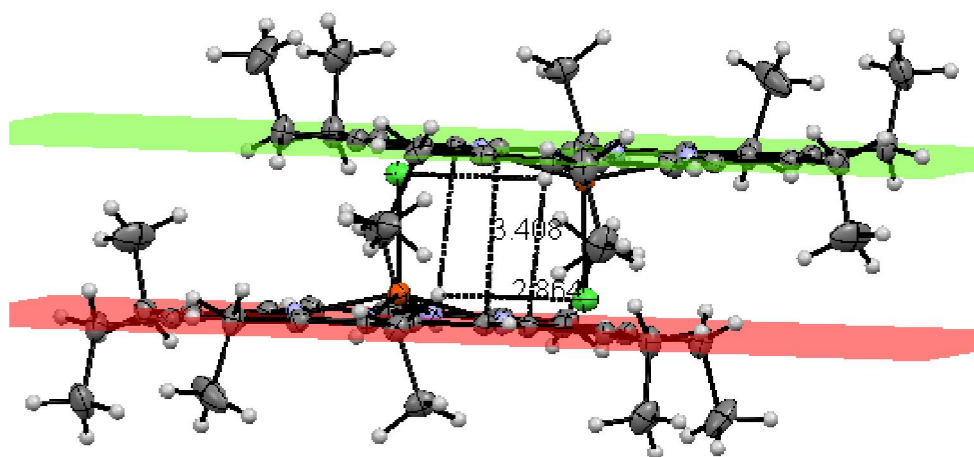


Figure. 3.11 Nonbonded interactions between two porphyrin rings in the monoclinic form of Fe(OEP)Cl showing the C–H... π and C–H...Cl distances.

Table 3.7 Selected Van der Waals Contacts in Triclinic and Monoclinic Fe(OEP)Cl.

Triclinic		Monoclinic	
interaction	Distance (Å)	interaction	Distance (Å)
H5...N1	3.269	H15...H17	2.228
H5...N2	3.263	H31b...H21a	2.277
H10...N2	3.260	H71a...H5a	2.255
H10...N3	3.258	H5...N21	3.275
H15...N3	3.259	H5...N22	3.266
H15...N4	3.262	H10...N22	3.267
H20...N1	3.264	H10...N23	3.270
H20...N4	3.271	H15...N23	3.266
H23a...N2	3.222	H15...N24	3.267
H24c...N3	3.292	H18e...N24	3.137
H25a...N1	3.002	H20...N21	3.276
H15...C32	3.538	H21b...N24	3.075
H22b...C30	3.555	H71b...N23	3.116
H25b...C3	3.531	H81b...N22	3.075
H26a...C25	3.502	H12a...C32	3.526
H26a...C28	3.549	H12e...C71	3.500
H26b...C7	3.346	H13b...C122	3.524
H26b...C25	3.465	H13d...C12	3.459
H28a...C34	3.515	H13e...C72	3.555

Table 3.7 (Continued).

Triclinic		Monoclinic	
Interaction	Distance (Å)	Interaction	Distance (Å)
H28c...C19	3.277	H17d...C22	3.542
H26c...C25	3.363	H17e...C15	3.525
H26c...C36	3.419	H18a...C20	3.524
H26c...C26	3.433	H18c...C16	3.519
H29a...C29	3.518	H18d...C81	3.564
H29a...C22	3.537	H18e...C17	3.528
H30a...C26	3.547	H18e...C14	3.563
H30b...C35	3.516	H21a...C171	3.538
H30c...C24	3.553	H22a...C1	3.530
H30c...C31	3.566	H32a...C122	3.542
H31a...C34	3.528	H32b...C122	3.538
H31b...C19	3.547	H32c...C21	3.525
H32a...C29	3.541	H32c...C22	3.555
H32a...C4	3.551	H72a...C9	3.550
H32b...C15	3.518	H82a...C181	3.550
H32c...C1	3.518	H82b...C181	3.546
H32c...C32	3.560		
H33b...C36	3.543		

In addition, these distortions are caused by only the weak nonbonding interactions, van der Waals, hydrogen bonding, axial ligation or by the environment of the heme (Jenzent, Ma and Shelnut, 1998). The orientations of the ethyl four up and down could possibly reduce the range of geometries possible to two equivalent orientations arising from steric effect between the methyl and chloride ion which can be seen by elongated of the C–H...Cl bond distance. However, the ethyl groups on porphyrins molecule also avoid contact with the adjacent porphyrin molecules which make close face-to-face contact (Olmstead, Costa, Maitra, Noll, Phillips, Van Calcar, and Balch, 1999).

3.4 Conclusion

In conclusion, the structure of Fe(OEP)Cl was characterized by FTIR and single crystal X-ray crystallography techniques and the supramolecular interactions analyzed with *ORTEP III* software. The new conformation Fe(OEP)Cl is characterized as falling in a triclinic space group. The crystal structure reveals a planar porphyrin macrocycle and the core conformation is in the wave mode. The arrangement of the ethyl groups in the triclinic form of Fe(OEP)Cl in the present work showed four ethyl groups of the half ring up and down. The arrangement of the ethyl groups may relate to a steric clash of the peripheral groups and favors a staggered configuration which leads to the dimeric formation via a slipped-parallel in the crystal packing. The arrangement of the ethyl groups may be reduce asymmetric unit in the unit cell when compare with the monoclinic form and changing in space group. Moreover, the C–H...Cl bond distance is prevent the close contact between two porphyrin rings

suggested that the crystal packing of the triclinic, Fe(OEP)Cl is held together by a very weak interactions.

3.5 References

- Bürgi, H. B., Restori, R., Schwarzenbach, D., Balch, A. L., Lee, W. J., Noll, B. C., and Olmstead, M. M. (1994). Nanocrystalline domains of a monoclinic modification of benzene stabilized in a crystalline matrix of C₆₀. **Chemistry of Materials**. 6: 1325-1329.
- Burnett, M. N. and Johnson, C. K. (1996). *ORTEP-III*: Oak Ridge Thermal Ellipsoid Plot Program for Crystal Structure Illustration, Report ORNL-6895, **Oak Ridge National Laboratory**, Tennessee, USA.
- Cheng, B., Safo, M. K., Orosz, R. D., Reed, C. A., Debrunner, P. G., and Scheidt, W. R. (1994). Synthesis, structure, and characterization of five-coordinate aquo(octaethylporphinato)iron(III). **Inorganic Chemistry**. 33: 1319-1324.
- Cullen, D. L. and Meyer, E. F. Jr. (1974). Crystal and molecular structure of the triclinic form of 1,2,3,4,5,6,7,8-octaethylporphyrinatonicel(II). A comparison with the tetragonal form. **Journal of the American Chemical Society**. 96: 2095-2102.
- Ellison, M. K., Schulz, C. E., and Scheidt, W. R. (2002). Structure of the deoxymyoglobin model [Fe(TPP)(2-MeIH)] reveals unusual porphyrin core distortions. **Inorganic Chemistry**. 41: 2173-2181.
- Hatano, K. and Uno, T. (1990). Preparation and molecular structure of (methoxo)-(octaethylporphinato) iron(III). *Bulletin Chemical Society Japan*, 63: 1825-1827.

- Medforth, C. J., Senge, M. O., Smith, M. K., Sparks, D. L., and Shelnut, J. A. (1992). Nonplanar distortion modes for highly substituted porphyrins. **Journal of the American Chemical Society**. 114: 9859-9869.
- Meyer, E. F. (1972). The crystal and molecular structure of nickel(II) octaethylporphyrin. **Acta Crystallographica B**. 28: 2162-2167.
- Neal, T. J., Cheng, B., Ma, J.-G., Shelnut, J. A., Schulz, C. E. and Scheidt, W. R. (1999). Conformational diversity in (octaethylporphinato)(trichloroacetato)-iron(III) derivatives. **Inorganica Chimica Acta**. 291: 49-59.
- Ohgo, Y., Neya, S., Ikeue, T., Takahashi, M., Takeda, M., Funasaki, N., and Nakamura, M. (2002). Molecular structural of five-coordinated halide ligated iron(III) porphyrin, porphycene, and corphycene complexes. **Inorganic Chemistry**. 41: 4627-4629.
- Ogoshi, H., Watanabe, E. Yoshida, Z., Kincaid, J., and Nakamoto, K. (1973). Synthesis and far infrared spectra of ferric octaethylporphine complexes. **Journal of the American Chemical Society**. 95: 2845-2849.
- Olmstead M. M., Costa, D. A., Maitra, K., Noll, B. C., Phillips, S. L., van Calcar, P. M., and Balch, A. L. (1999). Interaction of curved and flat molecule surfaces. The structures of crystalline compounds composed of fullerene (C₆₀, C₆₀O, C₇₀, and C₁₂₀O) and metal octaethylporphyrin units. **Journal of the American Chemical Society**. 121: 7090-7097.
- Puntharod, R., Webster, G. T., Asghari-Khiavi, Bambery, K. R., Safinejad, F., Rivadehi, S., Langford, S. L., Haller, K. J., and Wood, B. R. (2010). Supramolecular interactions playing an integral role in the near-infrared Raman “excitonic” enhancement observed in β-hematin (malaria pigment) and other

- related heme derivatives. **The Journal of Physical Chemistry B**. 114: 12104-12115.
- Puntharod, R. (2008). Synthesis and structural studies of malaria pigment model systems. Suranaree University of Technology, **Ph.D. thesis**. p.159.
- Safo, M. K., Buentello, K. E., Oliver, A. G., and Scheidt, W. R. (2010). Chlorido(2,3,7,8,12,13,17,18-octaethylporphyrinato)iron(III) dichloromethane sesquisolvate. **Acta Crystallographica E**. 66: m733.
- Scheidt, W. R. and Gouterman, M. (1983). **Iron Porphyrins**, Part One, edited by A. B. P. Lever and H. B. Gray: 89-139, Reading, MA: Addison-Wesley.
- Scheidt, W. R. and Lee, Y. J. (1987). Recent advance in the stereochemistry of metallotetrapyrroles. **Structural Bonding (Berlin)**. 64: 1-70.
- Scheidt, W. R., Song, H., Haller, K. J., Safo, M. K., Orosz, R. D., Reed, C. A., Debrunner, P. G., and Schulz, C. E. (1992). Characterization of Fe(OEP) π -Cation radicals. **Inorganic Chemistry**. 31: 939-941.
- Scheidt, W. R., in: K.M. Kadish, K.M. Smith, R. Guillard (Eds.). Systematics of the stereochemistry of porphyrins and metalloporphyrins. **The Porphyrin Handbook**, vol. 3, Academic Press, San Diego, CA, 2000: pp. 49-112.
- Shelnutt, J. A., Song, X.-Z., Ma, J.-G., Jia, S.-L., Jentzen, W., and Medforth, C. J. (1998). Nonplanar porphyrins and their significance in proteins. **Chemical Society Reviews**. 27: 31-41.
- Senge, M. O., in: K. M. Kadish, K. M. Smith, R. Guillard (Eds.). Highly substitute porphyrins. **The Porphyrin Handbook**, vol. 1, Academic Press, San Diego, CA, 2000: pp. 239-347.

- Senge, M. O. (2005). Chloro(2,3,7,8,12,13,17,18-octaethylporphyrinato)iron(III). **Acta Crystallographica E**. 61: m399-m400.
- Shelnutt, J. A., in: K. M. Kadish, K. M. Smith, R. Guilard (Eds.). Molecular simulations and normal-coordinate structural analysis of porphyrins. **The Porphyrin Handbook**, vol. 7, Academic Press, San Diego, CA, 2000: pp. 167-223.
- Spiro, T. G. (1985). Resonance Raman spectroscopy as a probe of heme protein structure and dynamics. **Advanced Protein Chemistry**. 37: 111-159.
- Teraoka, J. and Kitagawa, T. (1980). Raman characterization of axial ligands for penta- and hexacoordinate ferric high and intermediate-spin (octaethylporphyrinato)iron(III) complexes. Elucidation of unusual resonance Raman spectra of cytochrome *c'*. **The Journal of Physical Chemistry**. 8: 1928-1935.
- Uno, T., Hatano, K., Nishimura, Y., and Arata, Y. (1990). Spectrophotometric and resonance Raman studies on the formation of phenolate and thiolate complexes of (octaethylporphyrinato)iron(III). **Inorganic Chemistry**. 29: 2803-2807.
- Weiss, R., Fischer, J., Bulach, V., Schünemann, V., Gerdan, M., Trautwein, A. X., Shelnutt, J. A., Gros, C. P., Tabard, A., and Guilard, R. (2002). Structure and mixed spin state of the chloroiron(III) complex of 2,3,7,8,12,13,17,18-octaphenyl-5,10,15,20-tetraphenylporphyrin, Fe(dpp)Cl. **Inorganica Chimica Acta**. 337: 223-232.

CHAPTER IV

CONCLUSION

Malaria is a tropical disease that can cause death. Complete understanding of the relationship of electronic structure and conformation of malaria pigment and its properties is not clear because malaria pigment is a microcrystalline material which does not crystallize in a form suitable for single crystal X-ray crystallography. Part of the difficulty in obtaining suitable single crystals is presumably the extremely low solubility of malaria pigment. This study attempts to synthesize a potential malaria pigment model system based on PPIX or OEP porphyrins, which share similar heme core systems and substituents on each of the β -carbon positions. These model systems are five-coordinate, square-pyramidal, high-spin, iron(III) porphyrin complexes.

In the course of the study of a new polymorph of a previously structured malaria pigment model system was obtained. The crystallographic structural analysis demonstrated a new conformation of the peripheral ethyl groups in the new triclinic, P-1, form of Fe(OEP)Cl which has lower density than the previous studied monoclinic form. The porphyrin core of the new polymorph is nearly planar with the average displacement of the 24 atom of the core from the mean plane of only 0.03 Å. The porphyrin core conformation of the triclinic form shows the wave mode while the monoclinic form, the solvate and the $[\text{Fe}(\text{OEP}^\bullet)\text{Cl}]^+$ π -cation radical are in the saddled mode.

The ethyl groups of the triclinic Fe(OEP)Cl polymorph are arranged with four adjacent ethyl groups up (on the side of the axial ligand) and four down. The arrangement of the ethyl groups arises from steric repulsions between the peripheral substituents and favors the staggered conformation. The steric effect may increase the distance between the two porphyrin rings and leads to the slipped parallel form in crystal packing. Close intermolecular contacts between the two porphyrin rings are prevented by C–H...Cl interactions which stabilize a centrosymmetric, interaction dimer.



CURRICULUM VITAE

Name Ms. Saifon Archanachai Kohnhorst

Date of Birth 17 January 1973

Place of Birth Chaiyaphum, Thailand

Education

2002-2005 M.Sc. (Environmental Biology), Mahidol University.

1993-1997 B.Sc. (Applied Biology), Nakhon Pathom Ratchabhat University.

Experience

1997-2007 Technician, Biology Department, Faculty of Science, Mahidol University, Bangkok, Thailand. July 18-27, 2011 Certificate Course, ACA Summer Course – Small Molecule Crystallography, Indiana University of Pennsylvania, Indiana, PA, USA.

Awards Research Presentation award in PACCON 2009.

Grants and Fellowships 2550-2554 The Office of The Commission of Higher Education (CHE50- PHD-TH), Thailand. 2002-2005 Asia Development Bank Funds (ADB), Thailand.

Position and Place of Work Instructor, Department of Chemistry, Faculty of Science and Technology, Rajabhat Nakhon Ratchasima University.